INVESTIGATION OF ATOMIC NUCLEI VIA ELECTRONIC PROCESSES

Von der Fakultät für Elektrotechnik, Informationstechnik, Physik
der Technischen Universität Carolo-Wilhelmina zu Braunschweig

zur Erlangung des Grades eines Doktors
der Naturwissenschaften (Dr. rer. nat.)
genehmigte Dissertation

von ROBERT ALEXANDER MÜLLER
aus Darmstadt

eingereicht am: 6. August 2019
Disputation am: 20. September 2019

1. Referent: Prof. Dr. Andrey Surzhykov
2. Referent: Prof. Dr. Piet O. Schmidt

Druckjahr 2019

Robert Alexander Müller:
Investigation of Atomic Nuclei via Electronic Processes

SUPERVISORS:
Prof. Dr. Andrey Surzhykov
Prof. Dr. Piet O. Schmidt

Für meine Eltern

„Vielleicht“, meinte Momo, „braucht man dazu eben so eine Uhr.“ Meister Hora schüttelte lächelnd den Kopf. „Die Uhr allein würde niemand nützen. Man muß sie auch lesen können.“
— Michael Ende (Momo)

ABSTRACT

In atomic physics, nuclei are often described as a point-like charges with an infinite mass that binds the electrons. With more and more precise experimental techniques, however, this approximation is no longer sufficient and it is necessary to develop a better theoretical understanding of the ways atomic nuclei interact with the electron shell. We do observe for example small shifts in the lines of spectra of different isotopes of the same atomic species. In this thesis, we present calculations for these isotope shifts and use them to derive the difference between the nuclear charge radii of two thorium isotopes, ^{232}Th and ^{229}Th as well as ^{229}Th and the isomeric state ^{229m}Th. These results are of particular interest for the development of a future nuclear clock and coherent high-energy light sources. Moreover, we discuss precise isotope shift calculations for singly charged barium and compare them with a recent experiment. We motivate the relevance of such studies for the search for physics beyond the Standard Model.

Spectral lines, however, do not only shift but also split due to the non-point-like nature of atomic nuclei. From the spectroscopy of this hyperfine splitting, it is possible to extract the multipole moments of the nuclear electromagnetic field. As a part of this thesis, we present the first value of the nuclear magnetic dipole moment of the ^{229m}Th nuclear isomer that does not rely on previous calculations or measurements.

Having extracted several important properties of the ^{229}Th nucleus and the isomer ^{229m}Th using atomic theory we invert our view in the second part of this thesis. Namely, we want to use processes in the electron shell to populate the ^{229m}Th isomeric state. Preparatory to our calculations for the actual excitation of the isomer, we discuss the atomic structure of thorium. Of particular experimental interest is the level structure of singly charged thorium. In a recent study, we show the results of atomic structure calculations that help to interpret measured thorium spectra and can be used to estimate the probability of a nuclear excitation via the electron shell in this system. A deeper and more accurate discussion is performed for the comparably simple triply charged thorium ion. This study helps to test the various approximations necessary to discuss systems with a more complicated electronic structure. Bringing everything together the final publication presented in this thesis proposes an experimental setup to excite the ^{229}Th nucleus in a controlled way depending on the yet to be found energy of the nuclear isomeric state. This method is currently applied in an experiment at the German National Metrology Institute.

ZUSAMMENFASSUNG

Traditionell beschreibt die Atomphysik den Kern als eine Punktladung mit unendlicher Masse. Diese Näherung verliert durch immer präzisere Experimente mehr und mehr an Berechtigung und nötigt der theoretischen Physik eine immer detailliertere Beschreibung der Wechselwirkung zwischen der Elektronenhülle und dem Kern ab. So hängt beispielsweise die Frequenz eines bestimmten elektronischen Übergangs in einem bestimmten Atom oder Ion nicht nur von der elektronischen Struktur und der Kernladung, sondern auch von Masse und Volumen des Kerns ab. Diese sogenannte Isotopieverschiebung erlaubt es uns, die Differenzen zwischen den Ladungsradien von Atomkernen gleicher Ladung aber unterschiedlicher Masse zu berechnen.

Im Hinblick auf die Entwicklung einer Kernuhr sind die Eigenschaften des Thoriumisotops ^{229}Th und des Isomers ^{229m}Th von besonderem Interesse. Wir zeigen in dieser Arbeit die Änderung des Kernradius zwischen ^{232}Th und ^{229}Th und zwischen ^{229}Th und ^{229m}Th. Darüber hinaus können präzise Messungen der Isotopieverschiebung Indikatoren für mögliche Wechselwirkungen jenseits des Standardmodells sein. Mit Blick auf diese Möglichkeiten zeigen wir eine Studie der Isotopieverschiebung in einfach geladenem Barium als ersten Test der Leistungsfähigkeit der notwendigen theoretischen und experimentellen Methoden.

Zusätzlich zu den Verschiebungen von Spektrallinien aufgrund unterschiedlicher Kernmassen, spalten sich diese Linien durch die Wechselwirkung der Elektronen mit höheren Multipolmomenten des Kerns auf. Messungen dieser Hyperfeinstruktur können dazu genutzt werden ebendiese Momente zu bestimmen. In dieser Arbeit zeigen wir die erste Untersuchung der Hyperfeinstruktur von Th^{2+}. Wir nutzen unsere Ergebnisse, um die Kernmomente des ^{229}Th Isomers zu bestimmen.

Nachdem wir im ersten Teil dieser Arbeit wichtige Eigenschaften von ^{229}Th und ^{229m}Th bestimmt haben, kehren wir im zweiten Teil die Problematik um. Elektronische Prozesse können ebenfalls dazu genutzt werden den Kern zu beeinflussen. In einem ersten Schritt haben wir die Wahrscheinlichkeit einer Anregung von ^{229m}Th aus der mittleren Dichte der Energieniveaus von Th^{+} bestimmt. Eine tiefergehende Studie beschäftigt sich mit dem strukturell einfacheren dreifach geladenen Thorium und dient der Verifikation einiger Näherungen, die in komplexerem Systemen notwendig sind. Im letzten Teil dieser Arbeit schlagen wir ein Experiment zur Anregung von ^{229}Th durch einen Zweiphotonenübergang vor. Hierfür haben wir eine einfache Richtlinie entwickelt, die es erlaubt das Experiment, abhängig von der bis heute nicht genauer bestimmten Anregungsenergie von ^{229m}Th, optimal einzurichten.

CONTENTS

1 ATOMIC PHYSICS FOR NUCLEAR RESEARCH

In 1909 Geiger and Marsden investigated the scattering of α-particles by thin gold foils [1]. They found that some of the particles were deflected more than 90 degrees by the gold atoms. From these results Rutherford concluded that the positive charge of the atom has to be concentrated in a relatively small volume, contradicting Thomson's atomic model [2]. This conclusion marks the discovery of the atomic nucleus and at the same time started a whole new scientific branch in physics research.

The first experimental discovery of nuclear properties that influence atomic spectra has been made by Michelson and Morley [3], where they measured an unexpected splitting of spectral lines. At that time, however, no interpretation of this hyperfine structure of atomic levels could be given. It was Pauli later in 1924 who proposed a small nuclear magnetic moment for causing the splitting of fine structure levels in some atoms [4]. Shortly after the detection of the hyperfine structure, line shifts have been measured in atoms of the same species, leading to the discovery of nuclear isotopes. Those shifts have been explained by the movement of the nucleus [5] and its finite size [6]. Although all those breakthroughs have been made roughly 100 years ago, their implications are still highly relevant for modern atomic and nuclear physics.

Isotope Shifts and Physics Beyond the Standard Model

It has been found in precise measurements of atomic spectra that the frequency of spectral lines may depend on the way the investigated sample has been prepared. For example, a sample of naturally occurring lead has a different spectrum than lead that is a decay product of uranium [7]. The reason for this effect is differences in the composition of the atomic nuclei. Of course, the proton number Z of a certain element is fixed, the neutron number, however, and thus the total number of nucleons A of the atom can be different. There are two main consequences of this mass difference. First, the center of mass of the atom and thus, its kinetics, will change. Second, in addition to this so-called *mass shift*, the size of the nucleus also depends on A, giving rise to the *field shift* or *nuclear volume effect*. The first measurements of these effects led to the discovery of unknown isotopes, i.e. nuclei with the same charge Z but different mass number A. Moreover, the intensity of spectral lines from different

isotopes varies in a mixed sample. By that difference, it is possible to tell the relative abundance of isotopes in the sample, even from distant sources like stars and nebula.

Nowadays isotope shift measurements provide access to much more detailed information about atomic nuclei compared to the investigation of sample compositions. It is possible, for example, to derive precise information about nuclear charge radii from the spectroscopy of different isotopes of the same element [8, 9]. For such studies, precise atomic calculations are inevitable [10] [RAM1]. In most cases, the radius of the nucleus is determined from scattering experiments (see e.g. [11]). The radius difference between isotopes, however, can be obtained precisely and is an important quantity that can be used for the comparison of different nuclear models [12, 13, 14].

With measurements and theories becoming more and more precise, the number of effects that can be observed in experiments and need to be taken into account by theory keeps increasing constantly. Examples for that are higher-order relativistic interactions, Breit- and QED contributions to the isotope shift as well as nuclear polarization effects. This will make high-precision spectroscopy a valuable tool to test QED and to search for physics beyond the Standard Model. More and more proposals are made to use isotope shift spectroscopy combined with a King plot analysis [15] to put further criteria on the proposed fifth force and new light force carriers [16, 17]. We accompany the experimental starting point of such high-precision spectroscopy studies in this thesis. Our work on singly-charged earth-alkali metals [RAM1] serves as a benchmark for the theoretical and experimental methods needed for the proposed tests of the Standard Model. We show that the theory we use works reliably and can make precise predictions for experiments with unmatched accuracy.

Hyperfine Structure for the Extraction of Nuclear Moments

Aside from the shift of atomic levels and fluorescence lines due to the different mass and shape of different isotopes, we also observe a splitting of those lines in some atoms. This splitting originates from the coupling of the electron and its magnetic moment to the higher multipoles of the nuclear electromagnetic field. The first order hyperfine structure is caused by the coupling of the nuclear spin and the angular momentum of the electron shell and is proportional to the magnetic dipole moment of the nucleus. This, however, would suggest a uniform splitting of the line, which is not observed experimentally. Therefore, at least the coupling of the electron charge to the nuclear electric quadrupole moment needs to be taken into account to explain irregularities in the spacing of hyperfine lines. Of course, both the nuclear magnetic dipole and electric quadrupole moment can be calculated using nuclear theories. Such calculations, however, suffer from major uncertainties. We can circumvent those by

inverting the equations for the hyperfine splitting of atomic levels and use them to derive the nuclear moments from spectroscopic measurements. This method has been demonstrated successfully in combined theoretical and experimental approaches [18][RAM2]. The results of these considerations appear to be very precise. In fact, our calculations, that are discussed in more depth in Sec. 4.2 and [RAM2], are on the frontier of being sensitive to even more complex interactions such as the Bohr-Weisskopf effect.

The Thorium Nuclear Clock

Amongst the thousands of isotopes known today, there are only two that have a first excited state less than 100 eV above the ground state. One of them being ^{235}U with a first excited state at 76.5 eV, which is more than ten times lower than any other known nuclear transition [19]. Even more exceptional is the thorium isotope with mass number $A = 229$. The first excited state of ^{229}Th is only 8.28 eV above the ground state [20]. This makes the transition from the nuclear ground to this excited state accessible for modern tabletop lasers. Therefore a wide range of applications has been proposed to use this low energetic transition ^{229}Th [21, 22, 23, 24]. Out of these proposals, the usage of the 8.28 eV transition in thorium as a frequency standard by building a nuclear clock is probably the most famous. This idea has been first brought up by Peik and Tamm in 2003 [22] and later in 2015 discussed in more depth in Ref. [24].

In comparison to atomic transitions usually used as a frequency reference for clocks, a nuclear transition has several advantages. In particular, they are largely insensitive to systematic shifts like the Stark shift. Moreover nuclear transitions are very narrow and, thus, possibly enable us to construct a clock with an accuracy of 10^{-19} [25, 26]. This accuracy is competitive with the best atomic clocks proposed until now (see [27, 28] and references therein). Moreover, it is expected that a nuclear clock would be much more sensitive to physics beyond the Standard Model and variations of the fine structure constant α in particular [12, 13].

All potential applications mentioned above require a controlled interrogation of the 8.28 eV transition in ^{229}Th. The major obstacles for this are the small linewidth of the transition and the uncertainty with which the energy of the transition is determined up to now. Both rules out an excitation by a continuous scanning with an external spectroscopy laser. Therefore we devote the last two sections of this thesis to the controlled excitation of the first excited state of ^{229}Th. A number of ways have been proposed how this could be achieved [21, 29, 30, 31, 32]. In this thesis, however, we will focus on so-called *electron bridge processes*. These processes

use the electron shell as a mediator between the nucleus and the laser applied for the excitation [33, 34, 35, 36].

The probability for the excitation of the nucleus via an electron bridge process depends on the precise energy of the nuclear isomer and is very sensitive to the electronic structure of thorium. Therefore we present in section 4.3 an extensive study of the level structure of Th^+, one of the desired candidates for the first observation of an electron bridge process in thorium [RAM3]. Moreover, we take a more systematic look at the theory used to describe electron bridge processes in Sec. 4.3.1. In particular, we discuss the validity of common approximations used to calculate the excitation probability of thorium [RAM4]. We conclude this thesis with a detailed theoretical investigation of a scenario currently applied at the German National Metrology Institue *Physikalisch-Technische Bundesanstalt* (PTB) to excite ^{229}Th via a two-photon transition [RAM5].

2

THEORY OF MANY-ELECTRON SYSTEMS

In this chapter we will briefly lay down the theoretical methods used in the publications that are part of the present thesis. Our theory needs to perform two main tasks. For our study of electron bridge processes, we need to calculate two-photon transitions in complex atomic systems and the majority of our work requires the precise determination of atomic levels and transition matrix elements. For the latter we use a variety of methods starting from effective central potentials up to modern multi-configurational Dirac-Fock calculations and a combination of many-body perturbation theory and configuration-interaction.

EFFECTIVE CENTRAL POTENTIALS

Before we start describing many-electron effects we recall the case of a single relativistic electron with momentum $\boldsymbol{p}$ bound in a spherically symmetric potential $V^{nuc}(r)$. Such an electron is described by an eigenfunction of the Dirac Hamiltonian:

$$\hat{\mathcal{H}}^D = c\boldsymbol{\alpha}\cdot\hat{\boldsymbol{p}} + \beta m_e c^2 + \mathbb{1}\cdot V^{nuc}(\hat{r}) \tag{2.1}$$

where c is the speed of light in vacuum and m_e the electron rest mass. Moreover $\mathbb{1} = \mathrm{diag}(1,1,1,1)$ is the 4×4 identity matrix, $\boldsymbol{\alpha}$ denotes the vector of Dirac matrices and $\beta = \mathrm{diag}(1,1,-1,-1)$. The bound eigenfunctions of the Dirac Hamiltonian (2.1) are spherical Dirac spinors characterized by their principal and relativistic quantum numbers n and κ as well as the projection of the total angular momentum μ (see e.g. [37]):

$$\langle \boldsymbol{r}|n\kappa\mu\rangle = \psi_{n\kappa\mu}(\boldsymbol{r}) = \frac{1}{r}\begin{pmatrix} g_{n\kappa}(r)\chi^{\mu}_{\kappa}(\Omega) \\ \mathrm{i}f_{n\kappa}(r)\chi^{\mu}_{-\kappa}(\Omega)\end{pmatrix}. \tag{2.2}$$

Here $g_{n\kappa}(r)$ and $f_{n\kappa}(r)$ are the large and small radial components of the spinor and $\chi^{\mu}_{\kappa}(\Omega)$ are two-spinors describing the spin and angular dependencies of the wave function $\psi_{n\kappa\mu}(\boldsymbol{r})$.

After introducing the basic equations and notations for a relativistic single-electron system we can use them for the theoretical treatment of many-electron atoms. The most simple description of such an N-electron atom would be a product state $|\Psi\rangle = \Pi_{i=1}^{N}|n_i\kappa_i\mu_i\rangle$ of N spherical spinors (2.2) or *orbitals*. Such a state, however, entirely

neglects the interaction between the individual electrons. As a first step towards accounting for this interaction, we choose a semiclassical approach. Let us assume each electron is exposed to a screened nuclear potential

$$V(r) = V^{nuc}(r) + V^{H}(r), \tag{2.3}$$

where the first term is the well-known potential of the nucleus and the second term describes a spherically symmetric potential generated by the charge density of the electron cloud. We obtain this charge density from the expectation value of a δ-like operator. To begin with, we write it down for a single orbital with quantum numbers n, κ and μ:

$$\rho_{n\kappa\mu}(\boldsymbol{r}) = e \int \psi^{\dagger}_{n\kappa\mu}(\boldsymbol{r'})\delta^{(3)}(\boldsymbol{r}-\boldsymbol{r'})\psi_{n\kappa\mu}(\boldsymbol{r'})\mathrm{d}^3\boldsymbol{r'} = e\left|\psi_{n\kappa\mu}(\boldsymbol{r})\right|^2. \tag{2.4}$$

This charge density, however, is not spherically symmetric and thus we have to average it over the solid angle Ω before we can find an expression for $V^H(r)$. After averaging the charge density reads

$$\begin{aligned}\overline{\rho}_{n\kappa}(r) &= \frac{e}{4\pi r^2}\int_0^{\pi}\int_0^{2\pi}\left|\psi_{n\kappa\mu}(\boldsymbol{r})\right|^2 \mathrm{d}\varphi \sin\theta \mathrm{d}\theta \\ &= \frac{e}{4\pi r^2}\left[g_{n\kappa}(r)^2 + f_{n\kappa}(r)^2\right].\end{aligned} \tag{2.5}$$

Following Hartree we construct the classical force exerted by $\overline{\rho}_{n\kappa}(r)$ (2.5) onto an electron at r [38]:

$$F_{n\kappa}(r) = \frac{e}{2\pi\varepsilon_0 r^2}\int_0^r \rho_{n\kappa}(r')4\pi r^2 \mathrm{d}r'. \tag{2.6}$$

By integrating over this force we find the Hartree potential

$$\begin{aligned}\mathcal{V}^H_{n\kappa}(r) &= \int_r^{\infty} F_{n\kappa}(r')\mathrm{d}r' \\ &= \int_r^{\infty}\frac{e^2}{2\pi\varepsilon_0 r'^2}\int_0^{r'}\left[g_{n\kappa}(r'')^2 + f_{n\kappa}(r'')^2\right]\mathrm{d}r''\mathrm{d}r', \\ &= \int_0^{\infty}\frac{e^2}{2\pi\varepsilon_0 r_>}\left[g_{n\kappa}(r')^2 + f_{n\kappa}(r')^2\right]\mathrm{d}r'\end{aligned} \tag{2.7}$$

where in the second step we integrated by parts and $r_> = \max(r, r')$. Note here that this potential does only depend on the subshell, defined by n and κ and not on the particular state $|n\kappa\mu\rangle$.

Having constructed the Hartree potential $V^H_{n\kappa}(r)$ generated by a single orbital, we can use this result to describe a many-electron system with this semiclassical

approach. Let this system consist of one *single-electron configuration*, i.e. N electrons distributed over q subshells.Then the potential $V_A^H(r)$ experienced by an electron in the A-th subshell is obtained by summing (2.7) over all other electrons:

$$\begin{aligned} V_A^H(r) &= \sum_{B=1}^{q} (w_B - \delta_{AB}) \mathcal{V}^H_{n_B\kappa_B}(r) \\ &= \sum_{B=1}^{q} (w_B - \delta_{AB}) \int_0^\infty \frac{e^2}{2\pi\varepsilon_0 r_>} \left[g_{n_B\kappa_B}(r)^2 + f_{n_B\kappa_B}(r)^2 \right] \mathrm{d}r, \end{aligned} \tag{2.8}$$

where w_B is the number of electrons in subshell B. Using this equation to construct the screened potential $V_A^H(r)$ (2.3) we can obtain the wave function of all electrons in the configuration by solving the radial Dirac equation. This would, however, require to solve a system of q coupled Dirac equations, because the potential $V_A^H(r)$ experienced by an electron in subshell A depends on the wave functions of all electrons. Decoupling of these equations can be achieved with the *self consistent field* (SCF) approach. In this approach, we start with a set of trial spinors, one for each subshell in the configuration. From this set of spinors, we construct the potential $V_A^H(r)$ for all A and solve the Dirac equation for this potential. These solutions form the new set of trial spinors for the calculation of $V_A^H(r)$. This process is iterated until the solutions of the Dirac equation with potential $V_A^H(r)$ *self consistently* reproduce this potential. Especially for neutral systems and if the computations have to be very fast, we can further approximate $V_A^H(r)$ by taking

$$V_A^H(r) = \sum_{B=1}^{q} (w_B - \delta_{AB}) \mathcal{V}_B^H(r) \approx \sum_{B=1}^{q} w_B \mathcal{V}_B^H(r). \tag{2.9}$$

Here, the potential is the same for all subshells and, thus, needs to be calculated only once per iteration.

The Hartree approximation laid down above is a semiclassical and, originally, non-relativistic approach. Therefore it entirely neglects the Pauli exclusion principle and the correlation between the individual electrons imposed by it. We know that this correlation, that limits the number of electrons per subshell, weakens the screening of the nuclear potential. To correct for this overestimation, we can introduce another effective potential depending on the electron density and a free parameter x_α. This x_α-potential reads

$$V_A^{x_\alpha}(r) = \sum_{B=1}^{q} w_B \left[V_B^H(r) - x_\alpha \frac{e}{4\pi\varepsilon_0} \left(\frac{24}{\pi} \overline{\rho}_{n_B\kappa_B} \right)^{\frac{1}{3}} \right]. \tag{2.10}$$

Aside from plausible arguments, this potential can also be derived from density functional theory in a number of different ways (see e.g. [39] and references therein).

Each of these ways results in a slightly different value for x_α. In particular, we will refer to the case of $x_\alpha = \frac{2}{3}$ as the Kohn-Sham potential [40], as it has been used, e.g. in Ref. [RAM4]. Moreover x_α can be found by fitting the theory to experimentally measured energies.

THE RELATICISTIC DIRAC-HARTREE-FOCK EQUATIONS

In the previous section, we described a many-electron atom with an effective single-electron or independent particle model. This model is based on the approximation that the electrons interact only via their spherically averaged charge density. For a more accurate description, the interaction between individual electrons needs to be included explicitly in the Hamiltonian. We construct this full Hamiltonian of a N-electron system by summing over the single-electron Hamiltonians (2.1) of each electron and by including the interelectronic interaction:

$$\mathcal{H} = \sum_{a=1}^{N} \left(\mathcal{H}_i^D + \frac{1}{2} \sum_{\substack{b \neq a \\ b=1}}^{N} V^{e-e}(\boldsymbol{r}_a, \boldsymbol{r}_b) \right), \tag{2.11}$$

where the interaction of the a-th electron with the other $N-1$ electrons is contained in the sum of two-particle potentials $V^{e-e}(\boldsymbol{r}_a, \boldsymbol{r}_b)$. In leading order the interaction $V^{e-e}(\boldsymbol{r}_i, \boldsymbol{r}_j)$ is the Coulomb repulsion between the electrons a and b, represented by the following two-body operator:

$$V^{e-e}(r_{ab}) = \mathbb{1} \cdot \frac{e^2}{4\pi\varepsilon_0} \frac{1}{r_{ab}}, \tag{2.12}$$

where $r_{ab} = |\boldsymbol{r}_a - \boldsymbol{r}_b|$. This approximation neglects higher-order contributions to the electron-electron interaction, usually grouped under the term Breit interaction (see e.g. [41] and references therein).

In what follows we want to obtain the ground state energy of a system described by the Hamiltonian (2.11) and one single-electron configuration using a variational calculus. A proper description for the configuration is a single Slater determinant consisting of spherical Dirac spinors. The expectation value of $\mathcal{H}$ (2.11) with respect to such a determinant yields the so-called Dirac-Hartree-Fock (DHF) energy:

$$E^{DHF} = \sum_{a=1}^{N} \left[\langle a|\mathcal{H}_a^D|a\rangle + \frac{1}{2} \sum_{b=1}^{N} \left(\langle ab|V^{e-e}|ab\rangle - \langle ba|V^{e-e}|ab\rangle \right) \right], \tag{2.13}$$

where we abbreviated the quantum numbers of the states by their respective indices a and b, i.e. $|n_a\kappa_a\mu_a\rangle = |a\rangle$. The first term in Eq. (2.13) is the well-known single-electron energy of a hydrogen-like system with the potential $V^{nuc}(r)$. This energy

depends only on the principal and relativistic quantum numbers n and κ of the state and, therefore, is the same for all electrons in a subshell. We will, therefore, refer to this energy by E_A where A denotes the subshell. The evaluation of the matrix elements for the interelectronic interaction $\langle ab|V^{e-e}|ab\rangle$ and $\langle ba|V^{e-e}|ab\rangle$ needs a bit more work. First we expand the interaction potential into multipoles:

$$V^{e-e}(r_{12}) = \mathbb{1} \cdot \sum_{l=0}^{\infty} \sum_{m=-l}^{l} \frac{r_<^l}{r_>^{l+1}} C_{lm}^*(\theta_1, \phi_2) C_{lm}(\theta_1, \phi_2) \tag{2.14}$$

where $r_< = \min(r_1, r_2)$ and $r_> = \max(r_1, r_2)$ and $C_{lm}(\theta, \phi)$ are the normalized spherical harmonics

$$C_{lm}(\theta, \phi) = \sqrt{\frac{4\pi}{2l+1}} Y_{lm}(\theta, \phi). \tag{2.15}$$

With the help of the Wigner-Eckardt theorem we obtain:

$$\begin{aligned}\langle ab|V^{e-e}|ab\rangle =& (2j_a+1) \sum_l (j_a \mu_a l 0|j_a \mu_a)(j_b \mu_b l 0|j_b \mu_b) \\ & \times \langle \kappa_a||C_l||\kappa_a\rangle \langle \kappa_b||C_l||\kappa_b\rangle \langle n_a\kappa_a, n_b\kappa_b||\frac{r_<^l}{r_>^{l+1}}||n_a\kappa_a, n_b\kappa_b\rangle ,\end{aligned} \tag{2.16a}$$

$$\begin{aligned}\langle ba|V^{e-e}|ab\rangle =& \sqrt{(2j_a+1)(2j_b+1)} \sum_l (-1)^m (j_b \mu_b l - m|j_a \mu_a)(j_a \mu_a l m|j_b \mu_b) \\ & \times \langle \kappa_a||C_l||\kappa_b\rangle \langle \kappa_b||C_l||\kappa_a\rangle \langle n_b\kappa_b, n_a\kappa_a||\frac{r_<^l}{r_>^{l+1}}||n_a\kappa_a, n_b\kappa_b\rangle ,\end{aligned} \tag{2.16b}$$

where $j = |\kappa| + \frac{1}{2}$ is the total angular momentum of a single-electron orbital and $(j_1 m_1 j_2 m_2|j_3 m_3)$ are the Clebsch-Gordan coefficients. The reduced matrix elements $\langle \kappa_a||C_l||\kappa_b\rangle$, moreover, can be written as Clebsch-Gordan coefficients as well [41].The radial matrix elements represent the integrals

$$\begin{aligned}&\langle n_a\kappa_a, n_b\kappa_b||\frac{r_<^l}{r_>^{l+1}}||n_c\kappa_c, n_d\kappa_d\rangle \\ &\qquad = \int_0^\infty \int_0^\infty \left[g_{n_b\kappa_b}^*(r_1) g_{n_d\kappa_d}(r_1) + f_{n_b\kappa_b}^*(r_1) f_{n_d\kappa_d}(r_1)\right] \frac{r_<^l}{r_>^{l+1}} \\ &\qquad\qquad \times \left[g_{n_a\kappa_a}^*(r_2) g_{n_c\kappa_c}(r_2) + f_{n_a\kappa_a}^*(r_2) f_{n_c\kappa_c}(r_2)\right] \mathrm{d}r_1 \mathrm{d}r_2\end{aligned} \tag{2.17}$$

that are commonly solved numerically by means of Gauß-Legendre integration [42].

The direct $\langle ab|V^{e-e}|ab\rangle$ and exchange $\langle ba|V^{e-e}|ab\rangle$ energies derived above still depend on the magnetic quantum number μ_b of state b. It is a common approximation to average over this quantum number (configuration average), thus assuming that the interelectronic interaction V^{e-e} is approximately spherical. Note that this approximation is exact, if all subshells of the configuration are completely filled. The averaged matrix elements reduce to

$$\begin{aligned}\sum_{\mu_b}\frac{\langle ab|V^{e-e}|ab\rangle}{2j_b+1} =&(2j_a+1)\,\langle\kappa_a||C_0||\kappa_a\rangle\,\langle\kappa_b||C_0||\kappa_b\rangle \\ &\times\langle n_a\kappa_a,n_b\kappa_b||\frac{1}{r_>}||n_a\kappa_a,n_b\kappa_b\rangle\,,\end{aligned} \tag{2.18a}$$

$$\begin{aligned}\sum_{\mu_b}\frac{\langle ba|V^{e-e}|ab\rangle}{2j_b+1} =&(-1)^{j_b-j_a}\sum_l\langle\kappa_a||C_l||\kappa_b\rangle\,\langle\kappa_b||C_l||\kappa_a\rangle \\ &\times\langle n_b\kappa_b,n_a\kappa_a||\frac{r_<^l}{r_>^{l+1}}||n_a\kappa_a,n_b\kappa_b\rangle\,,\end{aligned} \tag{2.18b}$$

now depending only on the subshells A and B. Therefore we can introduce the shorthands:

$$E_{AB}^{dir}=\sum_{\mu_b}\frac{\langle ab|V^{e-e}|ab\rangle}{2j_b+1},\qquad E_{AB}^{ex}=\sum_{\mu_b}\frac{\langle ba|V^{e-e}|ab\rangle}{2j_b+1}, \tag{2.19}$$

which are the spherically averaged direct- and exchange interaction energies between two electrons in subshells A and B, respectively. We can use these energies to write down the spherically averaged Dirac-Hartree-Fock energy for a system with w_A electrons in subshell A and w_B electrons in subshell B:

$$\overline{E}^{DHF}=\sum_A w_A\left[E_A+\frac{1}{2}\sum_B w_B\left(E_{AB}^{dir}-E_{AB}^{ex}\right)\right]. \tag{2.20}$$

In order to find the ground state energy of the system we vary this energy with respect to the radial spinors $|n_A\kappa_A\rangle$. For this purpose we introduce a set of Lagrange multipliers λ_{AB} to enforce orthogonality between radial orbitals that belong to different subshells $A\neq B$. Thus, we have to vary the functional

$$E_A+\sum_B\left[\frac{w_B}{2}\left(E_{AB}^{dir}-E_{AB}^{ex}\right)+\delta_{AB}-\lambda_{AB}\,\langle n_A\kappa_A|n_B\kappa_B\rangle\right], \tag{2.21}$$

where we introduced the radial overlap integrals

$$\langle n_A\kappa_A|n_B\kappa_B\rangle=\int_0^\infty\left[g_{n_A\kappa_A}(r)g_{n_B\kappa_B}(r)+f_{n_A\kappa_A}(r)f_{n_B\kappa_B}(r)\right]\mathrm{d}r. \tag{2.22}$$

For clarity we will perform the variation of (2.21) term by term. Those terms that depend on one subshell A only, are straightforwardly obtained:

$$\delta E_A = 2\delta\left(\langle n_A\kappa_A|\right)|H_A^D|n_A\kappa_A\rangle\,, \tag{2.23a}$$

$$\delta\left(\langle n_A\kappa_A|n_A\kappa_A\rangle\right) = 2\delta\left(\langle n_A\kappa_A|\right)|n_A\kappa_A\rangle\,. \tag{2.23b}$$

All terms involving two subshells A and B require a little more effort, after some algebra we get:

$$\begin{aligned}\delta E_{AB}^{dir} =&(2j_a+1)\,\langle\kappa_a||C_0||\kappa_a\rangle\,\langle\kappa_b||C_0||\kappa_b\rangle\,2(1+\delta_{AB})\delta\left(\langle n_A\kappa_A|\right)\\ &\times\langle n_B\kappa_B||\frac{1}{r_>}||n_A\kappa_A, n_B\kappa_B\rangle\end{aligned} \tag{2.24a}$$

$$\begin{aligned}\delta E_{AB}^{ex} =&(-1)^{j_b-j_a}\sum_l\langle\kappa_a||C_l||\kappa_b\rangle\,\langle\kappa_b||C_l||\kappa_a\rangle\,2(1+\delta_{AB})\delta\left(\langle n_A\kappa_A|\right)\\ &\times\langle n_B\kappa_B||\frac{r_<^l}{r_>^{l+1}}||n_B\kappa_B, n_A\kappa_A\rangle\,.\end{aligned} \tag{2.24b}$$

The variation of the functional Eq. (2.21) must vanish for all $\delta\langle n_A\kappa_A|$ leading to the Dirac-Hartree-Fock equations:

$$\begin{aligned}0 =&H_A^D\,|n_A\kappa_A\rangle + \sum_B\left[\frac{w_B}{2}\right.\\ &\times\Bigg((2j_a+1)\,\langle\kappa_a||C_0||\kappa_a\rangle\,\langle\kappa_b||C_0||\kappa_b\rangle\,(1+\delta_{AB})\,\langle n_B\kappa_B||\frac{1}{r_>}||n_B\kappa_B\rangle\,|n_A\kappa_A\rangle\\ &-(-1)^{j_b-j_a}\sum_l\langle\kappa_a||C_l||\kappa_b\rangle\,\langle\kappa_b||C_l||\kappa_a\rangle\,(1+\delta_{AB})\,\langle n_B\kappa_B||\frac{r_<^l}{r_>^{l+1}}||n_A\kappa_A\rangle\,|n_B\kappa_B\rangle\Bigg)\\ &\left.-\lambda_{AB}\,|n_B\kappa_B\rangle\right]\,.\end{aligned} \tag{2.25}$$

It can be seen in these equations that the Lagrange multiplier λ_{AB} for $A = B$ can be interpreted as the energy of a single orbital in the subshell. Therefore the DHF equations (2.25) represent a coupled system of Dirac equations with eigenenergy λ_{AB} and two additional effective, electrostatic potentials $\langle n_B\kappa_B||\frac{1}{r_>}||n_B\kappa_B\rangle$ and $\langle n_B\kappa_B||\frac{r_<^l}{r_>^{l+1}}||n_A\kappa_A\rangle$. For the solutions of this set of coupled integro-differential equations commonly a self-consistent iterative approach is taken, very similar to the one discussed in Sec. 2.1. First, all integrals are evaluated using a set of trial functions, that can e.g. be obtained by the effective central potential approach (see Sec. 2.1).

Afterwards, the now decoupled single-electron Dirac equations are solved, and those solutions serve as the new set of trial functions and so on. We want to mention here that, above, we worked with wavefunctions that are normalized to unity. This has been done for clarity; in an actual implementation of the DHF approach, it is recommended to work with unnormalized wave functions instead, leading to an additional normalization factor of $\langle n\kappa|n\kappa\rangle^{1/2}$ in front of each radial integral. For an in-depth discussion of the numerical details, we refer the reader to Refs. [43, 41].

CONFIGURATION INTERACTION

For the derivation of the Dirac-Hartree-Fock equations (2.25) obtained in the previous section, we approximated a many-electron state by a single configuration of N electrons, distributed over q subshells. For a better description of such a state, we can expand it in the basis of all possible single-electron configurations, instead. Because we consider configurations consisting of bound-state orbitals this expansion is not complete. This, however, is a justified approximation as long as we perform calculations for levels (many-electron states) with energies well below the ionization threshold and not too strongly bound systems. In what follows we will assume that these requirements are fulfilled and, therefore, all possible single-electron configurations provide an approximately complete basis for the construction of a many-electron level.

After we have discussed the validity of describing a many-electron state in terms of a superposition of single-electron configurations we will now show how these configurations are constructed mathematically. First and foremost the function describing a configuration, from now on referred to as *configuration state function* (CSF), needs to be antisymmetrized to obey the Pauli exclusion principle. This requirement is already fulfilled by Slater determinants. Those consist of orbitals that have a well-defined parity p, total angular momentum j and total angular momentum projection μ. However, as it is easily seen, the operators corresponding to these quantum numbers do not commute with the many-electron Hamiltonian (2.11). Instead, not the individual orbitals but the many-electron state itself has to have a well-defined parity P and total angular momentum J with a projection M onto the quantization axis. This follows straight from the fact that each quantum mechanical system with a well-defined center of mass, has a well defined total angular momentum, as we already know from classical mechanics. Therefore Slater determinants cannot be used as configuration state functions, instead, they are constructed as a product state of orbitals (2.2) where all individual total angular momenta have been coupled to

a well defined J. We will identify CSFs by $|\gamma J^P M\rangle$, where γ denotes the electron configuration. Using these to expand a many-electron state we get

$$|\Gamma J^P M\rangle = \sum_\gamma c_{\Gamma\gamma} |\gamma J^P M\rangle \,, \tag{2.26}$$

where the expansion coefficients $c_{\Gamma\gamma}$ are the so-called *mixing coefficients* and we will refer to $|\Gamma J^P M\rangle$ as an atomic state function (ASF) that describes an atomic level Γ. Generally, an ASF does not correspond to a certain electron configuration and is identified by its level number Γ instead. This level number is the position of the ASF in a list of all levels with the same J and P ordered by energy.

In order to obtain the mixing coefficients $c_{\Gamma\gamma}$ we plug the ASF (2.26) into the Dirac equation with Hamiltonian $\mathcal{H}$ (2.11). After some algebra we find the matrix Hamiltonian form:

$$\hat{\mathcal{H}} \boldsymbol{c}_\Gamma = E_\Gamma \boldsymbol{c}_\Gamma \tag{2.27}$$

where $\hat{\mathcal{H}}$ is the many-electron Dirac Hamiltonian in the CSF basis and $\boldsymbol{c}_\Gamma$ is the vector of mixing coefficients for a particular level Γ. This eigenvalue problem can be solved algebraically, allowing us to obtain approximate solutions of the relativistic many-electron problem. It is worth noting that this *configuration interaction* (CI) description of the relativistic many-electron problem is exact if an infinite, complete basis set was used. In practice, however, the performance of the CI method strongly depends on the proper choice of the approximate, finite basis. Commonly this is done by starting with a reference configuration γ_0. This reference configuration should be chosen such that it already approximates the many-electron state as good as possible. In other words, ideally $c_{\Gamma\gamma_0}$ is one of the largest mixing coefficients. The other CSFs in the basis set are then generated by replacing one or more orbitals in the reference configuration with another one. To do this systematically we divide all orbitals into two groups as illustrated in Fig. 2.1. The inactive space contains all occupied orbitals from which no virtual excitations are allowed, so they are the same in all CSFs. Accordingly, all orbitals in the active space are subject to replacements. The size of the CSF set increases rapidly, the larger the active space is chosen and sets containing 10^5 up to almost 10^6 CSFs are common in high-precision calculations. The results of CI calculations are strongly dependent on the CSF set and the construction of the individual orbitals. Therefore it is extremely important to clearly communicate both together with any results obtained using the CI method. Moreover, it is equally important to be aware of the uncertainties of those results. Two different considerations are necessary to estimate these uncertainties. First one needs to estimate the magnitude of all effects not included in the theory. Breit interaction and QED effects, like vacuum polarization and the self-energy of electrons, for example, are usually

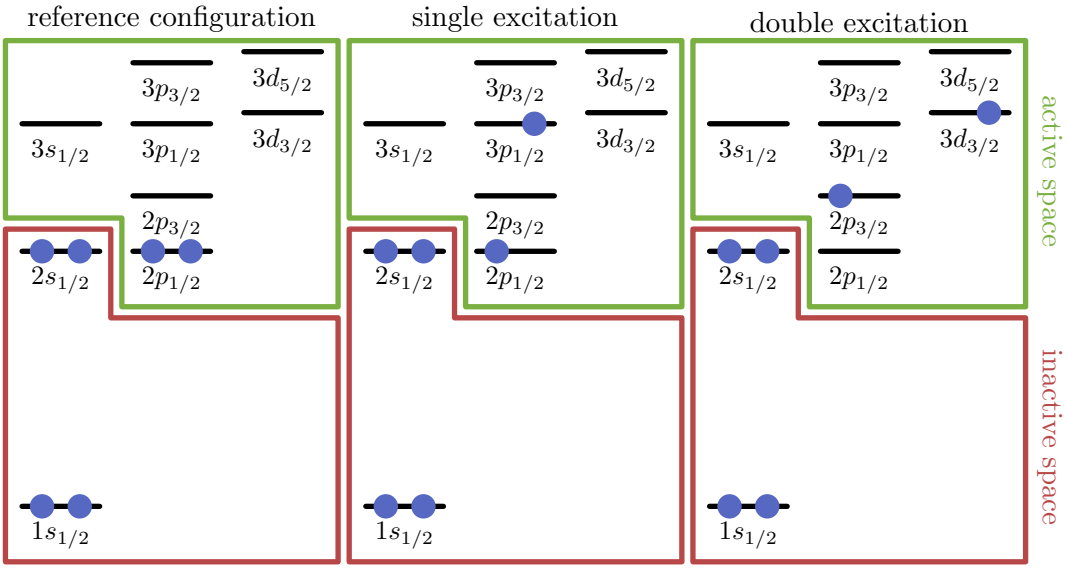

Figure 2.1: Active and inactive space for the construction of a CSF basis set using the example of a carbon-like ion. The inactive space consists of the $1s_{1/2}$ and $2s_{1/2}$ orbitals while the active space is formed by all orbitals in the $n = 3$ shell and the remaining states with $n = 2$. We show the reference configuration and two CSFs, one created by a single and the other one by a double virtual excitation.

incorporated only perturbatively in CI calculations. This procedure usually results in less numerical stability of the calculations and therefore it has to be carefully considered if those effects need to be calculated or not. An estimate of their magnitude can be obtained using simpler models like effective central potentials or the DHF approach. An example of such an estimate can be found e.g. in Ref. [RAM1].

Besides neglected effects, the numerical uncertainty of the CI method itself needs to be gauged. This can be done by carefully documenting the convergence behaviour of the calculations with increasingly larger basis sets. The size of the CSF basis, however, can be increased in several ways. It has proven useful to consider the following directions to enlarge the basis set. The zeroth-order calculation consists of γ_0, only and, thus, the result is given by a single CSF. Higher orders are obtained by adding orbitals to the active space which are not part of γ_0. This is referred to as adding correlation layers. Instead of adding correlation layers it is also possible to add previously inactive orbitals to the active space, usually called opening the core. Running several calculations with basis sets that are enlarged systematically by adding correlation layers and opening the core results in a two-dimensional convergence landscape, as seen in Fig. 2.2. This figure that shows the convergence of

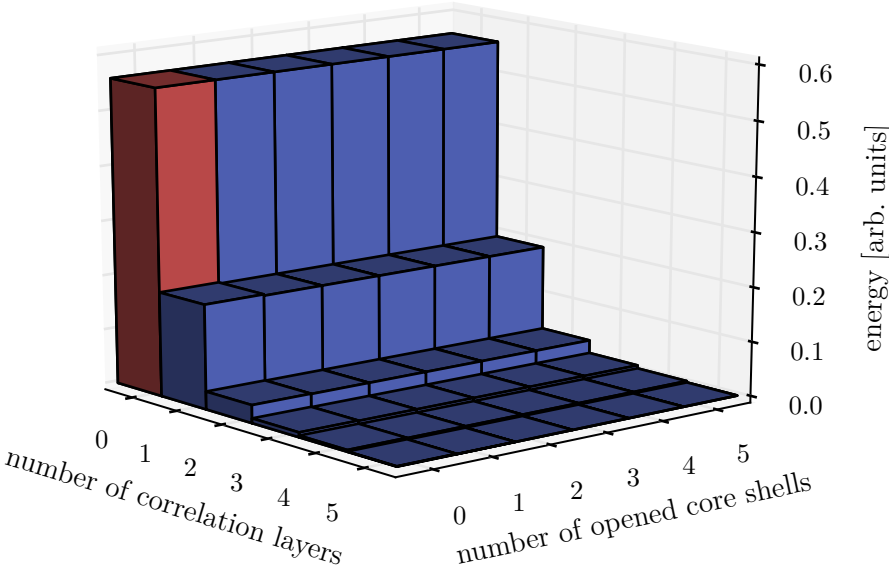

Figure 2.2: Convergence landscape of the [Xe].6s ground-state energy of Ba^+. The convergence is shown for an increasing number of opened core shells until all orbitals belong are added to the active space and subsequently added correlation layers up to $n = 12$. Consequently, the most left bar, colored red, corresponds to the DHF energy of the Ba^+ ground state.

the ground state energy of Ba^+ as we achieved it in our calculations presented in Ref. [RAM1]. As seen from this figure, the results converge fast towards the final value with an increasing number of correlation layers. In fact, the convergence with respect to opening the core appears to have a smaller effect in these calculations.

There is one caveat that needs to be taken into account: The CI method sometimes converges to local minima of the level energies. Therefore we recommend checking the convergence in a third dimension. Often the accuracy of CI calculations can be highly improved by starting not with one but several reference configurations. A good approach here is to subsequently add the configurations with the largest mixing coefficients $c_{\Gamma\gamma}$ to the set of reference configurations until convergence is achieved.

Finally, we can also increase the number of replacements or virtual excitations in the construction of the CSF set. It is not necessary to allow for multiple exci-

tations (usually three at maximum) from the entire active space since this would quickly enlarge the size of the CSF set, but it should be allowed from those orbitals that appear to strongly correlate with others in the calculations. This correlation is indicated by the mixing coefficients $c_{\Gamma\gamma}$. Comparing the configurations with the largest $c_{\Gamma\gamma}$ in the expansion we can identify those orbitals that are replaced most often. From these orbitals, multiple virtual excitations should be allowed. If after all, both additional reference configurations and multiple excitations do not change the results of a calculation, we usually consider it reliable and stable.

THE MULTI-CONFIGURATIONAL DIRAC-FOCK APPROACH

In this section we want to combine two theories for the treatment of many-electron systems to the *multi configurational Dirac-Fock* approach. This approach benefits from the optimization of the single-electron orbitals by solving the DHF equations as well as the asymptotically exact character of the CI method that only works with fixed orbitals. For this purpose we need to rederive the DHF equations for an atomic state function as the trial function (2.26), instead of a single configuration (2.13). The expectation value of the many-electron Hamiltonian (2.11) with respect to an ASF is

$$\langle \Gamma J^P M|\mathcal{H}|\Gamma J^P M\rangle = \sum_{\gamma\gamma'} c_{\Gamma\gamma'} c_{\Gamma\gamma} \langle \gamma' J^P M|\mathcal{H}|\gamma J^P M\rangle \,, \tag{2.28}$$

which can be separated into a diagonal and off-diagonal term:

$$\langle \Gamma J^P M|\mathcal{H}|\Gamma J^P M\rangle = \sum_{\gamma} c^2_{\Gamma\gamma} \langle \gamma J^P M|\mathcal{H}|\gamma J^P M\rangle + \sum_{\substack{\gamma\gamma' \\ \gamma\neq\gamma'}} c_{\Gamma\gamma'} c_{\Gamma\gamma} \langle \gamma' J^P M|\mathcal{H}|\gamma J^P M\rangle \,. \tag{2.29}$$

Here, the first term is the sum of DHF energies (2.13) of all configurations γ in the ASF. Therefore we may rewrite:

$$\langle \Gamma J^P M|\mathcal{H}|\Gamma J^P M\rangle = \sum_{\gamma} c^2_{\Gamma\gamma} E^{DHF}_{\gamma} + \sum_{\substack{\gamma\gamma' \\ \gamma\neq\gamma'}} c_{\Gamma\gamma'} c_{\Gamma\gamma} \langle \gamma' J^P M|\mathcal{H}|\gamma J^P M\rangle \,, \tag{2.30}$$

where it is seen now that we can understand the off-diagonal term as a multi-configurational correction to the individual DHF energies. A variation of this energy functional (2.30) results in a set of integro-differential equations very similar to Eq. (2.25) that can be solved iteratively as well. The solutions obtained this way now serve as orbitals for the construction of a CSF set to be used in the CI method

as described in the previous section 2.3. This improves the accuracy of the results significantly because the multi-configurational character of a many-electron state is already partially accounted for in the optimization of the single-electron orbitals. However, this gives rise to a number of numerical subtleties. We have discussed that it is necessary to repeat a CI calculation several times with successively enlarged CSF sets. As we can see from Eq. (2.30) this would lead to modified orbitals for each of these repetitions. But we find that the numerical stability of the iterative procedure for the solution of the MCDF equations (2.30) is impeded and sometimes does not converge if several orbitals with the same total angular momentum and parity are optimized simultaneously. Therefore we recalculate only those orbitals that have been added to the active space and keep all others as they have been calculated in the previous, lower order, calculation. This approach represents a good compromise between numerical stability, accuracy and fast convergence of the calculations. For a detailed discussion of several numerical tricks and improvements that can be made in an implementation of this method, we would like to refer the reader to the works of Froese-Fischer *et al.* [43] and Grant [41]. Both authors were deeply involved in the development of the GRASP2K code that has been used to obtain several of the results in this thesis and is one of the most commonly used implementations of the MCDF method.

CI AND MANY-BODY PERTURBATION THEORY

In the previous sections, we have discussed how we can describe many-electron systems by means of variational principles either with respect to the radial wavefunctions or by varying the coefficients of an expansion in configuration space. Eventually, we combined both of these approaches to form the MCDF method. This method, however, only accounts for the correlation between orbitals in the active and inactive space in a very limited way by opening the core in the CI part of the calculations. But enlarging the active space drastically increases the number of CSFs in the basis to an impractical amount. Many-body perturbation theory (MBPT), in contrast, is very powerful in treating core-core and core-valence correlations but only provides accurate results for systems with a single valence electron and closed shells otherwise. For more complicated systems it seems therefore natural to again combine methods for a gain of accuracy. Such a combination of MBPT and CI has been proposed by Dzuba *et al.* [44] and in a slightly different approach by Savukov and Johnson [45, 46]. Further development of this method has been presented by Dzuba and Flambaum [47] and, eventually, it was released as a program package by Kozlov *et al.* [48]. In this section, we will lay down the main idea of their theory.

The starting point of the combined CI-MBPT theory is an atomic state function and an active and inactive space of single-electron orbitals. Here, the active space consists only of the valence electrons and the correlation layers, while the inactive space contains all closed shells. With this active space and by fixing the number of virtual excitations a CSF set is constructed. We will call the space spanned by this set P. Moreover, we define the complement Q of P via the relation $P + Q = \mathfrak{H}_{CSF}$, where $\mathfrak{H}_{CSF}$ is the entire configuration space spanned by all possible CSFs. Let us define the projectors onto the spaces Q and P:

$$\begin{aligned} \mathcal{P} &= \sum_{\gamma \in P} |\gamma J^P M\rangle \langle \gamma J^P M| , \\ \mathcal{Q} &= \mathbb{1}_{\mathfrak{H}_{CSF}} - \mathcal{P}, \end{aligned} \tag{2.31}$$

where the sum runs over all configurations in the CSF set and $\mathbb{1}_{\mathfrak{H}_{CSF}}$ is the unity operator on $\mathfrak{H}_{CSF}$. With these projectors we can decompose the many-electron Hamiltonian (2.11) in the following way

$$\mathcal{H} = \mathcal{P}\mathcal{H}\mathcal{P} + \mathcal{Q}\mathcal{H}\mathcal{Q} + \mathcal{P}\mathcal{H}\mathcal{Q} + \mathcal{Q}\mathcal{H}\mathcal{P}, \tag{2.32}$$

where the first term is the Hamiltonian diagonalized by the CI method. The other terms describe core-core correlations on subspace Q and core-valence correlations. Let $|\Gamma J^P M\rangle$ be the exact wave function of a many-electron state that decomposes into $|\Gamma J^P M\rangle_{CI} = \mathcal{P}|\Gamma J^P M\rangle$ on the CI space P and $|\Gamma J^P M\rangle_{core} = \mathcal{Q}|\Gamma J^P M\rangle$ on Q. Plugging this decomposition $|\Gamma J^P M\rangle = |\Gamma J^P M\rangle_{CI} + |\Gamma J^P M\rangle_{core}$ into the Schrödinger-type eigenvalue equation $\mathcal{H}|\Gamma J^P M\rangle = E|\Gamma J^P M\rangle$ and projecting on either subspace P and Q we find the system of equations:

$$\mathcal{P}\mathcal{H}\mathcal{P}|\Gamma J^P M\rangle_{CI} + |\Gamma J^P M\rangle_{core} = E|\Gamma J^P M\rangle_{CI} \tag{2.33a}$$

$$\mathcal{Q}\mathcal{H}\mathcal{Q}|\Gamma J^P M\rangle_{core} + \mathcal{Q}\mathcal{H}\mathcal{P}|\Gamma J^P M\rangle_{CI} = E|\Gamma J^P M\rangle_{core} . \tag{2.33b}$$

Since we aim to find a representation of the ground and first few excited states of the many-electron system we need to solve these equations for $|\Gamma J^P M\rangle_{CI}$. Therefore let us define the Green's function on Q:

$$\mathcal{G}_Q(E) = (E - \mathcal{Q}\mathcal{H}\mathcal{Q})^{-1} \tag{2.34}$$

and use this to rewrite Eq. (2.33b) for $|\Gamma J^P M\rangle_{core}$:

$$|\Gamma J^P M\rangle_{core} = \mathcal{G}_Q(E)\mathcal{Q}\mathcal{H}\mathcal{P}|\Gamma J^P M\rangle_{CI} . \tag{2.35}$$

Plugging this into Eq. (2.33a) we find a Schrödinger-type equation for $|\Gamma J^P M\rangle_{CI}$:

$$[\mathcal{P}\mathcal{H}\mathcal{P} + \Sigma(E)]\,|\Gamma J^P M\rangle_{CI} = E\,|\Gamma J^P M\rangle_{CI}\,, \tag{2.36}$$

where we have introduced the operator

$$\Sigma(E) = \mathcal{P}\mathcal{H}\mathcal{Q}\mathcal{G}_Q(E)\mathcal{Q}\mathcal{H}\mathcal{P}. \tag{2.37}$$

Often this operator only weekly depends on E, thus we can approximate it by a constant $\Sigma(E_{av})$ and use the usual CI method explained in section 2.3 to calculate $|\Gamma J^P M\rangle_{CI}$ for the Hamiltonian $\mathcal{P}\mathcal{H}\mathcal{P} + \Sigma(E_{av})$.

To obtain the operator $\Sigma(E)$ we can apply many-body perturbation theory, starting with an effective mean-field Hamiltonian $\overline{\mathcal{H}}$ as it can be obtained by one of the self-consistent procedures discussed in Secs. 2.1-2.2. These Hamiltonians do not account for electron-electron correlation and, thus, act on single-electron orbitals, only. Therefore we find:

$$\mathcal{P}\overline{\mathcal{H}}\mathcal{Q} = \mathcal{Q}\overline{\mathcal{H}}\mathcal{P} = 0 \tag{2.38}$$

and, consequently, can write:

$$\Sigma(E) = \mathcal{P}(\mathcal{H} - \overline{\mathcal{H}})\mathcal{Q}\mathcal{G}_Q(E)\mathcal{Q}(\mathcal{H} - \overline{\mathcal{H}})\mathcal{P}. \tag{2.39}$$

Treating the difference between the mean-field and the full Hamiltonian $\mathcal{V}_{corr} = \mathcal{H} - \overline{\mathcal{H}}$, describing the higher-order correlation effects as a perturbation, we can expand the Green's function in a many-body perturbative manner:

$$\begin{aligned}\mathcal{G}_Q(E) &= (E - \mathcal{Q}\mathcal{H}\mathcal{Q})^{-1} \\ &= \mathcal{Q}\,(E - \mathcal{H})^{-1}\,\mathcal{Q} \\ &= Q\left(E - \overline{\mathcal{H}}\right)^{-1} Q + Q\left(E - \overline{\mathcal{H}}\right)^{-1} Q\mathcal{V}_{corr}Q\left(E - \overline{\mathcal{H}}\right)^{-1} Q + \ldots.\end{aligned} \tag{2.40}$$

This equation can be rewritten in matrix form in a single-electron orbital basis. We can use this expansion to find a representation of $\Sigma(E)$, where the shape of $\mathcal{V}_{corr}$ depends on the choice of the starting approximation. Often a DHF Hamiltonian (2.25) is chosen for $\overline{\mathcal{H}}$. For more details see Refs. [44, 47] and also Walter Johnson's Lectures on Atomic Physics [49].

3

INTERACTION OF ATOMS WITH LIGHT

Although it is textbook knowledge as found e.g. in Ref. [50], we will use this chapter to briefly recall how we describe the interaction of atoms with external fields. In Dirac's theory for point-like electrons this interaction is described by the *minimal coupling* between the electron and electromagnetic fields, represented by the replacement:

$$\mathrm{i}\hbar\frac{\partial}{\partial t} \to \mathrm{i}\hbar\frac{\partial}{\partial t} - e\phi \qquad , \qquad \boldsymbol{p} \to \boldsymbol{p} - e\boldsymbol{A}(\boldsymbol{r},t). \tag{3.1}$$

where ϕ is the scalar potential generated by the nucleus, and possibly the mean-field of the core electrons. The field $\boldsymbol{A}(\boldsymbol{r},t)$ is the vector potential of an external free electromagnetic field that interacts with the atom. Thus, with the replacements (3.1) the Hamiltonian for an atom interacting with an external light field can be written as

$$\mathcal{H} = \mathcal{H}^0 - \lambda ec\boldsymbol{\alpha}\cdot\boldsymbol{A}(\boldsymbol{r},t), \tag{3.2}$$

where λ is a small dimensionless parameter that is related to the ratio of the unperturbed electron momentum and the momentum transferred to the electron by the field $\boldsymbol{A}(\boldsymbol{r},t)$. The Hamiltonian $\mathcal{H}^0$ can be any Hamiltonian discussed in the previous chapter 2. If, however, $\mathcal{H}^0$ is a many-electron Hamiltonian the perturbation $\lambda ec\boldsymbol{\alpha}\cdot\boldsymbol{A}(\boldsymbol{r},t)$ needs to be summed over all electrons.

In the following we want to find the eigenfunctions and eigenenergies of the minimal coupling Hamiltonian (3.2) using perturbation theory. Let $|\Psi,t\rangle$ be a solution of the time-dependent eigenvalue problem

$$\mathcal{H}\,|\Psi,t\rangle = \mathrm{i}\hbar\partial_t\,|\Psi,t\rangle\,. \tag{3.3}$$

Then, the probability to find the atom in a particular state $|f\rangle$ at time t is

$$P_f(t) = |\langle f|\Psi,t\rangle|^2\,. \tag{3.4}$$

Moreover, let $|f\rangle$ be an eigenfunction of the unperturbed Hamiltonian $\mathcal{H}^0$, thus being either the solution of an (effective) single-electron problem as discussed in Secs. 2.1 and 2.2 or an atomic state function obtained by either of the methods described in sections 2.3, 2.4 or 2.5. The set of all eigenfunctions of $\mathcal{H}^0$ are a basis of the

Hilbert space belonging to $\mathcal{H}$. Therefore we can expand $|\Psi, t\rangle$ in the basis of $\mathcal{H}^0$ eigenfunctions

$$|\Psi, t\rangle = \sum\!\!\!\!\!\!\int_k c_k(t)\,|k\rangle\ \mathrm{e}^{-\frac{\mathrm{i}}{\hbar}E_k t}, \tag{3.5}$$

where $\sum\!\!\!\!\!\!\int_k$ sybolizes the sum over all bound and the integration over all continuum states that fullfill with $\mathcal{H}^0\,|k\rangle = E_k\,|k\rangle$. Plugging this expansion into Eq. (3.4), we find $P_f(t) = |c_f(t)|^2$. Entering it into the Schrödinger type equation (3.3) we obtain the relation

$$\mathrm{i}\hbar \sum\!\!\!\!\!\!\int_k \dot{c}_k(t)\,\mathrm{e}^{-\frac{\mathrm{i}}{\hbar}E_k t}\,|k\rangle = -\lambda e\boldsymbol{\alpha}\cdot\boldsymbol{A}(\boldsymbol{r},t)\sum\!\!\!\!\!\!\int_k c_k(t)\,\mathrm{e}^{-\frac{\mathrm{i}}{\hbar}E_k t}\,|k\rangle\,. \tag{3.6}$$

By multiplying from the left with $\langle f|$ we can obtain a differential equation for $c_f(t)$ that reads

$$\dot{c}_f(t) = \lambda\frac{\mathrm{i}ec}{\hbar}\sum\!\!\!\!\!\!\int_k c_k(t)\,\mathrm{e}^{\frac{\mathrm{i}}{\hbar}(E_f-E_k)t}\,\langle f|\boldsymbol{\alpha}\cdot\boldsymbol{A}(\boldsymbol{r},t)|k\rangle\,. \tag{3.7}$$

In order to solve this differential equation, we expand the coefficients $c_k(t)$ in powers of the perturbation strength λ:

$$c_k(t) = c_k^{(0)}(t) + \lambda c_k^{(1)}(t) + \lambda^2 c_k^{(2)}(t) + \ldots\,. \tag{3.8}$$

Entering this expansion into the differential equation (3.7) and taking the terms of equal power in λ on both sides of the equation, we get the recurrence relation:

$$\dot{c}_f^{(n+1)}(t) = \frac{\mathrm{i}ec}{\hbar}\sum\!\!\!\!\!\!\int_k c_k^{(n)}(t)\,\mathrm{e}^{\frac{\mathrm{i}}{\hbar}(E_f-E_k)t}\,\langle f|\boldsymbol{\alpha}\cdot\boldsymbol{A}(\boldsymbol{r},t)|k\rangle\,, \tag{3.9}$$

where the zeroth order is $\dot{c}_f^{(0)}(t) = 0$. The index n denotes the order of perturbation, thus we can use Eq. (3.9) to calculate the probability (3.4) order by order.

SINGLE PHOTON PROCESSES

In this section we will use the previously derived perturbative method (3.9) to express the transition probability for $n = 1$. Let us assume that the atom is prepared in an unperturbed state $|i\rangle$ at time $t = 0$. At this time the perturbing potential $\boldsymbol{A}(\boldsymbol{r},t)$ is zero and, thus,

$$c_k^{(0)}(t) = \delta_{ki}, \tag{3.10}$$

where we have used Eq. (3.5). Therefore the equation for the first order coefficient (3.9) reduces to

$$\dot{c}_f^{(1)}(t) = \frac{\mathrm{i}ec}{\hbar}\, \mathrm{e}^{\frac{\mathrm{i}}{\hbar}(E_f - E_i)t}\, \langle f|\boldsymbol{\alpha}\cdot\boldsymbol{A}(\boldsymbol{r},t)|i\rangle\,. \tag{3.11}$$

For a monochromatic electromagnetic field, we can seperate the time dependence of the vector potential $\boldsymbol{A}(\boldsymbol{r},t) = \boldsymbol{A}(\boldsymbol{r})\,\mathrm{e}^{-\mathrm{i}\omega t} + \boldsymbol{A}^*(\boldsymbol{r})\,\mathrm{e}^{\mathrm{i}\omega t}$ with the angular photon frequency ω. With this separation we can carry out the time integral in Eq. (3.11) from 0 to t:

$$\begin{aligned} c_f^{(1)}(t) =& \frac{\mathrm{i}ec}{\hbar}\int_0^t \Big(\mathrm{e}^{\frac{\mathrm{i}}{\hbar}(E_f - \hbar\omega - E_i)t'}\, \langle f|\boldsymbol{\alpha}\cdot\boldsymbol{A}(\boldsymbol{r})|i\rangle \\ &+ \mathrm{e}^{\frac{\mathrm{i}}{\hbar}(E_f + \hbar\omega - E_i)t'}\, \langle f|\boldsymbol{\alpha}\cdot\boldsymbol{A}^*(\boldsymbol{r})|i\rangle \Big)\, \mathrm{d}t' \\ =& ec\left(\frac{1 - \mathrm{e}^{\frac{\mathrm{i}}{\hbar}(E_f - \hbar\omega - E_i)t}}{E_i + \hbar\omega - E_f}\, \langle f|\boldsymbol{\alpha}\cdot\boldsymbol{A}(\boldsymbol{r})|i\rangle \right. \\ &\left. + \frac{1 - \mathrm{e}^{\frac{\mathrm{i}}{\hbar}(E_f + \hbar\omega - E_i)t}}{E_i - \hbar\omega - E_f}\, \langle f|\boldsymbol{\alpha}\cdot\boldsymbol{A}^*(\boldsymbol{r})|i\rangle \right), \end{aligned} \tag{3.12}$$

where we assumed that the field $\boldsymbol{A}(\boldsymbol{r},t)$ has been switched on adiabatically at $t = 0$ after the preparation of the initial state $|i\rangle$. Assuming that the observation of the system happens at asymptotic times, we define the transition rate:

$$w_{fi}^{(1)} = \lim_{t\to\infty} \frac{1}{t} \left| c_f^{(1)}(t) \right|^2, \tag{3.13}$$

which is essentially the probability (3.4) of the transition per unit time. With the definition of the δ-distribution $\delta(a) = \lim_{t\to\infty} \sin^2(at)/(\pi a^2 t)$ we can rewrite this rate and obtain:

$$\begin{aligned} w_{fi}^{(1)} =& 2\pi \frac{(ec)^2}{\hbar} \Big[\delta(E_f - \hbar\omega - E_i)\, |\langle f|\boldsymbol{\alpha}\cdot\boldsymbol{A}(\boldsymbol{r})|i\rangle|^2 \\ &+ \delta(E_f + \hbar\omega - E_i)\, |\langle f|\boldsymbol{\alpha}\cdot\boldsymbol{A}^*(\boldsymbol{r})|i\rangle|^2 \Big]. \end{aligned} \tag{3.14}$$

Here we see, why we refer to processes described by this first order perturbation theory as single-photon processes. The delta function $\delta(E_f \pm \hbar\omega - E_i)$ ensures energy conservation $E_f = E_i \pm \hbar\omega$ corresponding to the absorption or emission of one photon by the atom, depending on the energies of the initial and final state. The rate (3.14) is proportional to the module squared of the transition matrix element $\langle f|\boldsymbol{\alpha}\cdot\boldsymbol{A}(\boldsymbol{r})|i\rangle$. This matrix element can be calculated by means of any of the single- or many-electron theories discussed in chapter 2.

TWO-PHOTON PROCESSES

In the previous section, we calculated the rate for the transition $|i\rangle \to |f\rangle$ by solving the differential equation (3.9) for $n = 0$. There we have seen that this rate corresponds to the emission or apsorption of a single photon. Based on these results, we calculate in this section the second order $n = 1$, which is of major importance for our works [RAM4] and [RAM5] constituting parts of this thesis. Therefore we write down Eq. (3.9) for $n = 1$ and find:

$$\dot{c}_f^{(2)}(t) = \frac{\mathrm{i}ec}{\hbar} \sum\!\!\!\!\!\!\int_k c_k^{(1)}(t)\, \mathrm{e}^{\frac{\mathrm{i}}{\hbar}(E_f - E_k)t} \langle f|\boldsymbol{\alpha}\cdot\boldsymbol{A}(\boldsymbol{r},t)|k\rangle\,. \tag{3.15}$$

For simplicity we assume a monochromatic, ingoing wave $\boldsymbol{A}(\boldsymbol{r},t) = \boldsymbol{A}(\boldsymbol{r})\,\mathrm{e}^{-\mathrm{i}\omega t}$. With this, the integration of this equation is readily performed and after taking the limit $t \to \infty$ we get

$$w_{fi}^{(2)} = (2\pi)^2 \frac{(ec)^4}{\hbar} \delta(E_f - E_i - 2\hbar\omega) \left| \sum\!\!\!\!\!\!\int_k \frac{\langle f|\boldsymbol{\alpha}\cdot\boldsymbol{A}(\boldsymbol{r})|k\rangle \langle k|\boldsymbol{\alpha}\cdot\boldsymbol{A}(\boldsymbol{r})|i\rangle}{E_i - E_k + \hbar\omega} \right|^2 \tag{3.16}$$

From the energy conserving prefactor $\delta(E_f - E_i - 2\hbar\omega)$ we can conclude that this coefficient determines the probability for the absorption of two equal photons. For the description of different processes, the absorption and subsequent emission of a photon for example, we have to modify the vector potential accordingly, i.e.:

$$\boldsymbol{A}(\boldsymbol{r},t) = \boldsymbol{A}(\boldsymbol{r})\,\mathrm{e}^{-\mathrm{i}\omega t} + \boldsymbol{A}^*(\boldsymbol{r})\,\mathrm{e}^{\mathrm{i}\omega t} \tag{3.17}$$

In order to obtain the second order rate for the transition from $|i\rangle$ to $|f\rangle$, we can apply the same steps as in the previous section 3.1. There is however, one problem remaining. The coefficient $c_f^{(2)}(t \to \infty)$ still contains the sum and integration over the complete set of $\mathcal{H}^0$-eigenfunctions. Generally this sum/integral can not be performed analytically and, therefore, we will discuss two methods used in this thesis to approximate $c_f^{(2)}$.

B-Spline Pseudobasises

It is a common method to solve the radial Dirac equation by expanding the radial orbitals into a finite basis set while the spin-angular function $\chi_\kappa^\mu(\Omega)$ is fixed by the symmetry of the orbital. Generally such an expansion can be written as

$$\frac{1}{r}\begin{pmatrix} g_{n\kappa}(r) \\ f_{n\kappa}(r) \end{pmatrix} = \sum_{i=1}^{2n} c_i u_i(r). \tag{3.18}$$

Early implementations of this method for the solution of the Dirac equation can be found e.g. in Refs. [51, 52]. A popular choice for the finite set of $u_i(r)$, first introduced by Johnson *et al.* [53, 54] are a set B-splines of order k [55]. These splines are piecewise polynomial functions of order $k-1$ on a sequence of knots $\{t_0, t_1, \ldots, t_n\}$. These knots do not have to be pairwise distinct but we require $t_i \leq t_{i+1}$. With these prerequisites, the i-th B-spline of first order fulfills the condition:

$$B_i^k(r) = \begin{cases} 1 & \text{for} \quad t_i \leq r < t_{i+1} \\ 0 & \text{otherwise} \end{cases} \tag{3.19}$$

The higher-order B-splines are then constructed from the recursion formula

$$B_i^{k+1}(r) = \frac{r - t_i}{t_{i+k} - t_i} B_i^k(r) + \frac{t_{i+k+1} - r}{t_{i+k+1} - t_{i+1}} B_{i+1}^k(r). \tag{3.20}$$

In their works Johnson *et al.* [53] chose to expand the large and small component of the radial wave function into B-splines separately:

$$\begin{aligned} u_i(r) &= \begin{pmatrix} B_i^k(r) \\ 0 \end{pmatrix} \qquad \text{for } i \leq n \\ u_i(r) &= \begin{pmatrix} 0 \\ B_{i-n}^k(r) \end{pmatrix} \quad \text{for } i > n. \end{aligned} \tag{3.21}$$

This representation of the radial wavefunctions, however, raises a major problem. Due to the finity of the basis set, unphysical, so-called *spurious states* occur amongst the solutions for positive κ [56, 53]. As shown by Shabaev *et al.* these spurious states can be avoided by using a coupled expansion of the large and small component of the radial wave function in a so-called dual kinetic balance (DKB) approach [57]. The DKB approach uses a different expression for the basis elements $u_i(r)$:

$$\begin{aligned} u_i(r) &= \begin{pmatrix} B_i^k(r) \\ \frac{1}{2m_e c} \left(\partial_r + \kappa/r\right) B_i^k(r) \end{pmatrix} \qquad \text{for } i \leq n \\ u_i(r) &= \begin{pmatrix} \frac{1}{2m_e c} \left(\partial_r - \kappa/r\right) B_{i-n}^k(r) \\ B_{i-n}^k(r) \end{pmatrix} \quad \text{for } i > n. \end{aligned} \tag{3.22}$$

The variation of the expectation value of the Dirac Hamiltonian $\mathcal{H}^D$ with respect to this expansion yields the eigenvalue equation

$$\frac{1}{2} \left(\langle u_i | \mathcal{H}^D | u_k \rangle + \langle u_k | \mathcal{H}^D | u_i \rangle \right) c_k = E \, \langle u_i | u_k \rangle \, c_k, \tag{3.23}$$

that can be diagonalized algebraically to calculate the expansion coefficients c_k (3.18). These coefficients form the DKB B-spline basis set. Because this basis set is finite, its energy spectrum is discrete. Thus it spans not only the majority of bound eigenfunctions of $\mathcal{H}^D$ but also represents a discretized positive and negative continuum. Therefore it can be entered into Eq. (3.16) to obtain a good approximation of the two-photon transition rate. This approach has already provided very precise results for atoms and ions with only one or two electrons above a closed-shell configuration, as presented e.g. in Refs. [58, 59]. Moreover it has been extended to non-local potentials as in the DHF approach (see Sec. 2.2) to make it applicable for more complex electronic structures [60].

Direct Summation of Many-Electron Amplitudes

For complex many-electron systems represented by atomic state functions (2.26) an approximation of the continuum is not easily obtained. There are some methods for the description of few-electron systems like lithium-like ions [61, 62], but an adaption for larger active spaces has not been established yet.

For photon energies well below the ionization threshold and low-intensity fields, we can assume that bound states only represent a sufficient basis (cf. Sec. 2.3). Thus we use one of the methods shown in Secs. 2.2 - 2.5 to calculate all states in an energy interval $[E_i + \hbar\omega - \Delta E/2, E_i + \hbar\omega + \Delta E/2]$ around the energy of the system after the absorption of one photon. Afterwards we calculate the transition matrix elements $\langle f|\boldsymbol{\alpha} \cdot \boldsymbol{A}(\boldsymbol{r})|k\rangle$ and $\langle k|\boldsymbol{\alpha} \cdot \boldsymbol{A}(\boldsymbol{r})|i\rangle$ for all $|k\rangle$ with E_k in this interval. Plugging these matrix elements into Eq. (3.16) we can reduce the infinite sum and integral to a finite sum over bound atomic states. In the literature, this method is referred to as *direct summation* of transition amplitudes. Within the validity of the approximation $E_i + 2\hbar\omega$ being well below the ionization threshold, this approach has been applied in many studies leading to several well-acknowledged results [36, 63, 64] and has been applied successfully within this thesis as well [RAM5].

4

PROBING THE NUCLEUS

An atom or ion is an inseperable combination of electrons and a positively charged nucleus. However even in contemporal physics we mostly see a strict separation; nuclear physics describes the properties of atomic nuclei and hardly recognizes the electrons surrounding them. Atomic physics, in contrast, is devoted to the dynamics of the electron shell and commonly treats nuclei just as an electrostatic binding potential for the electrons. This is a missed opportunity: The unequaled precision of modern laser spectroscopy allows to extract nuclear properties from atomic spectra [RAM1] [65, 66, 67].

In this chapter, we will discuss various examples of how nuclear properties influence electronic observables with increasing complexity. We will show how precise many-body calculations can be used to tell these effects apart and to derive nuclear moments and radii from spectroscopic measurements. Eventually, we will turn the perspective around and discuss how the electron shell of an atom can be utilized to influence the state of the nucleus.

ISOTOPE SHIFTS

In our derivation of the theories to describe many-electron systems (see Ch. 2), we have assumed that the nucleus of an atom has an infinite mass. For the precision achieved by nowadays experiments, however, this assumption is no longer justified. Accurate measurements reveal slight differences in the energies of atomic levels can be identified between different isotopes, i.e. nuclei with the same nuclear charge Z but a different number of nucleons A. This difference is the so-called isotope shift of atomic levels and is not covered by basic theories describing the nucleus as an infinitely heavy point charge.

Theoretically, we distinguish between two kinds of isotope shifts. The *mass shift* (MS) or kinetic isotope shift arises due to the finite mass of the nucleus, and the *field shift* (FS), also called nuclear volume effect, that originates from the difference between the nuclear potentials $V^{nuc,A}(r)$ of isotopes with different size. Below we will discuss both, the effects of different nuclear sizes and a displacement of the center of mass from the coordinate center on atomic spectra.

Field Shift

In chapter 2 we only required that the potential generated by the nuclear charge is spherically symmetric. For the majority of applications, it is safe to approximate this potential by the Coulomb potential of a point charge. Such a point source is theoretically comfortable to treat and allows to solve the Dirac equation (2.1) analytically, but does only approximate the nucleus in zeroth order. A simple but more realistic description of the nuclear charge distribution is given by a homogeneously charged sphere of radius R and constant charge density ρ:

$$\rho^{nuc}(r, R) = \begin{cases} \rho_0 & \text{for} \quad r < R \\ 0 & \text{for} \quad r \geq R \end{cases}. \tag{4.1}$$

This model is adequate to cover the nature of the field isotope shift. A more natural, smooth model for the nuclear charge is given by the Fermi distribution:

$$\rho^{nuc}(r) = \frac{\rho_0}{1 + \mathrm{e}^{(r-b)/a}}, \tag{4.2}$$

where c is the radius at which $\rho_N(b) = \frac{\rho_0}{2}$ and $a \approx 0.5\,\mathrm{fm}$ is taken from nuclear theory [68]. Both the Fermi distribution and the uniformly charged sphere describe a spherically symmetric nucleus. Although we know that nuclei, especially in their ground state, can be aspherical, the difference between such a spheroid charge distribution and Eqs. (4.1) and (4.2) is marginal and will therefore be neglected in our considerations.

Besides its charge Ze, the size of a nucleus is one of its main characteristics. It is given by the root-mean-square (rms) radius R_{rms} of the nuclear charge distribution, calculated from the radial expectation value:

$$R_{rms} = \langle r^2 \rangle^{\frac{1}{2}} = \left(\frac{\int \rho_N(r) r^2 \mathrm{d}^3\boldsymbol{r}}{\int \rho_N(r) \mathrm{d}^3\boldsymbol{r}} \right)^{\frac{1}{2}}, \tag{4.3}$$

where the denomiator corresponds to the total charge Ze of the nucleus. The rms radius of atomic nuclei is usually obtianed experimentally and then used to fix the free parameters of the nuclear charge models (4.1) and (4.2). If no experimental data is available an empirical approximation for R_{rms} can be used

$$R_{rms} = (0.836 A^{\frac{1}{3}} + 0.570)\mathrm{fm}. \tag{4.4}$$

This approximation is applicable for $A > 9$ and accurate to less than a tenth of a femtometer.

The nuclear charge distributions derived above can be used to discuss the influence of different nuclear sizes on an atomic level. The isotope shift between two isotopes with mass numbers A and A' can be determined within first-order pertubation theory:

$$\begin{aligned}\Delta E_{k,FS}^{AA'} &= -\langle k|V^{nuc,A}(r) - V^{nuc,A'}(r)|k\rangle \\ &= -\int |\langle \boldsymbol{r}|k\rangle|^2 \left(V^{nuc,A}(r) - V^{nuc,A'}(r)\right) \mathrm{d}^3\boldsymbol{r}\end{aligned} \tag{4.5}$$

where $V^{nuc,A}(\boldsymbol{r})$ is the potential of a nucleus with mass number A. It has been shown that the probability density of a state $|k\rangle$ inside the nucleus can be approximated by a spherically symmetric even polynomial [69]:

$$|\langle \boldsymbol{r}|k\rangle|^2 \approx \sum_{n=0}^{3} b_{k,n} r^{2n}. \tag{4.6}$$

The expansion coefficients $b_{k,n}$ represent the $2n$-th derivative of the probability density $|\langle \boldsymbol{r}|k\rangle|^2$ at the origin $r = 0$. Plugging this expansion into Eq. (4.5) we get the following integral

$$\Delta E_{k,FS}^{AA'} = -4\pi \sum_{n=0}^{3} b_{k,n} \int \left[V^{nuc,A}(r) - V^{nuc,A'}(r)\right] r^{2n+2} \mathrm{d}r, \tag{4.7}$$

which, after integrating by parts, becomes:

$$\begin{aligned}\Delta E_{k,FS}^{AA'} &= -4\pi \sum_{n=0}^{3} \frac{b_{k,n}}{(2n+2)(2n+3)} \int r^{2n+4} \nabla^2 \left[V^{nuc,A}(r) - V^{nuc,A'}(r)\right] \mathrm{d}r \\ &= (4\pi)^2 \sum_{n=0}^{3} \frac{b_{k,n}}{(2n+2)(2n+3)} \int r^{2n+4} \left[\rho^{nuc,A}(r) - \rho^{nuc,A'}(r)\right] \mathrm{d}r \\ &= -4\pi Ze \sum_{n=0}^{3} \frac{b_{k,n}}{(2n+2)(2n+3)} \Delta\langle r^{2n+2}\rangle^{AA'}.\end{aligned} \tag{4.8}$$

With the field shift constant $F_{k,n}$ defined by

$$F_{k,n} = 4\pi Ze \frac{b_{k,n}}{(2n+2)(2n+3)} \tag{4.9}$$

we can write down the field isotope shift (4.8) in the compact form

$$\Delta E_{k,FS}^{AA'} = -\sum_{n=0}^{3} F_{k,n} \Delta\langle r^{2n+2}\rangle^{AA'}. \tag{4.10}$$

In most calculations of the field shift only the first term of this expansion, proportional to the mean-square radius difference $\Delta\langle r^2\rangle^{AA'}$ (cf. (4.3)) of the nucleus, is considered. The field shift constant corresponding to this term is $F_{k,0}$. As we can see from Eq. (4.6) this constant is proportional to the electron density at the nucleus $|\langle 0|k\rangle|^2$.

An important property of Eq. (4.10) to be noted is that the empirical, nuclear quantities are separated from the field shift constant that can be obtained theoretically to a very good accuracy. This will later allow us to determine the nuclear radius from isotope shift measurements and to construct quantities that are very robust against the uncertainties of nuclear experiments and theory.

Mass Shift

Although an atomic nucleus is at least three orders of magnitude heavier than the electron shell, the center of mass (cms) of an atom is not at its center. In the theory chapter we were discussing solutions of the Dirac equations obtained in the rest frame of the nucleus assuming that it coincides with the atomic cms. In this frame the kinetic energy of an atom with N electrons and a nucleus with mass M_A reads:

$$T^A(\boldsymbol{p}_N, \boldsymbol{p}_1, \ldots, \boldsymbol{p}_n) = \frac{\boldsymbol{p}_N^2}{2M_A} + \sum_{n=1}^{N} \frac{\boldsymbol{p}_n^2}{2m_e}, \tag{4.11}$$

where $\boldsymbol{p}_N$ is the momentum of the nucleus and $\boldsymbol{p}_n$ the momentum of the n-th electron. Nonrelativistically we can rewrite this kinetic energy in the cms frame using the transformation

$$\begin{aligned} \boldsymbol{R} &= \frac{M_A \boldsymbol{r}_N + m_e \sum_{n=1}^{N} \boldsymbol{r}_n}{M_A + N m_e} \\ \boldsymbol{\rho} &= \boldsymbol{r}_N - \boldsymbol{r}_n, \end{aligned} \tag{4.12}$$

where $\boldsymbol{R}$ is the center of mass and $\boldsymbol{\rho}_n$ the coordinate of the n-th electron with respect to the nucleus. In these coordinates the kinetic energy of the atom with reduced mass $\mu = \frac{m_e M_A}{m_e + M_A}$ reads

$$T^A(\boldsymbol{P}, \boldsymbol{\pi}_1, \ldots, \boldsymbol{\pi}_n) = \frac{1}{2\mu} \sum_{n=1}^{N} \boldsymbol{\pi}_n^2 + \frac{1}{M_A} \sum_{n<k} \boldsymbol{\pi}_n \cdot \boldsymbol{\pi}_k + \frac{\boldsymbol{P}^2}{2(M_A + N m_e)}, \tag{4.13}$$

where $\boldsymbol{\pi}_n$ is the conjugated momentum to $\boldsymbol{\rho}_n$ and $\boldsymbol{P}$ is the momentum of the center of mass motion, i.e. the atom as a whole. In the cms rest frame, where $\boldsymbol{P} = 0$ this reduces to

$$T^A(0, \boldsymbol{\pi}_1, \ldots, \boldsymbol{\pi}_n) = \frac{1}{2m_e} \sum_{n=1}^{N} \boldsymbol{\pi}_n^2 + \frac{1}{2M_A} \sum_{n=1}^{N} \boldsymbol{\pi}_n^2 + \frac{1}{M_A} \sum_{n<k} \boldsymbol{\pi}_n \cdot \boldsymbol{\pi}_k, \tag{4.14}$$

The first term of this equation is the well known kinetic energy of all electrons. The second and third term are the nonrelativistic corrections due to the finite mass of the nucleus. We distinguish both of these terms by their nature. The normal mass shift (NMS)

$$T^A_{NMS}(\boldsymbol{\pi}_1, \ldots, \boldsymbol{\pi}_n) = \frac{1}{2M_A} \sum_{n=1}^{N} \boldsymbol{\pi}_n^2, \tag{4.15}$$

occurs due to the reduced mass of the electron and can already be observed in hydrogen-like systems. The specific mass shift (SMS)

$$T^A_{SMS}(\boldsymbol{\pi}_1, \ldots, \boldsymbol{\pi}_n) = \frac{1}{M_A} \sum_{n<k} \boldsymbol{\pi}_n \cdot \boldsymbol{\pi}_k \tag{4.16}$$

has its origin in the polarization of the electron shell. Therefore a specific mass shift can only be observed in many electron systems. The total mass isotope shift of a level $|k\rangle$ between two isotopes A and A' is then:

$$\begin{aligned} \Delta E^{AA'}_{k,MS} &= \langle k|T^A_{NMS} - T^{A'}_{NMS}|k\rangle + \langle k|T^A_{SMS} - T^{A'}_{SMS}|k\rangle \\ &= \frac{M_A - M_{A'}}{M_A M_{A'}} K_k. \end{aligned} \tag{4.17}$$

Similar to Eq. (4.10) the mass shift separates into a prefactor depending on the properties of the nucleus and the mass shift constant K_k that depends solely on the electronic structure of the atom. Therefore accurate many-electron theories are of major importance for isotope shift studies, in particular because the specific and normal mass shift are of the same order.

Up to now we have only discussed the nonrelativistic contributions to the mass shift. The mass shift, however, can be also derived in a strictly relativistic framework. Especially in heavy systems, where the electron motion is strongly governed by relativistic effects, a nonrelativistic treatment of the mass shift is not sufficient. Going through the derivations of the relativistic mass shift is beyond the scope of this thesis and, therefore, we only give the results of these calculations here up to the order $(v/c)^2$ and m_e/M_A [70, 71, 72]:

$$\begin{aligned} &T^A_{NMS}(\boldsymbol{\pi}_1, \ldots, \boldsymbol{\pi}_n; \boldsymbol{\rho}_1, \ldots, \boldsymbol{\rho}_n) = \\ &\qquad \frac{1}{2M_A} \sum_{n=1}^{N} \boldsymbol{\pi}_n^2 - \frac{Ze^2}{4\pi\varepsilon_0 m_e c^2} \frac{1}{\rho_n} \left[\boldsymbol{\alpha}_i + \frac{(\boldsymbol{\alpha}_i \cdot \boldsymbol{\rho}_n)\boldsymbol{\rho}_n}{\rho_n^2} \right] \cdot \boldsymbol{\pi}_n, \end{aligned} \tag{4.18a}$$

$$\begin{aligned} &T^A_{SMS}(\boldsymbol{\pi}_1, \ldots, \boldsymbol{\pi}_n; \boldsymbol{\rho}_1, \ldots, \boldsymbol{\rho}_n) = \\ &\qquad \frac{1}{M_A} \sum_{n<k} \boldsymbol{\pi}_n \cdot \boldsymbol{\pi}_k - \frac{Ze^2}{4\pi\varepsilon_0 m_e c^2} \frac{1}{\rho_n} \left[\boldsymbol{\alpha}_i + \frac{(\boldsymbol{\alpha}_i \cdot \boldsymbol{\rho}_n)\boldsymbol{\rho}_n}{\rho_n^2} \right] \cdot \boldsymbol{\pi}_k. \end{aligned} \tag{4.18b}$$

Table 4.1: Calculation of the nuclear charge radii difference between the thorium isomers with mass number $A = 229$ and $A = 232$ using theoretical values for the mass shift (MS), the field shift constant $F_{fi,0}$ and the experimentally obtianed net isotope shift from Refs. [73, 14]. The investigated levels are denoted by $a : 5f6d(J = 4) : 0\,\mathrm{cm}^{-1}$, $b : 6d^2(J = 2) : 63\,\mathrm{cm}^{-1}$, $c : 5f^2(J = 4) : 15\,148\,\mathrm{cm}^{-1}$, $d : 5f6d(J = 1) : 20\,711\,\mathrm{cm}^{-1}$, $e : 5f^2(J = 4) : 21\,784\,\mathrm{cm}^{-1}$ and $f : 5f^2(J = 0) : 29\,300\,\mathrm{cm}^{-1}$. Our results are compared to calculations by Safronova *et al.* [14]

transition	$\Delta E^{232,229}_{fi,MS}$	$F_{fi,0}$	$\Delta E^{232,229}_{exp.}$	$\delta\langle r^2\rangle^{232,229}$	$\delta\langle r^2\rangle^{232,229}$ [14]
	GHz	GHz/fm^2	GHz	fm^2	fm^2
$a \to c$	−0.296(17)	−29(6)	6.8(2)[14]	0.24(5)	0.335(43)
$a \to e$	−0.282(13)	−23(6)	5.2(2)[14]	0.24(6)	0.332(54)
$b \to d$	−0.357(20)	−47(2)	8.2(2)[73]	0.18(2)	0.315(32)
$d \to f$	−0.294(38)	−27(10)	6.2(3)[73]	0.24(30)	0.312(42)

In all calculations presented in this thesis we used the relativistic operators above to calculate the mass shift constant K_k. Those operators now do not only depend on the momenta of the electrons but also on their positions relative to the nucleus. This makes the integration of the corresponding matrix elements numerically more challenging, however relativistic effects cannot be neglected in high precision calculations.

Isotope Shift Calculations for the Extraction of Nuclear Properties

Combining the results of the previous sections we can write down the total isotope shift of one level $|k\rangle$ between an isotope with mass number A and a reference isotope A_0:

$$\Delta E_k^{A_0 A} = \Delta E_{k,MS}^{A_0 A} + \Delta E_{k,FS}^{A_0 A} \tag{4.19}$$

or explicitely

$$\Delta E_k^{A_0 A} = \frac{M_A - M_{A_0}}{M_A M_{A_0}} K_k - F_{k,0}\delta\langle r^2\rangle^{A_0 A}, \tag{4.20}$$

where we omitted higher order contributions to the field shift (cf. (4.10)). The energy of a single level, however, cannot be measured experimentally. Instead the energy

difference between two levels is observed as a spectral line. This difference is subject to an isotope shift as well, which for a transition from $|i\rangle$ to $|f\rangle$ reads:

$$\begin{aligned}\Delta E_{fi}^{A_0 A} &= \Delta E_f^{A_0 A} - \Delta E_i^{A_0 A} \\ &= \frac{M_A - M_{A_0}}{M_A M_{A_0}} K_{fi} - F_{fi,0} \delta\langle r^2\rangle^{A_0 A},\end{aligned} \tag{4.21}$$

where $K_{fi} = K_f - K_i$ and $F_{fi,0} = F_{f,0} - F_{i,0}$. As we can see from this equation, it is possible to extract the difference of the nuclear radius between isotopes A and A_0 from a measurement of $\Delta E_{fi}^{A_0 A}$. For this purpose the electronic structure of the atom in question has to be known precisely, in order to accurately determine the mass- and field shift constants. In such a calculation the specific mass shift is the largest source of uncertainty, and is therefore sometimes even omitted completely [74, 75, 76].

Of particular interest for this thesis are the charge radii of nuclear isomers, which are excited states of nuclei having the same mass but possibly different R_{rms}. As motivated in Sec. 1 we are especially interested in the isomer ^{229m}Th. The reason for the special properties of the ^{229}Th nucleus and the low energy of its first excited state are still under debate [12, 77, 13]. Therefore it is of major importance to investigate the properties of this nucleus with increasing precision. In a recent experiment, the isotope shift of four transitions in doubly charged thorium has been measured. The measurements have been performed for $^{229}\mathrm{Th}^{2+}$ and the reference isotope $^{232}\mathrm{Th}^{2+}$ [73, 14]. Moreover these measurements included the isomeric shift $\Delta E_{fi}^{229,229m}$. The ratio between this shift and the isotope shift has been obtained to $\Delta E_{fi}^{229m,229} / \Delta E_{fi}^{232,229} = 0.035(4)$. Using this ratio and precise CI-MBPT (see Sec. 2.5) calculations Safronova *et al.* were able to extract not only values for the difference between mean square radii $\delta\langle r^2\rangle^{232,229} = 0.299\,\mathrm{fm}^2$ but also $\delta\langle r^2\rangle^{229m,229} = 0.0105(13)\,\mathrm{fm}^2$. To complement their calculations, we have performed an analogue investigation using Multi-Configurational Dirac-Fock theory (cf. Sec. 2.4). As seen in table 4.1 our values for the radius change $\delta\langle r^2\rangle^{232,229}$ are always smaller than the ones obtained by Safronova *et al.* , but still agree within 1σ of the estimated accuracy, except for the transition $b \to d$. From our results shown in the table we can estimate the difference between the mean square radius of ^{229}Th and ^{229m}Th to $\delta\langle r^2\rangle^{229m,229} = 0.008(1)\,\mathrm{fm}^2$, which also agrees well with the value of $\delta\langle r^2\rangle^{229m,229} = 0.0105(13)\,\mathrm{fm}^2$ presented in Ref. [14]. Unfortunately, these values still do not allow to conclude what are the physics behind the unique nuclear structure of ^{229}Th as we will discuss in more detail in Sec. 4.2. Therefore experiments on $^{229}\mathrm{Th}^{3+}$ would be beneficial, because much more precise theoretical results can be obtained for this essentially hydrogen-like system.

King Plot Nonlinearities

While we can theoretically separate the different contributions to the isotope shift, in an experiment only the total isotope shift is measured. With a series of measurements, however, it is possible to extract certain effects from experimental data using a so-called King plot [15]. To create such a plot the isotope shift $\Delta E_{fi}^{A_0 A}$ of two transitions $|i_1\rangle - |f_1\rangle$ and $|i_2\rangle - |f_2\rangle$ is measured for a series of isotopes A with respect to a reference isotope A_0. From those two datasets we can take the ratio $\Delta E_{f_2 i_2}^{A_0 A} / \Delta E_{f_1 i_1}^{A_0 A}$ and, after some algebra, obtain

$$\frac{M_A M_{A_0}}{M_A - M_{A_0}} \Delta E_{f_1 i_1}^{A_0 A} = \frac{F_{f_1 i_1,0}}{F_{f_2 i_2,0}} \frac{M_A M_{A_0}}{M_A - M_{A_0}} \Delta E_{f_2 i_2,0}^{A_0 A} + K_{f_1 i_1} - \frac{F_{f_1 i_1,0}}{F_{f_2 i_2,0}} K_{f_2 i_2}. \quad (4.22)$$

By introducing the modified isotope shifts $\Delta \widetilde{E}_{fi}^{A_0 A} = \frac{M_A M_{A_0}}{M_A - M_{A_0}} \Delta E_{fi}^{A_0 A}$ this simplifies to the linear equation

$$\Delta \widetilde{E}_{f_1 i_1}^{A_0 A} = \frac{F_{f_1 i_1,0}}{F_{f_2 i_2,0}} \Delta \widetilde{E}_{f_2 i_2}^{A_0 A} + K_{f_1 i_1} - \frac{F_{f_1 i_1,0}}{F_{f_2 i_2,0}} K_{f_2 i_2}, \quad (4.23)$$

which describes the graph drawn in a King plot. An example of such a plot is shown in Fig. 4.1. As seen in the figure, Eq. (4.23) describes a line with its slope given by the ratio of field shift constants $f = F_{f_2 i_2,0} / F_{f_1 i_1,0}$. The y-intercept of the curve depends on both, this ratio and the mass shift parameters of both transitions.

It is important to note that in Eq. (4.23) all dependencies on nuclear parameters other than the mass have been cancelled out. Therefore the King plot only depends on the electron dynamics of the atom and thus is a very stable and sensitive tool for benchmarking many-electron theories and the search for New Physics [78] [RAM1]. Of special interest are King plots for transitions that are degenerated in a non-relativistic framework, e.g. $1s_{1/2} \rightarrow 2p_{1/2}$ and $1s_{1/2} \rightarrow 2p_{3/2}$. For such a system the slope of the King plot differs from one solely due to relativistic effects. Such a study has been performed for the Ca^+ ion. This ion has a ground state configuration of $[\mathrm{Ar}].4s\,^2S_{1/2}$ and the isotope shift has been measured for the transitions $D1 = [\mathrm{Ar}].4s\,^2S_{1/2} \rightarrow [\mathrm{Ar}].4p\,^2P_{1/2}$ and $D2 = [\mathrm{Ar}].4s\,^2S_{1/2} \rightarrow [\mathrm{Ar}].4p\,^2P_{3/2}$ [78]. In this work Shi *et al.* found a slope of the King plot that is much larger than theoretically predicted. Indeed it even exceeded estimations by a purely hydrogenic model which is believed to yield an upper threshold for $F_{D2,0} / F_{D1,0}$.

To get a better hold on the possible reasons for the difference between the theoretical slope of the King plot for Ca^+ and the experimental results in Ref. [78], we performed a study on the Ba^+ ion [RAM1]. The electronic structure of singly charged barium is very similar to Ca^+ with one $6s$ electron above a closed xenon configuration and, therefore, Ba^+ serves as a good comparison to better understand the isotope

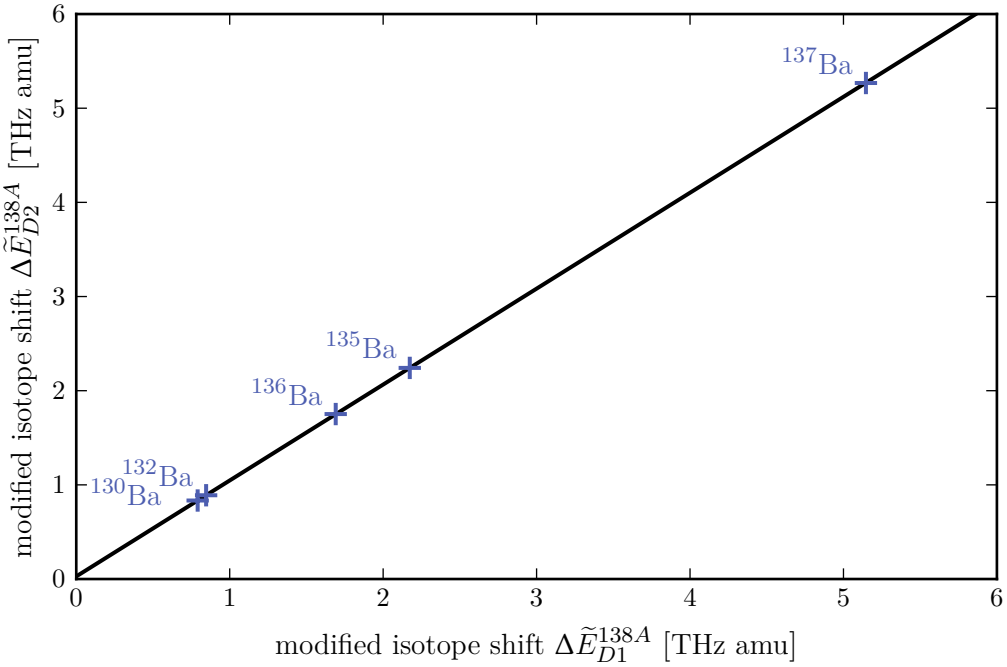

Figure 4.1: King plot for two transitions in Ba^+ shown for five isotopes with ^{138}Ba as the reference. The transitions are $D1 = [\mathrm{Xe}].6s\,^2S_{1/2} \rightarrow [\mathrm{Xe}].6p\,^2P_{1/2}$ and $D2 = [\mathrm{Xe}].6s\,^2S_{1/2} \rightarrow [\mathrm{Xe}].6p\,^2P_{3/2}$. The black line shows the linear fit of experimental data represented by the blue crosses. The data is taken from [RAM1].

shift in singly charged earth alkali metals. For the King plot we chose the same transitions $D1 = [\mathrm{Xe}].6s\,^2S_{1/2} \rightarrow [\mathrm{Xe}].6p\,^2P_{1/2}$ and $D2 = [\mathrm{Xe}].6s\,^2S_{1/2} \rightarrow [\mathrm{Xe}].6p\,^2P_{3/2}$ as in [78] and analyzed them with surpassing accuracy. We extracted the ratio of field shift constants $f_{exp} = \frac{F_{D2,0}}{F_{D1,0}} = 1.0186(9)$ from the King plot shown in Fig. 4.1 and compared it to theoretical results using increasingly detailed models. The results of these calculations are displayed in Tab. 4.2. There we see that the hydrogenic model overestimates f as expected and we achieve an excellent agreement with the experimental field shift ratio. The numerical uncertainty of the final theoretical result $f_{theo.} = 1.0206(3)_{\mathrm{num}}(4)_{\mathrm{sys}}$ has been estimated using the convergence analysis scheme described in section 2.3. The systematic uncertainty is given by possible contributions from the Breit interaction, vacuum polarization and self-energy, that have not been taken into account in the MCDF computations. For more details on this analysis, we refer the reader to our publication [RAM1].

The excellent agreement of our results with the experimental King plot presented in Ref. [RAM1] allows us to narrow down possible reasons for the disagreement between experiment and theory in the calcium case [78]. Since barium has a higher

Table 4.2: Results for the field shift ratio $f = F_{D2,0}/F_{D1,0}$ for the transitions $D1 =$ [Xe].$6s\,^2S_{1/2} \rightarrow$ [Xe].$6p\,^2P_{1/2}$ and $D2 =$ [Xe].$6s\,^2S_{1/2} \rightarrow$ [Xe].$6p\,^2P_{3/2}$ in Ba^+. We compare the hydrogenic model, DHF and MCDF calculations to the experimental result (see also Ref. [RAM1]).

Model	hydrogenic	DHF	MCDF	experimental
f	1.04231	1.0201	$1.0206(3)_{num}(4)_{sys}$	1.0186(9)

nuclear charge than calcium, Breit and QED effects are enhanced. However, we found that they do not give a considerable contribution to the field shift ratio of the investigated transitions in Ba^+. Therefore we can exclude them as possible reasons for the discrepancy in the calcium experiment. Many-electron correlations, in contrast, are weaker in heavier systems. This leaves us with two possible solutions for the calcium puzzle. One being that the many-electron dynamics have not been completely under control, which might be indicated by the disagreement of the different theories amongst each other. This, however, still leaves the question of why the hydrogenic model fails to serve as an upper boundary for f. The other option is that there has been an overseen systematic shift of the measurements. By reproducing the experiment using a different method and comparing the results will help to narrow down those possible systematics and, eventually, may lead to a better understanding of the physics involved which is highly desirable for both theory and experiment.

As seen from Eq. (4.23), a King plot is strictly linear. This is, however, only true within the approximations applied to derive Eq. (4.23) (cf. Sec. 4.1). Higher order contributions to both the field and the mass shift lead to nonlinearities of the King plot. In systems, where these effects are small, the linearity of a King plot can be used as a probe for New Physics that modifies the coupling between light and fermions. Recently a number of proposals have been made, how the methods benchmarked by works like ours, can be used to derive upper boundaries on the properties of new particles [16, 17]. Until now, however, the experimental and theoretical accuracy necessary to be sensitive to those particles is not reached, yet. Moreover the already known sources for King plot nonlinearities remain to be seen experimentally. Therefore a steady process in benchmark studies involving well known systems like e.g. Ca, Ba or other alkali metals is inevitable to draw strong conclusions from possible nonlinearities in a King plot.

HYPERFINE STRUCTURE

In the previous section we have discussed energy shifts of atomic levels caused by the finite nuclear mass and volume. These shifts were derived, assuming that the electron interacts with a finite-mass nucleus, described by a spherically symmetric charge distribution. Nuclei, however, can be non-spherical and may also have a spin, resulting in an additional magnetostatic field. Therefore we have to consider the full potential of the nuclear electromagnetic field:

$$V^{nuc}(\boldsymbol{r}) = e\phi(\boldsymbol{r}) - ec\hat{\boldsymbol{\alpha}} \cdot \boldsymbol{A}(\boldsymbol{r}) \tag{4.24}$$

If we expand both, the scalar and vector potential into multipoles, we can treat all terms except for the spherically symmetric $V^{nuc}(r)$ as a perturbation. This perturbation can be factorized in terms of irreducible tensors

$$\mathcal{H}^{HFS} = \sum_{k=1}^{\infty} \sum_{q=-1}^{1} T_q^{(k)} M_q^{(k)}, \tag{4.25}$$

where the operator $T_q^{(k)}$ acts solely on the electronic and $M_q^{(k)}$ on the nuclear degrees of freedom [43]. Explicitly the first orders of the multipole expansion yield:

$$\begin{aligned} M_q^{(1)} &= \mu_q \quad \text{nuclear magnetic dipole operator,} \\ M_q^{(2)} &= Q_q \quad \text{nuclear electric quadrupole operator.} \end{aligned} \tag{4.26}$$

The expectation values of μ_0 and Q_0 with respect to a nuclear state $|IM_I\rangle$ with $M_I = I$ correspond to the nuclear magnetic dipole and electric quadrupole moments μ and Q [49]. Similarly we can obtain the operators acting on the electron wave function:

$$\begin{aligned} T_q^{(1)} &= -\frac{e}{4\pi\varepsilon_0}(-1)^q \frac{[\boldsymbol{r} \times \boldsymbol{\alpha}]_q}{cr^3}, \\ T_q^{(2)} &= -\frac{e}{4\pi\varepsilon_0} \frac{C_{2q}(\boldsymbol{r}/r)}{r^3}, \end{aligned} \tag{4.27}$$

where C_{2q} are the second order normalized spherical harmonics (2.15). With the explicit expressions for the higher multipoles of the nuclear electromagnetic field we can use first order pertubation theory to obtain the corresponding corrections to the energies of atomic levels. We perform the perturbative calculations with respect to eigenstates $|FM_F\rangle$ of the total angular momentum of the atom $\boldsymbol{F}^2 = (\boldsymbol{J} + \boldsymbol{I})^2$. These states are obtained by coupling eigenstates of the nuclear total angular momentum $|IM_I\rangle$ and the total angular momentum of the electron shell $|J\mu_J\rangle$:

$$|FM_F\rangle = \sum_{\mu_J M_I} (J\mu_J I M_I | FM_F) \, |J\mu_J\rangle \, |IM_I\rangle \,, \tag{4.28}$$

With respect to these states the first order energy correction caused by the Hamiltonian (4.24) is

$$\begin{aligned} E^{(M1)} &= \sum_{q=-1}^{q} \langle FM_F|T_q^{(1)}\mu_q|FM_F\rangle \\ E^{(E2)} &= \sum_{q=-1}^{q} \langle FM_F|T_q^{(2)}Q_q|FM_F\rangle\,. \end{aligned} \tag{4.29}$$

Using the Wigner-Eckardt theorem we can split those equations into products of electronic matrix elements and properties of the nucleus:

$$\begin{aligned} E^{(M1)} &= \frac{1}{2}AC \\ E^{(E2)} &= B\frac{\frac{3}{4}C(C+1) - I(I+1)J(J+1)}{2I(2I-1)J(2J-1)}, \end{aligned} \tag{4.30}$$

where $C = F(F+1) - J(J+1) - I(I+1)$ is a angular momentum dependent prefactor and A and B are the so called magnetic dipole and electric quadrupole hyperfine constants, respectively. These constants are proportional to the nuclear magnetic dipole and electric quadrupole moment

$$\begin{aligned} A &= \frac{\mu}{I}\left[J(J+1)(2J+1)\right]^{-\frac{1}{2}}\langle\alpha J||T^{(1)}||\alpha J\rangle \\ B &= 2Q\left[\frac{J(2J-1)}{(J+1)(2J+1)(2J+3)}\right]^{\frac{1}{2}}\langle\alpha J||T^{(2)}||\alpha J\rangle\,, \end{aligned} \tag{4.31}$$

where $\langle\alpha J||T^{(k)}||\alpha J\rangle$ is the reduced matrix element of the operator $T^{(k)}$. We see from Eq. (4.30) that the perturbation not only shifts the energy levels of the atom but also splits them, depending on the value of the total angular momentum F. This is the so called *hyperfine splitting* of atomic levels.

As we have motivated above, we can observe a splitting of spectral lines that depends on the properties of both the electron shell and the nucleus. Therefore hyperfine spectroscopy can be used as a tool to infer the spin and the multipole moments of the nucleus. While the first is straightforwardly obtained by counting the number of lines an atomic level splits into, the latter is usually achieved by combining results from experiment and theory. For this purpose, we recall from Eq. (4.31) that A and B depend on both, the nuclear moments and the electronic structure of the atom. The latter can be calculated very precisely using modern codes and methods, as e.g. outlined in Secs. 2.3-2.4. The results of these calculations, the reduced matrix elements $\langle\alpha J||T^{(k)}||\alpha J\rangle$ in particular, only weakly depend on nuclear properties via the nuclear mass and charge radius. Therefore we can consider them as *ab initio*

Table 4.3: Magnetic dipole and electric quadrupole hyperfine constants of two states (a):[Rn].$6d^2$ at $63\,\mathrm{cm}^{-1}$ and (b) [Rn].$5f6d$ at $20\,711\,\mathrm{cm}^{-1}$ in $^{229}\mathrm{Th}^{2+}$. Our results using both the MCDF and CI-MBPT method are compared to experimental values. For the calculation of the A and B constants we used $\mu = 0.36\mu_N$ and $Q = 3.11\,\mathrm{eb}$ [18] (see also [RAM2]).

level	A[MHz]			B[MHz]		
	MCDF	CI-MBPT	exp. [73]	MCDF	CI-MBPT	exp. [73]
(a)	162(8)	143(47)	151(8)	71(7)	68(23)	73(27)
(b)	90(4)	109(36)	88(5)	689(110)	839(220)	901(18)

atomic physics results that allow us to obtain the electronic parts A/μ and B/Q of the hyperfine constants. Dividing the measured values of the hyperfine constants by these electronic parts it is possible to derive very precise values for μ and Q.

In this thesis, we are especially interested in the properties of ^{229}Th and the ^{229m}Th isomer to gain a better understanding for the mechanisms that lead to the emergence of the low lying isomeric state at 8.28 eV. In a first advance, Campbell *et al.* recorded the hyperfine split spectrum of the electronic ground and first excited state of $^{229}\mathrm{Th}^{3+}$ confined to a linear Paul trap [79]. By fitting the second-order model (4.30) to their recorded spectra, the authors obtained the hyperfine constants A and B of these states. In combination with calculations by Safronova *et al.* it was possible to calculate the widely accepted values of $\mu = 0.360(7)\mu_N$ and $Q = 3.11(6)\,\mathrm{eb}$ for the nuclear magnetic dipole and electric quadrupole moments of ^{229}Th [18].

Recently Thielking *et al.* recorded hyperfine spectra of two transitions in doubly charged thorium [73]. The exciting novelty in their experiment was that they recorded these spectra not only for the nucleus being in the ground but also in the first excited, isomeric state. From these spectra, again, the A and B constants of two states in $^{229}\mathrm{Th}^{2+}$ as well as A_m and B_m of the same states in $^{229m}\mathrm{Th}^{2+}$ could be extracted. With the ratios $A/A_m = \mu/\mu_m$ and $B/B_m = Q/Q_m$ and the results of Safronova *et al.* , values for the nuclear magnetic dipole moment μ_m and electric quadrupole moment Q_m of the nuclear isomer ^{229m}Th have been found [73]. In particular, the value for μ_m appeared to disagree strongly with previous theoretical estimates [80, 81] by almost an order of magnitude. Possible reasons for this discrepancy had to be either errors in the experiment by Thielking *et al.* [73], the derivation of the value for μ by Safronova *et al.* [18] and Campbell *et al.* [79] or, more likely, theoretical inaccuracies in the nuclear models used in Refs. [80, 81].

The findings of Thielking *et al.* , however, relied on the previous calculation of the magnetic moment of the ground state nucleus. Therefore we carried out an in-

Table 4.4: Electronic parts of the magnetic dipole and electric quadrupole hyperfine constants of two states (a):[Rn].$6d^2$ at $63\,\mathrm{cm}^{-1}$ and (b) [Rn].$5f6d$ at $20\,711\,\mathrm{cm}^{-1}$ in $^{229m}\mathrm{Th}^{2+}$. Together with the measured values of A_m and B_m we display the derived magnetic dipole and electric quadrupole constant of the ^{229m}Th isomer (see also [RAM2]).

energy level	A/μ_m [MHz/μ_N]		A [MHz]	μ_m [μ_N]	
	MCDF	CI-MBPT	exp. [73]	MCDF	CI-MBPT
(a)	749	660	−263(29)	−0.35	−0.40
(b)	419	506	−151(22)	−0.36	−0.30

dependent and to the best of our knowledge first theoretical study of the hyperfine structure of $^{229}\mathrm{Th}^{2+}$ and $^{229m}\mathrm{Th}^{2+}$ [RAM2]. The main results of this study were obtained using the MCDF method and verified by a set of CI-MBPT calculations. The first part of our investigation of the thorium hyperfine structure was the calculation of hyperfine constants (4.31) using $\mu = 0.36\mu_N$ and $Q = 3.11\,\mathrm{eb}$ and compare them to the experimental values. This comparison is shown in Tab. 4.3. We see in the table that our results obtained using the MCDF method agree perfectly with the experimental values, except for the electric quadrupole constant B of the state [Rn].$5f6d(J = 1^-)$ at $20\,711\,\mathrm{cm}^{-1}$. Generally our values obtained using CI and MBPT suffer from a larger uncertainty, however they additionally ensure that we converged to proper results in our MCDF calculations.

The comparison of our calculations with the measured values of the hyperfine constants A and B of $^{229}\mathrm{Th}^{2+}$ wer performed to ensure the validity of our numerical method. In a second step we used this method to calculate the reduced matrix elements of the hyperfine operators $T^{(1)}$ and $T^{(2)}$. We used those to calculate the electronic part of A and B [18][RAM2]. As discussed above, these can be used together with experimentally obtained hyperfine constants to precisely derive the magnetic dipole and electric quadrupole moment of a nucleus. We performed this derivation for the nuclear magnetic dipole moment of the $^{229m}\mathrm{Th}^{2+}$ isomer. As seen in Tab. 4.4 our results yield an average value for $\mu_m = -0.35\mu_N$. This value agrees very well with the $-0.37(6)\mu_N$ that has been obtained using the results of Safronova *et al.* [18]. Therefore our calculations provide not only the first independent derivation of the nuclear moments of ^{229m}Th that that does not rely on Ref. [18] but also gives further evidence that the calculated value of $\mu_m = -0.076\mu_N$ [80, 81] has been obtained under assumptions that do not reflect the nuclear structur of the thorium nucleus with mass number $A = 229$.

In an attempt to resolve the discrepancy between theoretical and experimental values for the magnetic dipole moment μ_m of the ^{229m}Th nuclear isomer Minkov and Pálffy recently proposed a new nuclear model that predicts μ_m very well [82]. Regrettably, their method cannot reproduce the ground state properties of ^{229}Th up to a similar accuracy. Therefore the quest for a precise description of the thorium nucleus with mass number $A = 229$ is continuing. A better understanding of its structure, however, would be very important to conclusively determine how sensitive the nuclear transition from ^{229}Th to ^{229m}Th is with respect to changes of the fine structure constant. It has been estimated that this transition might be orders of magnitude more sensitive to α-variations than any atomic clock system known until now [12, 13]. This estimation, however, relies on the fact that the low energy of the isomeric state is caused by a cancellation of two independent effects: An excitation of the unpaired nucleon combined with a simultaneous change of the Coulomb energy of the nucleus. Both of these effects usually cause energy changes in the keV region, and only if they cancel their difference can be as small as the 8.28 eV energy of the isomeric state.

The sensitivity of the transition from the nuclear ground to its first excited state in thorium to variations of the fine structure constant α can be calculated using a simple model put forward by Berengut *et al.* [13] and V. V. Flambaum [12]. The free parameters of this model are the nuclear charge radius difference $\delta\langle r^2\rangle^{229m,229}$ and the ratio of the nuclear quadrupole moments Q/Q_m of ^{229}Th and ^{229m}Th, respectively. Both of these quantities have been obtained in either this or the previous section of the present thesis (see also [14] and [RAM2]). To date, the theoretical and experimental accuracy up to which we are able to determine $\delta\langle r^2\rangle^{229m,229}$ and Q/Q_m limits the significance of the conclusions drawn from the Berengut model [13]. While the sensitivity of the transition from ^{229}Th to ^{229m}Th to α-variations is most probably about three to four orders of magnitude higher than in atomic transitions, it cannot be excluded that the nuclear transition in thorium is not sensitive to such variations at all. The latter has been suspected by Hayes *et al.* [77], who also critiqued Ref. [13] based on their nuclear calculations. Therefore both, the sensitivity of the nuclear transition to the variation of α as well as the excitation mechanism forming ^{229m}Th are still an open question.

COMBINED NUCLEAR AND ELECTRONIC TRANSITIONS

After our discussion of several methods how we can use atomic physics to investigate the properties of atomic nuclei, we will turn our perspective around. The low energy of the isomer ^{229m}Th relative to the ground state, for which we discussed possible

reasons in the previous sections, opens up opportunities for several new technologies. In particular the construction of a clock based on the ^{229}Th$\rightarrow^{229m}$Th transition has been investigated thoroughly in the recent decade [22, 25, 26, 24]. For this purpose, however, it is necessary to drive this transition as a frequency reference. The width of the transition is very small, depending on the charge state ranging from $\Delta E/E = 10^{-20}$ to $\Delta E/E = 10^{-11}$[83]. Since the energy of the transition is known only up to 0.17 eV, direct laser excitation of the transition using laser scanning would take impractical amounts of time [20]. Until this uncertainty is significantly reduced, other methods need to be employed to prepare thorium nuclei in the ^{229m}Th isomeric state. Up to now most experiments with samples that contained the nuclear isomer have been performed using a ^{233}U sample that naturally decays via α-decay to the ^{229m}Th isomer with a branching ratio of about 2 % [84, 85]. Here we want to discuss alternative processes for the excitation of the nuclear isomeric state at 8.28 eV which involve the electron shell.

Electron Bridge

There are several misunderstandings and ambiguities regarding the naming of possible excitation mechanisms for the preparation of the ^{229m}Th via processes in the electron shell. For the sake of clarity, we will refer to all of these by *electron bridge processes* throughout this thesis and in the publications that are part of it. For further specification, we will use Feynman diagrams or pictorial sketches.

Let us first discuss the most simple case of how the electron shell can be used to excite its nucleus. This mechanism, shown in Fig. 4.2, resembles the core of every more elaborate electron bridge process. Initially, the electron shell is prepared in an excited state $|i\rangle$ and the nucleus is in its ground state $|G\rangle$. After the exchange of a virtual photon, the nucleus is excited to the isomeric state $|IS\rangle$ and the electron shell relaxes to some final state $|f\rangle$ that has a lower energy than $|i\rangle$. This process is very similar to the time-inverse of internal conversion, except that both the initial and final electron states are bound. The corresponding matrix element can be found by applying Feynman rules [41]:

$$M_{f,IS\leftarrow i,G} = -\mathrm{i}\int_{-\infty}^{\infty} \langle f, IS|\gamma^\mu\gamma^\nu D^F_{\mu\nu}|i, G\rangle \,\mathrm{d}t, \tag{4.32}$$

where γ^μ are the Dirac matrices defined by $\gamma^\mu\gamma^\nu + \gamma^\nu\gamma^\mu = 2\eta^{\mu\nu}\mathbb{1}$ with the Minkowski metric $\eta = \mathrm{diag}(-1, 1, 1, 1)$. Moreover, we have introduced the photon propagator $D^F_{\mu\nu}$ in Feynman gauge.

In order to perform the time integration in the matrix element (4.32) of the simple electron bridge process shown in Fig. 4.2, we assume that the width of the nuclear

Figure 4.2: Feynman diagram of a simple electron bridge process. The electron shell is prepared in an excited state $|i\rangle$ and decays to the final state $|f\rangle$ by emitting a virtual photon that excites the nucleus from its ground state $|G\rangle$ to the excited, isomeric state $|IS\rangle$.

isomeric state is negligibly small and the widths of the atomic levels are given by Γ_i and Γ_f, respectively. With these assumptions we find:

$$M_{f,IS\leftarrow i,G} = -\frac{\mathrm{i}}{\varepsilon_0} \frac{\Gamma_i + \Gamma_f}{(\epsilon_f - \epsilon_i - \hbar\omega_N)^2 + \frac{(\Gamma_i+\Gamma_f)^2}{4}} \left\langle f, IS \left| \frac{\mathrm{e}^{\mathrm{i}\omega_N |\boldsymbol{r}-\boldsymbol{R}|/c}}{|\boldsymbol{r}-\boldsymbol{R}|} \right| i, G \right\rangle, \quad (4.33)$$

where $\boldsymbol{r}$ and $\boldsymbol{R}$ are the coordinades of the electron and the nucleus, respectively and $\epsilon_{i/f}$ denotes the energies of the initial and final electronic state. Moreover we have introduced the frequency of the nuclear transition $\hbar\omega_N = \epsilon_{IS} - \epsilon_G$.

The prefactor of the matrix element in Eq. (4.33) is a Lorentz function. In the limit of vanishing widths of the electronic levels it reduces to a delta function $\delta(\epsilon_f - \epsilon_i - \hbar\omega_N)$. Therefore the process described by the Feynman diagram 4.2 is strongly suppressed if the splitting between the electronic states $\epsilon_f - \epsilon_i$ is not close to the energy of the nuclear excitation $\hbar\omega_N$. We will refer to this requirement as the *resonance condition* for electron bridge processes. Because of the negligibly small width of the nuclear levels, it is unlikely that this condition is fulfilled exactly by an atomic transition. Therefore several proposals have been made how to circumvent or weaken it. If, for example, we consider a decay from $|i\rangle$ to several $|f\rangle$, it becomes apparent that a system with a dense, ideally overlapping level structure is desirable for the electron bridge process.

The discussion of electron bridge processes in this thesis is focused on the excitation of the ^{229m}Th isomeric state. Therefore a couple of requirements have to be fulfilled to acquire a long lifetime of ^{229m}Th. It is necessary to investigate thorium in a charge state that energetically forbids internal conversion from the isomeric state. Neutral thorium has an ionization energy of 6.3 eV and, therefore, internal conversion is possible, lowering the lifetime of the isomer by about nine orders of magnitude [83]. With 12.1 eV, the ionization threshold of Th^+ is larger than the energy of the nuclear excitation of about 8 eV. Therefore electron bridge processes will more likely be observed in singly or higher charged thorium.

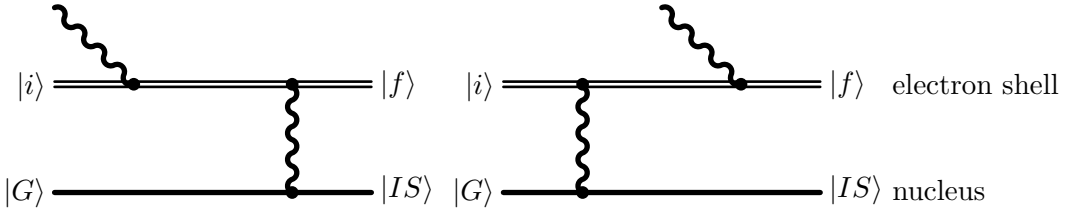

Figure 4.3: Feynman diagrams of an electron bridge process. The electron shell is excited from its ground state $|i\rangle$ by an external laser and decays to the final state $|f\rangle$ by emitting a virtual photon that excites the nucleus from its ground state $|G\rangle$ to the excited, isomeric state $|IS\rangle$.

In its ground state, singly charged thorium has three valence electrons above a closed radon core in a superposition of a [Rn].$6d7s^2$ and [Rn].$6d7s^2$ configuration with total angular momentum $J = 3/2$. The electronic structure of Th^+ is dominated by d- and f-orbitals in low lying states and, therefore, strong core-valence correlations lead to a large level density. Experimentally an extensive catalogue of even parity states in Th^+ with total angular momenta between $J = \frac{1}{2}$ and $J = \frac{7}{2}$ has been created. First measurements identified energy levels with even parity up to 6.2 eV [86]. Later this has been extended to 8.3 eV [87]. With the estimates for the energy of the nuclear isomer increasing from 3.5 eV [88] to the newest result of 8.28 eV [20] it became necessary to investigate the level structure of Th^+ for even higher energies. Therefore, we recently identified several dozens of previously unknown levels of Th^+ with energies up to 9.8 eV [RAM3]. The density of these newly identified levels has then been compared to theoretical results from the MCDF method. This comparison has been performed as a cross-check to ensure that, especially at the fringes of the investigated energy range, no levels have been overseen.

Although we do not know the transition amplitude of the nuclear transition, we want the electron bridge process to be stronger than the spontaneous decay of the nucleus. Therefore we introduce the *enhancement factor* β that is the width of the electron bridge process divided by the spontaneous decay width of the nucleus. This factor can be estimated from the level density of an atom or ion and gives a good hold on how probable the observation of an electron bridge process is in a particular system. For the case of Th^+, we derived an average enhancement of $0.5 \times 10^3 < \beta < 6 \times 10^3$ for a supposed $\hbar\omega_N = 8.28\,\text{eV}$ [RAM3]. Therefore we were able to confirm the calculations of Porsev *et al.* [36] that are referenced frequently but had yet to be verified.

The relative enhancement β of an electron bridge process with respect to the spontaneous decay has been investigated by us in more detail for the Th^{3+} ion, which has a [Rn].$5f$ ground state with only a single valence electron. This yields a

considerably simpler electronic structure than we observe in Th^+ [RAM4]. In this work, we did not only consider the excitation of the nucleus as shown in Fig. 4.2 but also the preparation of the atom in a, possibly virtual, excited state. It is evident from the Feynman diagrams that contribute to this scenario 4.3 that such a mechanism is a second-order process as discussed in Sec. 3.2 and, therefore, requires the calculation of the electron propagator. Recent calculations of this propagator by Porsev *et al.* use the direct summation method (cf. Sec. 3.2.2), neglecting the supposedly small exchange and interference terms in the matrix element [36]. Our work [RAM4] aims to investigate the justification of this neglection and its effect on the enhancement factor β. We used the B-spline pseudobasis approach (cf. Sec. 3.2.1) to calculate β for the process shown in Fig. 4.3 in Th^{3+} considering both the positive and negative Dirac continuum and including the interference between both Feynman diagrams. Our calculations show that the direct summation approach can provide accurate results for triply charged thorium, although a stronger influence of the positive continuum for lower charge states of thorium is expected. The neglection of interference, however, has shown to have a stronger influence on the results and we conclude that it should be included in high precision calculations.

Nuclear Excitation via a Two-Photon Decay

Both processes discussed in the previous section relied on a weakening of the resonance condition (4.33) due to a dense level structure. It has been shown by Porsev *et al.* that this approach works for singly charged thorium, yielding a minimal enhancement of $\beta \geq 10^3$ [36]. In this section, we want to formulate a scenario that benefits from a rich level structure but does not rely on it. Therefore we consider a two-photon decay from an excited state $|i\rangle$ of a thorium ion to some final state $|f\rangle$. One of the photons with energy $\hbar\omega$ is emitted and the other one is a virtual photon that excites the nucleus like in Fig. 4.2. The corresponding Feynman diagrams are shown in Fig. 4.4, where we see that, again, the calculation of the electron propagator is required by one of the methods discussed in Sec. 3.2. We know from energy conservation, that the sum of both photon energies $\hbar\omega$ and $\hbar\omega_N$ has to be equal to the energy difference between the excited and the finale state $\epsilon_f - \epsilon_i$. The energy share between both photons, however, is continuous and, therefore, the resonance condition can be always fulfilled.

The nuclear excitation by a two-photon electronic transition (NETP) has been first introduced for highly charged few-electron systems [89]. Those first calculations were performed for helium-like actinium, Ac^{87+}. For their study, the authors chose the isotope ^{255}Ac that has an excited nuclear state at 40.09 keV above the ground

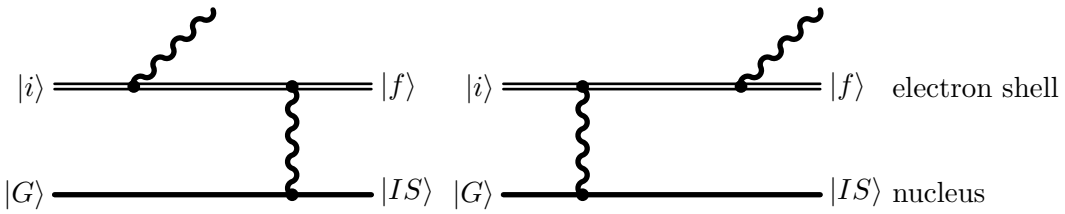

Figure 4.4: Feynman diagrams for the excitation of a nucleus via a two-photon decay of the electron shell. The atom decays from an excited state $|i\rangle$ via the emission of one real and one virtual photon to the final state $|f\rangle$. The virtual photon is exchanged with the nucleus and drives the $|G\rangle \rightarrow |IS\rangle$ transition.

state. By ionizing one of the K-shell electrons in Ac^{86+}, helium-like actinium can be prepared in the excited $1s2s^1S_0$ state at 89.218 keV. From this state, the NETP process can occur and there are two possible ways to witness the successful excitation of the nucleus. One option is to record the spectrum of real photons with energy $\hbar\omega$. This spectrum will have a narrow resonance peak at $\epsilon_i - \epsilon_f - 40.09\,\text{keV}$. Its observation will require a fine resolution of the spectrometer otherwise it will be averaged out. The second possibility is to observe the delayed emission of a photon from the spontaneous decay of the nucleus. Because of its small width, the nuclear excited state is much longer-lived than the initial electronic state of the NETP process. Therefore it is possible to distinguish between photons that are emitted during a normal two-photon decay (i.e. the emission of two real photons) of $1s2s^1S_0$ and photons emitted from the nucleus by the time they are observed. If the measurement is started after a certain time interval after which we can safely assume that all electronic levels are decayed, we can conclude that any observed photon has to come from the nucleus, as discussed in high detail in Ref. [89].

As a part of this thesis, we transferred the idea of NETP to more complex atomic systems [RAM5]. In particular, we investigated the excitation of the thorium ^{229m}Th nuclear isomer in $^{229}Th^{2+}$. The major difference between this ion and helium like actinium is the number of real intermediate levels between the excited and the final state. Those will appear as resonances in the spectrum of the emitted real photon, even if no nuclear excitation occurs. Therefore it will not be possible to confirm a nuclear excitation by an analysis of the spectrum of the real photon. Instead, we propose another method to distinguish the electronic two-photon decay from NETP. Since it has been shown that the hyperfine structure of $^{229m}Th^{2+}$ can be observed experimentally, it is an excellent probe to confirm the presence of the nuclear isomer in a trap. This monitoring of the hyperfine structure of doubly charged thorium can be included in the preparation of the initial excited state for the two-photon nuclear excitation process.

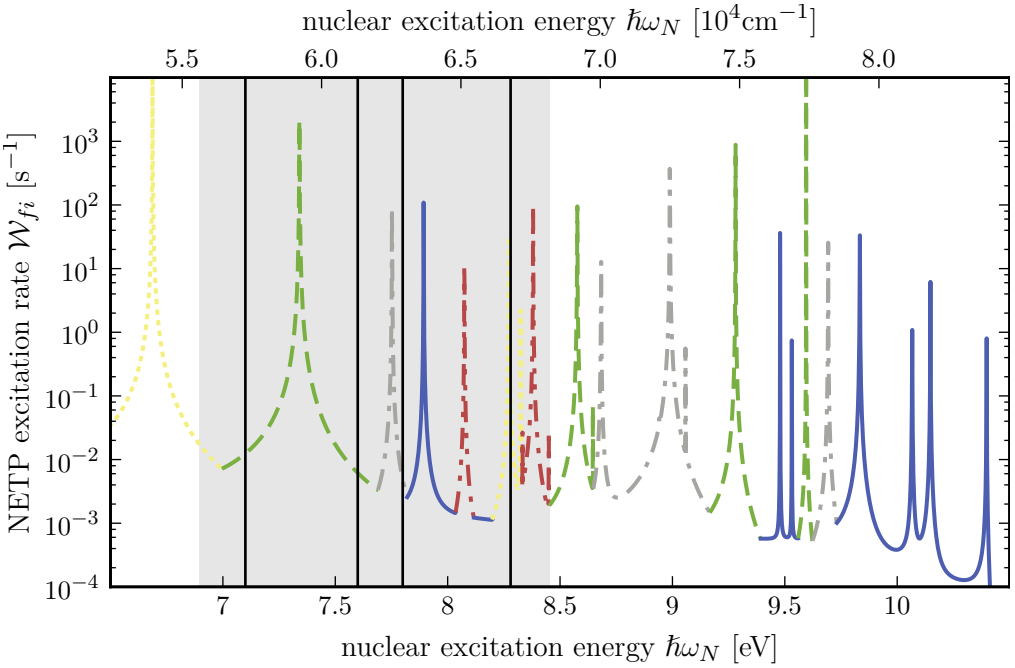

Figure 4.5: Envelope of the probability of NETP for different upper states. The colors are distributed as follows: yellow dotted line: $5f8s(J = 2) : 74\,644\,\mathrm{cm}^{-1}$, green dashed line: $5f7d(J = 2) : 79\,916\,\mathrm{cm}^{-1}$, grey dash-dotted line: $5f7d(J = 2) : 83\,237\,\mathrm{cm}^{-1}$, blue solid line: $5f7d(J = 3) : 84\,374\,\mathrm{cm}^{-1}$ and red dash-double dotted line: $5f7d(J = 2) : 78\,333\,\mathrm{cm}^{-1}$. The black vertical lines show the supposed energies of the low lying isomeric state according to Refs. [90, 91, 92, 20] with the corresponding uncertainty interval shown by the grey-shaded area.

The presence of many real intermediate states between the initial and final state of NETP in Th^{2+}, however, raises the question which initial state provides the best probability for the excitation of the nucleus. The answer to this question, however, strongly depends on the energy of the isomeric state that is only known up to a precision of 0.17 eV, which is much more than the usual width of an electronic level. Therefore we have to treat the excitation energy of the isomer $\hbar\omega_N$ as a free parameter of our theory. Doing so our work aims to provide a precise guideline for NETP experiments on $^{229}Th^{2+}$ at the German National Metrology Institute (PTB). The essence of this guideline is shown in Fig. 4.5. The optimal experimental configuration for the observation of the NETP process is shown by the color of the graph at a certain supposed nuclear excitation energy on the x-axis. For more details on how this graph is constructed, we refer the reader to our publication [RAM5]. Based on our analysis and the latest measurement of $\hbar\omega_N$, we recommend exciting

the $5f8s(J = 2) : 74\,644\,\mathrm{cm}^{-1}$ state to achieve the maximum probability. By the time this thesis is submitted our guideline is implemented, but unfortunately, the excitation of the thorium isomer remains to be observed.

5

PUBLICATIONS

In this chapter we reprint the publications that are part of this thesis in the order in which they are discussed in Ch. 4. This order does not correspond to the submission or publication date, but rather the development of the ideas and the story around the topic of this thesis starting from nuclear effects on the electron shell leading to a proposal for an experimental scenario for the excitation of the ^{229m}Th nuclear isomer.

Collinear laser spectroscopy at ion-trap accuracy: Transition frequencies and isotope shifts in the $6s\,^2S_{1/2} \rightarrow 6p\,^2P_{1/2,3/2}$ transitions in Ba^+

Phillip Imgram,[1,*] Kristian König,[1] Jörg Krämer,[1] Tim Ratajczyk,[1] Robert A. Müller,[2,3] Andrey Surzhykov,[2,3] and Wilfried Nörtershäuser[1]

[1]*Institut für Kernphysik, Technische Universität Darmstadt, 64289 Darmstadt, Germany*

[2]*Physikalisch-Technische Bundesanstalt, 38116 Braunschweig, Germany*

[3]*Technische Universität Braunschweig, 38106 Braunschweig, Germany*

(Received 7 November 2018; published 18 January 2019)

The rest-frame transition frequencies of the $6s\,^2S_{1/2} \rightarrow 6p\,^2P_{1/2}$ (D_1) and $6s\,^2S_{1/2} \rightarrow 6p\,^2P_{3/2}$ (D_2) lines in the stable isotopes of Ba^+ were measured with an accuracy better than 200 kHz through (quasi)simultaneous collinear and anticollinear laser spectroscopy, leading to an improvement in the accuracy of the isotope shifts by more than an order of magnitude compared to previous data. The ratio of the field-shift constants in the D_1, D_2 fine-structure doublet has been determined to $f = 1.0186(9)$ through a King plot analysis. These collinear laser spectroscopy measurements have reached an accuracy comparable to ion-trap measurements on allowed dipole transitions. Our result provides an accurate benchmark for atomic many-body calculations and is compared to pure Dirac-Hartree-Fock calculations and to elaborate multiconfigurational Dirac-Fock calculations. The influence of correlation effects and the Breit interaction on the isotope shift in Ba^+ are discussed.

DOI: 10.1103/PhysRevA.99.012511

I. INTRODUCTION

Precise measurements of the isotope shift are important in various fields and have many applications reaching from nuclear physics [1,2] to astronomy, astrophysics [3–7], and cosmology [8–10]. One of the first applications of collinear laser spectroscopy (CLS) was the investigation of short-lived isotopes for the extraction of nuclear ground-state properties from the isotope shift and hyperfine structure (hfs) of optical spectra [11–13]. In astronomy and astrophysics, isotope shift information is used to probe the isotopic composition of distant stars [3–7,14] and to search for changes of the fine-structure constant α in ancient times of the universe [8–10,15]. Recently, it was even proposed to use isotope shift measurements to search for short-range interactions mediated by a new boson [16–18].

In the past, combined experimental and theoretical studies have proven to be a powerful tool to investigate nuclear structure, e.g., in the case of the thorium ^{229}Th and its isomer [19,20] or for a search for physics beyond the standard model [21]. Often these studies involve elaborate atomic structure calculations, for which high-precision benchmarks are desirable. Such a benchmark is provided by the ratio of the coefficients F_i/F_j of the nuclear volume effect (or field shift) in two fine-structure transitions i and j which share the same lower state and excite into a fine-structure doublet of a higher state. It is well suited since the ratio can be experimentally determined with high precision by measuring the isotope shift

$$\delta\nu_{i,j}^{A,A'} = \nu_{i,j}^{A'} - \nu_{i,j}^{A} = K_{i,j}\frac{M_{A'} - M_A}{M_A M_{A'}} + F_{i,j}\delta\langle r_c^2\rangle^{A,A'} \quad (1)$$

between two isotopes A and A' with masses M_A and $M_{A'}$ in both transitions i and j. The slope in the King plot of the two transitions immediately provides the ratio [22]. While the mass shift constants $K_{i,j}$ play a subordinate role in this analysis, the ratio F_i/F_j is especially sensitive to relativistic effects since it can only differ from 1 due to the relativistic admixture of other wave functions to the wave functions of the involved state. These admixtures arise from states with the same total angular momentum J but different orbital angular momentum. The first experimental resolution of the J dependence in singly ionized barium was achieved in the $6s$-$6p$ and $5d$-$6p$ doublets with CLS [23,24].

Barium with proton number $Z = 56$ has seven stable isotopes and has been among the favorite candidates for testing new methods in laser spectroscopy for a long time. Recently, it has also become a candidate for parity-violation experiments which lead to transition frequency measurements in an ion trap [25]. Ba^+ also gained new interest from theory after the highly accurate measurement of the J dependence in the $4s \rightarrow 4p$ doublet of Ca^+ in an ion trap [26]. There the ratio of the field-shift coefficients strongly deviated from theoretical predictions which were thought to be well under control and reliable within the quoted uncertainties in medium- and high-Z ions. Therefore, it came as a surprise that the measured ratio in Ca^+ ions was far off theoretical expectations of all high-accuracy calculations. The ratio was even larger than calculated for pure hydrogenic wave functions that do not take into account electron-electron correlations. These correlations will, however, only reduce the field-shift ratio and from a theoretical point of view there is no way that theory can accommodate for this deviation. As barium is an alkaline-earth metal like calcium and therefore has a similar atomic structure, this work targets an improved and more accurate

*pimgram@ikp.tu-darmstadt.de

measurement of the ratio of the field-shift constants in Ba^+ in order to contribute to a better understanding of the inconsistencies in Ca^+ [27]. Moreover, additional high-accuracy data can be used to search for King linearity violation and to constrain new-physics contributions as it has been performed in [16,17] using the calcium data. Recent online experiments applying collinear laser spectroscopy have produced results with uncertainties between 2 MHz and 0.7 MHz in the isotope shift of Be^+ [28] and 0.5 MHz at best for absolute transition frequencies. The latter was comparable to the best previous measurements on Li^+ ions applying CLS in combination with saturation spectroscopy in $^{6,7}Li^+$ ions [29].

Here we present measurements of transition frequencies and isotope shifts in the $6s\,^2S_{1/2} \rightarrow 6p\,^2P_{1/2}$ (D_1) and $6s\,^2S_{1/2} \rightarrow 6p\,^2P_{3/2}$ (D_2) transitions of all seven stable Ba^+ isotopes with uncertainties of 200 kHz or less, an accuracy so far only achieved for these and other E_1 transitions with atom and ion traps [25,26,30]. This is important since high-precision CLS is not merely complementary to ion-trap measurements but provides access to transitions between short-lived atomic states in neutral, singly, and highly charged ions that are not accessible for ion trap experiments. For He-like ions, this has already been demonstrated, albeit at much lower accuracy in [31–34]. In the long run, our aim is to measure absolute transition frequencies in He-like ions of Be, B, and C to extract absolute charge radii purely from optical transitions as suggested for helium in [35]. This endeavor requires advanced calculations of QED terms of the order of $\alpha^7 m$ and transition frequency measurements with accuracy of about 100–200 kHz in transitions starting from the $1s2p\,^3S_1$ state with lifetimes reaching from 1.8 s (Be^{2+}) down to 21 ms in C^{4+}. Work on the theoretical side has recently started and the numerically most demanding part, the calculation of the relativistic corrections to the Bethe logarithm, has been achieved [35]. Here we demonstrate that the required experimental accuracy is available. The extraction of all-optical charge radii of light isotopes in He-like systems will shed light on those determined from elastic electron scattering and are expected to provide even higher accuracy. The comparison of these radii with muonic atom experiments that are currently prepared might also contribute to the explanation of the proton radius puzzle [36–38] and serve as a test of universality of electromagnetic interactions of leptons in the standard model [35].

We apply (quasi)simultaneous collinear and anticollinear excitation with two laser beams, one in a copropagating (ν_+) and a second one in a counterpropagating (ν_-) geometry [28,39,40]. The alternating excitation of fast ions in both directions at the same velocity allows for the determination of the rest-frame transition frequency ν_0 directly from the product of the two laboratory-frame resonance frequencies

$$\nu_\pm = \nu_0\gamma(1 \pm \beta) \Rightarrow \nu_0 = \sqrt{\nu_+\nu_-}, \tag{2}$$

with the Lorentz factor $\gamma = (1-\beta^2)^{-1/2}$ and the dimensionless ion velocity $\beta = v/c$. Transition frequencies and isotope shifts in both transitions of the Ba^+ fine-structure doublet and the ratio of their field-shift constants are determined with very high accuracy.

II. EXPERIMENT

The experiment was performed at the Collinear Apparatus for Laser Spectroscopy and Applied Science (COALA) at TU Darmstadt, Germany. The beamline was originally designed for accurate high-voltage evaluations based on CLS [41,42]. During this endeavor all systematics of the apparatus were well understood and minimized. Now the beamline is also destined for conventional but highly accurate CLS.

The Ba^+ ions are produced in a surface ionization source on a potential $U_{\mathrm{acc}} = 17$ kV with respect to the ground potential of the beamline. After initial acceleration, the ions are collimated and superimposed with the laser beams through electrostatic deflectors and lenses. Ion beam shape and current can be monitored with fluorescence screens and Faraday cups in two beam-diagnostic stations located 2.5 m apart, before and after the fluorescence detection region (FDR). To control the overlap of laser beams and the ion beam, adjustable iris diaphragms are also part of the beam diagnostic chambers limiting the angular misalignment between ion and laser beam to $\theta < 1.5$ mrad. The FDR can be floated on a potential U_{offset} up to 20 kV, allowing for postacceleration of the ions. The ions are tuned to resonance with the Doppler-shifted laser frequency by an additional variable potential U_{scan} ranging from -500 V to 500 V with respect to U_{offset}. The two light collection systems in the FDR consist of elliptical mirrors which image light emitted along the ion beam onto a line outside the optical windows from where it is transported to Sens-Tech P25PC photomultiplier tubes using a compound parabolic concentrator. The latter suppresses laser stray light by discriminating according to the incidence angle in the focal plane of the mirror system.

Laser light for both transitions $\lambda_{D_1} = 493$ nm and $\lambda_{D_2} = 455$ nm is produced with two frequency-doubled continuous-wave Sirah MATISSE 2 TS Ti:sapphire lasers. A Menlo Systems FC1500 frequency comb is used to measure the fundamental frequency of both lasers. One of the two MATISSE lasers is stabilized by a wavemeter, while the other one is stabilized to an iodine-stabilized helium-neon laser by a transfer cavity setup. Both stabilization schemes provide long-term stability with standard deviations of $\sigma_{\mathrm{WM}} = 509(14)$ kHz and $\sigma_{\mathrm{TC}} = 251(4)$ kHz relative to the chosen fundamental frequency. Finally, the blue laser light is transported to the beamline through polarization maintaining optical fibers. A $\lambda/2$ waveplate and a polarizer in front of the beamline viewport ensure linear polarization of the laser light, which has typically 10 μW in laser power. Furthermore, two iris diaphragms outside the beamline allow a superposition of the collinear and anticollinear laser beams to better than $\theta_{\mathrm{l}} < 0.9$ mrad, which is crucial for suppressing systematic shifts by angular misalignment of the laser beams.

III. RESULTS

The fixed-frequency collinear and anticollinear lasers are used in an alternating scheme to excite the Doppler-shifted transitions in ions with the matching velocities. In order to use Eq. (2), the velocity β of the ions has to be identical during the collinear and anticollinear excitation. Therefore, the ions have to be in resonance with the lasers at the same ion energy.

TABLE I. Transition frequencies ν_{D_1,D_2} in the $6s\,^2S_{1/2} \rightarrow 6p\,^2P_{1/2}$ and $6s\,^2S_{1/2} \rightarrow 6p\,^2P_{3/2}$ transition of Ba^+ ions and corresponding isotope shifts. The number in the first set of parentheses denotes the statistical uncertainty and in the second set the total uncertainty. All values are in MHz.

A	$\nu_{D_1}^A$ (this work)	$\delta\nu_{D_1}^{138,A}$ (this work)	$\delta\nu_{D_1}^{138,A}$ (Ref. [24])	$\nu_{D_2}^A$ (this work)	$\delta\nu_{D_2}^{138,A}$ (this work)	$\delta\nu_{D_2}^{138,A}$ (Ref. [24])
138	607 426 262.600 (33) (126)	0	0	658 116 486.035 (24) (124)	0	0
137	607 426 534.810 (49) (145)	272.210 (192)	271.1 (1.7)	658 116 764.655 (51) (145)	278.620 (190)	279.0 (2.6)
136	607 426 442.790 (69) (140)	180.190 (188)	179.4 (1.8)	658 116 672.730 (57) (135)	186.695 (183)	186.9 (2.1)
135	607 426 612.605 (70) (153)	350.005 (198)	348.6 (2.1)	658 116 847.077 (60) (136)	361.042 (184)	360.7 (2.2)
134	607 426 485.803 (66) (139)	223.203 (188)	222.6 (3.0)			233.9 (3.7)
132	607 426 541.362 (133) (181)	278.762 (220)	278.9 (4.0)	658 116 779.071 (130) (178)	293.036 (217)	294.9 (4.2)
130	607 426 615.420 (142) (187)	352.820 (225)	355.3 (4.4)	658 116 857.849 (138) (184)	371.814 (222)	372.3 (4.9)

In the case of the Doppler tuning where a scanning potential is used to change the ion velocity, the laser frequencies have to be set in a way that the resonances appear at the same scanning voltage $U_+ = U_-$. It is more practical, however, to tolerate small remaining voltage differences $\delta U = U_+ - U_-$ between the corresponding centers of gravity and correct them during data analysis by calculating the required shift of one of the laser frequencies, e.g., ν_+, using the linear approximation $\delta\nu = \frac{\partial\nu_D}{\partial U}\delta U$, where

$$\frac{\partial\nu_D}{\partial U} = \frac{\nu_0}{mc^2}\left(e + \frac{e(mc^2+eU)}{\sqrt{eU(2mc^2+eU)}}\right) \tag{3}$$

is the differential Doppler shift. Hence, the transition rest-frame frequency was calculated according to

$$\nu_0 = \sqrt{\left(\nu_+ - \frac{\partial\nu_D}{\partial U}\delta U\right)\nu_-}. \tag{4}$$

The isotope-dependent photon recoil $\delta\nu_{rec} = h\nu_{photon}^2/2m_0c^2$ was taken into account ($\delta\nu_{rec} \approx 7$ kHz) but is not significant at the current level of accuracy.

The measurements of all isotopes were repeated ten times; only for the D_1 line in $^{138}Ba^+$, 40 data points were taken, spread over several days to check for day-to-day drifts. Obvious drifts were not observed, neither were systematic differences between the first and the second chamber of the FDR. The weighted average of all measurements are listed in Table I. Statistical uncertainties (first set of parentheses) were obtained either as the standard error of the mean or the propagated weighted uncertainties, whichever was larger.

Systematic uncertainties include the alignment uncertainties of the two laser beams and the ion beam (100 kHz), a small asymmetry in the spectral line shape (see Fig. 1) due to inelastic collision of the ions (70 kHz), and a small remaining dependence of a voltage measurement in hyperfine structure spectra for the odd isotopes due to the large hfs splitting corresponding to more than 1000 V in Doppler tuning (60 kHz). The influences of the Zeeman effect, the ac Stark effect, or photon recoil shifts due to repeated photon scattering were investigated and found to be insignificant at the current level of accuracy (less than 10 kHz).

Our results are listed in Table I and were used to perform a King plot analysis according to [22]

$$\mu\,\delta\nu_{D_2}^{138,A} = f\mu\,\delta\nu_{D_2}^{138,A} + k, \tag{5}$$

with the inverse mass factor $\mu := m_{138}m_A/(m_{138} - m_A)$, the relation between the field and mass shift $k := K_{D_2} - fK_{D_1}$, and the ratio of the field shifts $f := F_{D_2}/F_{D_1}$. Figure 2 shows the excellent linearity of the data points, which demonstrates the high quality. A linear fit performed with the algorithm of York *et al.* [43] taking x and y uncertainties into account resulted in a slope of $f = 1.0186(9)$ and an intersection with the y axis of $k = 27.86(1.04)$ GHz amu. The measurement of the rest-frame transition frequencies presented here is an extremely precise measurement performed with CLS. Not only does our result $\nu_{D1,\,\mathrm{CLS}}^{138} = 607\,426\,262.60(13)$ MHz agree with the recent trap result $\nu_{D1,\,\mathrm{trap}}^{138} = 607\,426\,262.5(2)$ MHz [25], but we even improve its accuracy by almost a factor of 2. Moreover, since we have measured all stable isotopes with similar accuracy, the uncertainty of the isotope shifts is

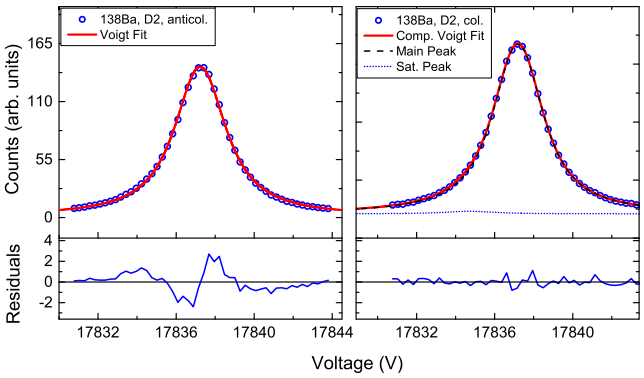

FIG. 1. Shown on the right is the collinear and and on the left the anticollinear D_2 fluorescence spectra of $^{138}Ba^+$. For demonstration, a usual Voigt fit has been used (left) which reveals a clear asymmetry in the residuals. This has been improved by a compound of two Voigt profiles (right). Thereby, the reduced $\chi_r^2 = \chi^2/(\text{degree of freedom})$ has been lowered from $\chi_r^2 = 12$ to $\chi_r^2 = 1.6$. Although the center frequencies are shifted up to 400 kHz by the compound fit, the rest-frame transition frequency ν_0 is only shifted up to 70 kHz. This shift has been included in the systematic uncertainty. The reason for such satellite peaks is inelastic collisions of the ions and is explained in detail in [28]. All spectra were fitted with the composite line profile.

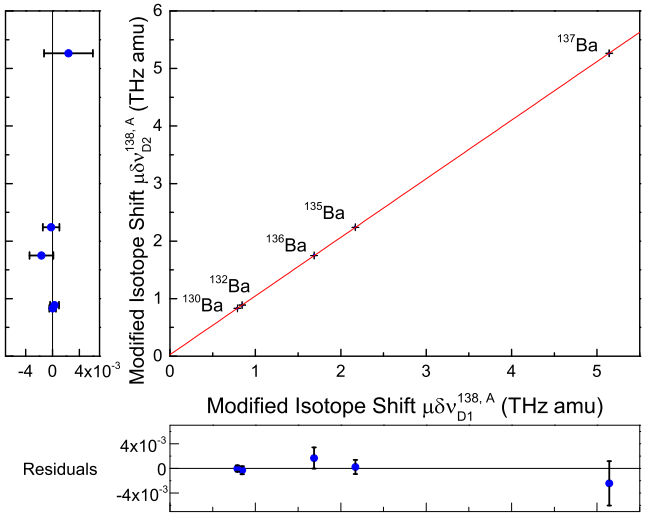

FIG. 2. King plot of the D_2 versus D_1 transition in Ba^+. The line is a regression of Eq. (5) taking uncertainties in both directions into account. The high linearity demonstrates the excellent quality of the data.

reduced by at least an order of magnitude compared to the previous study [24], resulting in a field-shift ratio determination with a relative uncertainty less than 0.1%. Furthermore, our result for the field-shift ratio is within 2σ of the previous value $f_{\mathrm{Wendt}} = 1.025(3)$ [24].

IV. THEORY

We used the multiconfigurational Dirac-Fock (MCDF) method implemented in the GRASP2K package [44] to calculate the isotope shift and especially the ratio of field-shift constants for the transitions $6s\,^2S_{1/2} \rightarrow 6p\,^2P_{1/2}$ and $6s\,^2S_{1/2} \rightarrow 6p\,^2P_{3/2}$ in Ba^+. The MCDF method is based on an expansion of many-electron wave functions into a basis of so-called configuration state functions (CSFs) (for more details see, e.g., [45,46]). The choice and composition of this basis is crucial to obtain precise results. We built the CSF set with single excitations up to $n = 12$ and $l = 4$ from the reference states $[\mathrm{Xe}] + 6s$, $[\mathrm{Xe}] + 6p$, $[\mathrm{Xe}] + 7s$, and $[\mathrm{Xe}] + 7p$, where the xenon core is fully opened. Moreover, we include (double) core-valence excitations from the $5p$ shell.

The estimation of the theoretical uncertainty is of major importance for a meaningful comparison to high-precision measurements. Generally, it consists of two parts: (i) the numerical uncertainty, e.g., due to a lack of convergence, and (ii) the uncertainty introduced by effects that have been neglected in the calculations. The first can be obtained by analyzing the convergence behavior of a set of several calculations, with increasing numbers of both correlation layers and open core shells. More difficult is the estimation of the magnitude of neglected effects. In our calculation neither Breit interaction nor the effects from self-energy or vacuum polarization are taken into account. To obtain the influence of these effects we employed two methods. First we calculated the field-shift constants using the Dirac-Hartree-Fock (DHF) method, where the Breit Hamiltonian can be included in the self-consistent iterative process [47]. By comparing DHF results with and without Breit interaction taken into account, we obtain the approximate uncertainty introduced by disregarding this effect. Second, we estimate the influence of the neglected self-energy and vacuum polarization on the field shift from calculations for the same barium isotope but in the hydrogenlike charge state using the analytical formulas from Ref. [48]. We expect these effects to be of similar relative magnitude in the Ba^+ case, as it is indicated in Refs. [49,50].

V. DISCUSSION

Before we present the field-shift ratio calculated with the MCDF approach it is instructive to compare the experimental results with a more simple model. The first approximation is the hydrogenic model [48]. Here we obtain $f_{\mathrm{hyd}} = 1.04231$, which is significantly larger than the experimental result of $f = 1.0186(9)$. However, as it has been also discussed in [26], the effective nuclear charge is largely reduced from $Z = 56$ due to correlation effects, which, as a consequence, will reduce the field-shift ratio f. This can already be seen in the DHF result, yielding $f_{\mathrm{DHF}} = 1.0201$. With the MCDF method we obtain $f_{\mathrm{MCDF}} = 1.0206(3)_{\mathrm{num}}(4)_{\mathrm{sys}}$, which agrees well with our experimental findings. As discussed in Sec. IV, the numerical uncertainty has been determined by analyzing the convergence behavior of f with respect to an increase of the basis size. It turns out that the systematic uncertainty due to approximations is of the same order of magnitude. The main contribution originates from the self-energy effects on the field shift calculated using the hydrogenic model [48]. The effect caused by vacuum polarization, in turn, is one order of magnitude smaller. Our DHF calculations show that the effect of Breit interaction on f is similarly small. From these results, we can draw conclusions for the yet still unexplained calcium case: Both QED and Breit effects on the field-shift ratio in Ba^+ are comparably small. Our calculations using the model [48] show that they are expectedly one order of magnitude smaller for the case of Ca^+. Therefore, the disagreement between experiment and theory for calcium must be explained by correlation effects that are not well enough under control or systematic experimental shifts that have not been taken into account.

In summary, we have performed collinear laser spectroscopy on seven stable barium isotopes and significantly improved the transition frequencies, the isotope shifts, and the ratio of the field-shift factors of the D_1- and D_2-like transitions in Ba^+ even compared to recent optical spectroscopy on laser-cooled ensembles in an ion trap. The result is very different from the situation found with Ca^+, where a strong deviation between experiment and theory was reported [26]. The present work can help to encircle the reason for this deviation: In the case of Ba^+ we concluded that both QED and Breit interaction contributions to f must be small. In the case of Ca the nuclear charge is 65% smaller and hence these effects should be even smaller while electron correlations are more important. Therefore, additional data on the isotope shifts and f factor of the corresponding transitions in Sr^+ with $Z = 38$ will be helpful to further understand the anomalous behavior in Ca^+. Recent work has provided improved data [51], but accuracy has yet to be improved by another order of magnitude.

ACKNOWLEDGMENTS

We acknowledge financial support from the German Federal Ministry for Education and Research (BMBF) under Contract No. 05P15RDFN1, the Helmholtz International Center for FAIR within the LOEWE program by the State of Hesse and funding by the Deutsche Forschungsgemeinschaft (DFG) Project No. 279384907 SFB 1245. Installation of COALA was supported by the DFG under Grant INST No. 163/392-1 FUGG. P.I. and T.R. acknowledge support from HGS-HIRE.

[1] K. Blaum, J. Dilling, and W. Nörtershäuser, Phys. Scr. **T152**, 014017 (2013).

[2] P. Campbell, I. D. Moore, and M. R. Pearson, Prog. Part. Nucl. Phys. **86**, 127 (2016).

[3] F. Castelli and S. Hubrig, Astron. Astrophys. **421**, L1 (2004).

[4] C. R. Cowley and S. Hubrig, Astron. Astrophys. **432**, L21 (2005).

[5] J. Leenaarts, J. de la Cruz Rodríguez, O. Kochukhov, and M. Carlsson, Astrophys. J. Lett. **784**, L17 (2014).

[6] D. L. Lambert and C. Allende Prieto, Mon. Not. R. Astron. Soc. **335**, 325 (2002).

[7] L. Mashonkina and G. Zhao, Astron. Astrophys. **456**, 313 (2006).

[8] M. G. Kozlov, V. A. Korol, J. C. Berengut, V. A. Dzuba, and V. V. Flambaum, Phys. Rev. A **70**, 062108 (2004).

[9] T. Ashenfelter, G. J. Mathews, and K. A. Olive, Phys. Rev. Lett. **92**, 041102 (2004).

[10] Y. Fenner, M. T. Murphy, and B. K. Gibson, Mon. Not. R. Astron. Soc. **358**, 468 (2005).

[11] R. Neugart, Nucl. Instrum. Methods Phys. Res. **186**, 165 (1981).

[12] A. C. Mueller, F. Buchinger, W. Klempt, E. W. Otten, R. Neugart, C. Ekström, and J. Heinemeier, Nucl. Phys. A **403**, 234 (1983).

[13] E. W. Otten, in *Treatise on Heavy Ion Science, Volume 8: Nuclei Far From Stability*, edited by D. A. Bromley (Springer US, Boston, 1989), pp. 517–638.

[14] R. L. Kurucz, Phys. Scr. **T47**, 110 (1993).

[15] J. C. Berengut, V. A. Dzuba, V. V. Flambaum, J. A. King, M. G. Kozlov, M. T. Murphy, and J. K. Webb, in *From Varying Couplings to Fundamental Physics*, edited by C. Martins and P. Molaro (Springer, Berlin, 2011), pp. 9–16.

[16] J. C. Berengut, D. Budker, C. Delaunay, V. V. Flambaum, C. Frugiuele, E. Fuchs, C. Grojean, R. Harnik, R. Ozeri, G. Perez, and Y. Soreq, Phys. Rev. Lett. **120**, 091801 (2018).

[17] C. Frugiuele, E. Fuchs, G. Perez, and M. Schlaffer, Phys. Rev. D **96**, 015011 (2017).

[18] V. V. Flambaum, A. J. Geddes, and A. V. Viatkina, Phys. Rev. A **97**, 032510 (2018).

[19] M. S. Safronova, U. I. Safronova, A. G. Radnaev, C. J. Campbell, and A. Kuzmich, Phys. Rev. A **88**, 060501 (2013).

[20] R. A. Müller, A. V. Maiorova, S. Fritzsche, A. V. Volotka, R. Beerwerth, P. Glowacki, J. Thielking, D.-M. Meier, M. Okhapkin, E. Peik, and A. Surzhykov, Phys. Rev. A **98**, 020503 (2018).

[21] J. C. Berengut, V. A. Dzuba, V. V. Flambaum, and S. G. Porsev, Phys. Rev. Lett. **102**, 210801 (2009).

[22] W. King, *Isotope Shifts in Atomic Spectra* (Springer Science+Business Media, New York, 1984).

[23] M. Van Hove, G. Borghs, P. De Bisschop, and R. Silverans, J. Phys. B **15**, 1805 (1982).

[24] K. Wendt, S. Ahmad, F. Buchinger, A. Mueller, R. Neugart, and E.-W. Otten, Z. Phys. A **318**, 125 (1984).

[25] E. A. Dijck, M. Nuñez Portela, A. T. Grier, K. Jungmann, A. Mohanty, N. Valappol, and L. Willmann, Phys. Rev. A **91**, 060501 (2015).

[26] C. Shi, F. Gebert, C. Gorges, S. Kaufmann, W. Nörtershäuser, B. K. Sahoo, A. Surzhykov, V. A. Yerokhin, J. C. Berengut, F. Wolf, J. C. Heip, and P. O. Schmidt, Appl. Phys. B **123**, 2 (2016).

[27] M. R. Kalita, J. A. Behr, A. Gorelov, M. R. Pearson, A. C. DeHart, G. Gwinner, M. J. Kossin, L. A. Orozco, S. Aubin, E. Gomez, M. S. Safronova, V. A. Dzuba, and V. V. Flambaum, Phys. Rev. A **97**, 042507 (2018).

[28] A. Krieger, W. Nörtershäuser, C. Geppert, K. Blaum, M. L. Bissel, N. Frömmgen, M. Hammen, K. Kreim, M. Kowalska, J. Krämer, R. Neugart, G. Neyens, R. Sánchez, D. Tiedemann, D. Yordanov, and M. Zakova, Appl. Phys. B **123**, 15 (2017).

[29] E. Riis, A. G. Sinclair, O. Poulsen, G. W. F. Drake, W. R. C. Rowley, and A. P. Levick, Phys. Rev. A **49**, 207 (1994).

[30] V. Batteiger, S. Knünz, M. Herrmann, G. Saathoff, H. A. Schüssler, B. Bernhardt, T. Wilken, R. Holzwarth, T. W. Hänsch, and T. Udem, Phys. Rev. A **80**, 022503 (2009).

[31] T. P. Dinneen, N. Berrah-Mansour, H. G. Berry, L. Young, and R. C. Pardo, Phys. Rev. Lett. **66**, 2859 (1991).

[32] T. J. Scholl, R. Cameron, S. D. Rosner, L. Zhang, R. A. Holt, C. J. Sansonetti, and J. D. Gillaspy, Phys. Rev. Lett. **71**, 2188 (1993).

[33] J. K. Thompson, D. J. H. Howie, and E. G. Myers, Phys. Rev. A **57**, 180 (1998).

[34] E. G. Myers, H. S. Margolis, J. K. Thompson, M. A. Farmer, J. D. Silver, and M. R. Tarbutt, Phys. Rev. Lett. **82**, 4200 (1999).

[35] V. A. Yerokhin, V. Patkóš, and K. Pachucki, Phys. Rev. A **98**, 032503 (2018).

[36] R. Pohl *et al.*, Nature (London) **466**, 213 (2010).

[37] R. Pohl, R. Gilman, G. A. Miller, and K. Pachucki, Annu. Rev. Nucl. Part. Sci. **63**, 175 (2013).

[38] S. Schmidt *et al.*, J. Phys.: Conf. Ser. **1138**, 012010 (2018).

[39] W. Nörtershäuser, D. Tiedemann, M. Žáková, Z. Andjelkovic, K. Blaum, M. L. Bissell, R. Cazan, G. W. F. Drake, C. Geppert, M. Kowalska, J. Krämer, A. Krieger, R. Neugart, R. Sánchez, F. Schmidt-Kaler, Z.-C. Yan, D. T. Yordanov, and C. Zimmermann, Phys. Rev. Lett. **102**, 062503 (2009).

[40] A. Krieger, K. Blaum, M. L. Bissell, N. Frömmgen, C. Geppert, M. Hammen, K. Kreim, M. Kowalska, J. Krämer, T. Neff, R. Neugart, G. Neyens, W. Nörtershäuser, C. Novotny, R. Sánchez, and D. T. Yordanov, Phys. Rev. Lett. **108**, 142501 (2012).

[41] J. Krämer, K. König, C. Geppert, P. Imgram, B. Maaß, J. Meisner, E. W. Otten, S. Passon, T. Ratajczyk, J. Ullmann, and W. Nörtershäuser, Metrologia **55**, 268 (2018).

[42] K. König, C. Geppert, J. Krämer, B. Maaß, E. W. Otten, T. Ratajczyk, and W. Nörtershäuser, Hyperfine Interact. **238**, 24 (2017).

[43] D. York, N. M. Evensen, M. L. Martinez, and J. D. B. Delgado, Am. J. Phys. **72**, 367 (2004).

[44] P. Jönsson, G. Gaigalas, J. Bieroń, C. F. Fischer, and I. Grant, Comput. Phys. Commun. **184**, 2197 (2013).

[45] C. Froese-Fischer, T. Brage, and P. Johnsson, *Computational Atomic Structure: An MCHF Approach* (Taylor & Francis, London, 1997).

[46] I. P. Grant, *Relativistic Quantum Theory of Atoms and Molecules: Theory and Computation* (Springer Science+Business Media, New York, 2007).

[47] O. Zatsarinny and C. Froese Fischer, Comput. Phys. Commun. **202**, 287 (2016).

[48] V. A. Yerokhin, Phys. Rev. A **83**, 012507 (2011).

[49] N. A. Zubova, Y. S. Kozhedub, V. M. Shabaev, I. I. Tupitsyn, A. V. Volotka, G. Plunien, C. Brandau, and T. Stöhlker, Phys. Rev. A **90**, 062512 (2014).

[50] N. A. Zubova, A. V. Malyshev, I. I. Tupitsyn, V. M. Shabaev, Y. S. Kozhedub, G. Plunien, C. Brandau, and T. Stöhlker, Phys. Rev. A **93**, 052502 (2016).

[51] B. Dubost, R. Dubessy, B. Szymanski, S. Guibal, J.-P. Likforman, and L. Guidoni, Phys. Rev. A **89**, 032504 (2014).

Rapid Communications

Hyperfine interaction with the ^{229}Th nucleus and its low-lying isomeric state

Robert A. Müller,[1,2,*] Anna V. Maiorova,[3] Stephan Fritzsche,[4,5] Andrey V. Volotka,[4] Randolf Beerwerth,[4,5] Przemyslaw Glowacki,[1,†] Johannes Thielking,[1] David-Marcel Meier,[1] Maksim Okhapkin,[1] Ekkehard Peik,[1] and Andrey Surzhykov[1,2]

[1]*Physikalisch-Technische Bundesanstalt, D-38116 Braunschweig, Germany*
[2]*Technische Universität Braunschweig, D-38106 Braunschweig, Germany*
[3]*Center for Advanced Studies, Peter the Great St. Petersburg State Polytechnical University, Polytekhnicheskaya 29, 195251 St. Petersburg, Russia*
[4]*Helmholtz Insitute Jena, D-07743 Jena, Germany*
[5]*Friedrich-Schiller-University Jena, D-07743 Jena, Germany*

(Received 31 January 2018; published 20 August 2018)

The thorium nucleus with a mass number $A = 229$ has attracted much interest because its extremely low-lying first excited isomeric state at about 8 eV opens the possibility for the development of a nuclear clock. Both the energy of this state as well as the nuclear magnetic dipole and electric quadrupole moment of the ^{229m}Th isomer are subjects of intense research. The latter can be determined by investigating the hyperfine structure of thorium atoms or ions. Due to its electronic structure and the long lifetime of the nuclear isomeric state, Th^{2+} is especially suitable for such kinds of studies. In this Rapid Communication, we present a combined experimental and theoretical investigation of the hyperfine structure of the $^{229}Th^{2+}$ ion in the nuclear ground state, where a good agreement between theory and experiment is found. For the nuclear excited state we use our calculations in combination with recent measurements [J. Thielking *et al.*, Nature (London) **556**, 321 (2018)] to obtain the nuclear dipole moment of the isomeric state $\mu_{\rm iso} = -0.35\mu_{\rm N}$, which is in contradiction to the theoretically predicted value of $\mu_{\rm iso} = -0.076\mu_{\rm N}$ [A. M. Dykhne and E. V. Tkalya, JETP Lett. **67**, 251 (1998)].

DOI: 10.1103/PhysRevA.98.020503

Introduction. While the energy levels of atomic nuclei are usually several keV, if not MeV, apart, ^{229}Th exhibits an extremely low-lying isomeric state ^{229m}Th with an excitation energy of only about 8 eV [1–3]. Since this energy can be reached by current laser systems and the nuclear isomer is very long lived, it has been proposed to build a nuclear clock based on the transition from the nuclear ground to the isomeric state [4]. The precision of this clock has been estimated to 10^{-19} s [5,6]. Therefore such a clock might be sensitive to temporal drifts of the quantum chromodynamics (QCD) coupling constant and the fine-structure constant. In fact, it was shown that the transition from the nuclear ground to the isomeric state could be orders of magnitude more sensitive to temporal variations of the fine-structure constant α than electronic transitions [7–10].

The experimental realization of a nuclear clock requires precise knowledge of the nuclear properties of both the nuclear ground and the first excited isomeric states. Most of the important quantities are not known to a high precision so far. The exact energy of the isomer, for example, remains to be determined. The currently accepted value of 7.8(5) eV has been obtained by a comparison of fluorescence lines in the keV regime from higher excited states of the ^{229}Th nucleus [11,12]. For the search for possible variations of the fundamental constants, the moments of the nuclear ground and isomeric states [8,9] are of major importance. The moments of the ground-state nucleus have been extracted to a good precision by a combination of theory and experiment in Th^{3+} [13]. Moreover, recently, the first measurements of the moments of the nuclear isomer have been presented [7]. Since these were partially contradicting previous calculations [10,14], a theoretical explanation is still pending.

A well-established and precise method for determining nuclear moments is hyperfine spectroscopy: the measurement of the hyperfine splitting of electronic levels. The precise analysis of such experimental data requires both theoretical and experimental efforts. A theoretically challenging, but experimentally convenient, system for hyperfine spectroscopy of thorium is the charge state Th^{2+}, which resembles a two-valence electron system. The ionization threshold of this ion is well above the low-lying nuclear resonance [15] and the density of low energetic electronic levels is much smaller than in the case of Th^{+}. Therefore the longevity of the nuclear isomer is increased, allowing for a better measurement statistic. However, except for the recent experiment [7], neither experimental nor theoretical values for the hyperfine structure in $^{229}Th^{2+}$ have been presented so far.

In this Rapid Communication, we present a comparative study of experimental values and theoretical calculations for the hyperfine splitting in both $^{229}Th^{2+}$ and $^{229m}Th^{2+}$. Our theoretical results are obtained using two different methods, a combination of configuration interaction and second-order many-body perturbation theory (CI+MBPT) and the

*robert.mueller@ptb.de
†Present address: Poznań University of Technology, 60-965 Poznań, Poland.

multiconfigurational Dirac-Fock approach (MCDF). The combination of these theories and experimental data allows for an evaluation of the $^{229m}Th^{2+}$ nuclear magnetic dipole and electric quadrupole moment, independent on previous determinations of these quantities [13]. This might support future investigations of possible variations of the fundamental constants.

Hyperfine structure of thorium ions. Hyperfine spectroscopy is the measurement of the splitting of atomic levels due to the coupling of the nuclear spin $\vec{I}$ and the total angular momentum $\vec{J}$ of the electronic state to the combined total angular momentum $\vec{F} = \vec{I} + \vec{J}$. The energy shift induced by that coupling can be calculated using first-order perturbation theory,

$$E_{M1} = \frac{1}{2}AC, \tag{1a}$$

$$E_{E2} = B\frac{\frac{3}{4}C(C+1) - I(I+1)J(J+1)}{2I(2I-1)J(2J-1)}, \tag{1b}$$

where $C = F(F+1) - J(J+1) - I(I+1)$. The subscript $M1$ refers to the energy shift due to the interaction of the electron shell with the magnetic dipole moment of the nucleus, while $E2$ is the corresponding shift due to the nuclear electric quadrupole moment. Usually, multipoles higher than the $E2$ interaction are negligible.

The hyperfine energies (1) scale with the so-called *hyperfine constants* A and B. For an electronic state characterized by its total angular momentum J and further quantum numbers γ, these constants are obtained as [16]

$$A = \frac{\mu_I}{I}\frac{1}{\sqrt{J(J+1)(2J+1)}}\langle\gamma J||\vec{T}^1||\gamma J\rangle, \tag{2a}$$

$$B = 2Q\left[\frac{J(2J-1)}{(J+1)(2J+1)(2J+3)}\right]^{\frac{1}{2}}\langle\gamma J||\vec{T}^2||\gamma J\rangle, \tag{2b}$$

It can be seen from the equation that A and B are proportional to the nuclear magnetic dipole and electric quadrupole moment μ_I and Q, respectively. The operators $\vec{T}^k$ are the electronic parts of the hyperfine interaction. Relation (2) can be used to extract the nuclear moments from the hyperfine splitting of atomic lines.

Numerical calculations. The theoretical determination of the hyperfine constants A and B and hence the hyperfine structure of Th^{2+} requires the evaluation of the many-electron matrix elements of the hyperfine operator $\vec{T}^k$ [cf. Eq. (2)]. We therefore need to obtain a precise representation of the many-electron wave functions of the corresponding states. In this Rapid Communication, we apply two different methods to approximate these wave functions.

The first technique we use to calculate the hyperfine constants in $^{229}Th^{2+}$ is the relativistic configuration interaction (CI). In CI, the ansatz for a many-electron wave function with a well-defined parity Π and total angular momentum J is a superposition of N so-called configuration state functions (CSFs) [16],

$$\Psi(\Pi, J) = \sum_{i=1}^{N} c_i \Phi_i(\Pi, J). \tag{3}$$

With these basis functions, the Hamiltonian matrix and its eigenvalues are calculated. The entries of the corresponding eigenvectors are the expansion coefficients c_i. This reduces the problem of constructing a complicated many-electron wave function to the diagonalization of a matrix.

The relativistic CI approach is well known for its performance to calculate the atomic structure of highly charged ions and is being actively developed to include QED corrections to atomic processes up to a very high precision [17–20]. For the determination of hyperfine constants in Th^{2+}, however, the correlation between core electrons and core-valence correlations are of major importance, which are typically neglected in CI for practical reasons. To overcome these problems, many-body perturbation theory (MBPT) can be used to account for core-core and core-valence correlations, while the dynamics of the valence electrons are still treated using CI. The results presented here were obtained using the package published in Ref. [21]. A detailed description of the method can be found, e.g., in Refs. [22–24].

Accurate wave functions can be constructed alternatively by applying the multiconfigurational Dirac-Fock (MCDF) method [16]. Here, the wave functions are also constructed as a superposition of CSFs. However, in contrast to CI, the CSFs are not fixed, but iteratively optimized to achieve self-consistency of the result. For our calculations we utilized the newest version of the GRASP2K package [25].

Experimental method. For the experimental investigation of the $^{229}Th^{2+}$ hyperfine structure we use ions stored in a radio-frequency linear Paul trap [26]. The ions are cooled to room temperature by collisions with a buffer gas (He) at 0.1 Pa pressure, which also depopulates metastable states via collisional quenching. To prepare a sample of Th^{2+} ions we first load 10^5 Th^+ ions into the trap via laser ablation and then generate doubly charged ions via photoionization. We reach a stable amount of 10^3 Th^{2+} ions, defined by an equilibrium of the ionization rate and losses due to chemical reactions with impurities in the buffer gas.

We study single-photon excitations at two different frequencies which can be addressed by external-cavity diode lasers (see Fig. 1). The levels $5f^2(J=4) : 15\,148\ \mathrm{cm}^{-1}$ and $5f^2(J=4) : 21\,784\ \mathrm{cm}^{-1}$ are excited from the electronic ground state $5f6d(J=4) : 0\ \mathrm{cm}^{-1}$ via laser radiation at 660.1 and 459.1 nm, respectively. Both upper levels possess a fluorescence decay channel in the visible spectrum that is detectable by photomultiplier tubes. In addition, the decay from $5f^2(J=4) : 2\,1784\ \mathrm{cm}^{-1}$ is spectrally separated from the excitation, allowing for a detection free from the background of laser stray light.

Furthermore, our analysis includes hyperfine spectroscopy data from a previous experiment [7], which utilizes Doppler-free two-step laser excitation to achieve a higher resolution [27,28]. This experiment was conducted at the Maier-Leibnitz-Laboratorium at LMU Munich using a ^{233}U source, which produces thorium recoil ions via alpha decay with 2% of the ions being in the isomeric nuclear state. The selected transition in this case was from the $6d^2(J=2) : 63\ \mathrm{cm}^{-1}$ electronic state to $5f^2(J=0) : 29\,300\ \mathrm{cm}^{-1}$ via the $5f6d(J=1) : 20\,711\ \mathrm{cm}^{-1}$ intermediate state, using laser radiation at 484.3 nm for the first and 1164.3 nm for the second step.

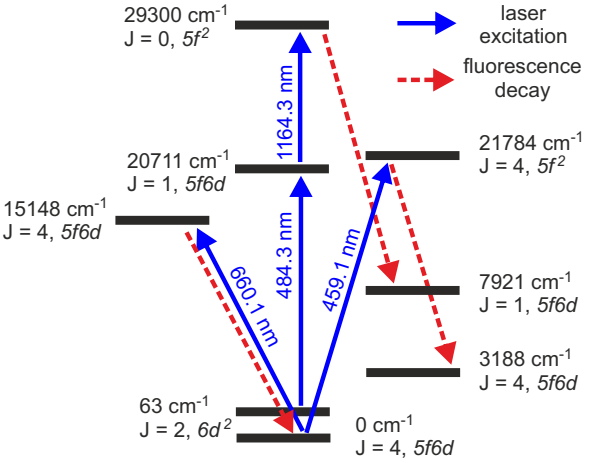

FIG. 1. Scheme of the investigated $^{229}Th^{2+}$ levels. The transitions and electronic configurations of Th^{2+} levels relevant to the experiment are depicted, labeled by their energy in cm^{-1} and the electronic angular momentum J. Laser excitation is shown with solid arrows and fluorescence detection with dashed arrows.

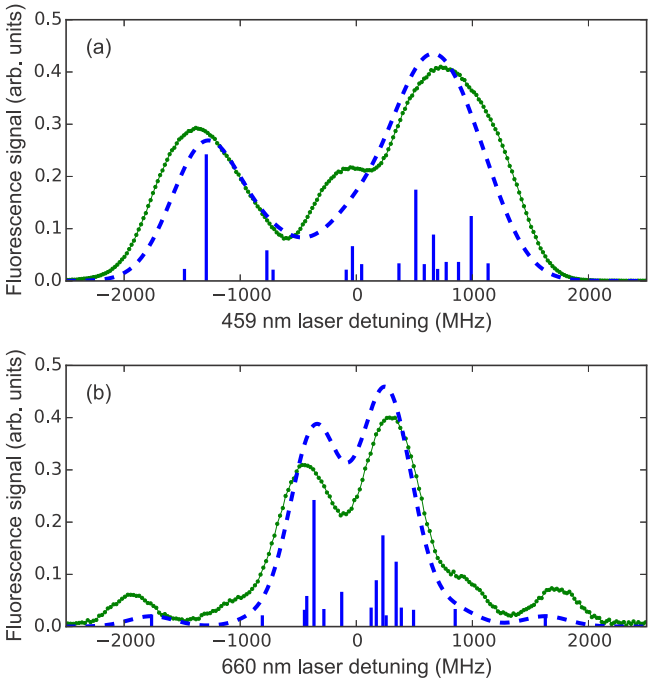

FIG. 2. Recorded $^{229}Th^{2+}$ hyperfine spectra. (a) Transition $5f6d(J=4): 0\ cm^{-1}$ to $5f^2(J=4): 21\,784\ cm^{-1}$, (b) transition $5f6d(J=4): 0\ cm^{-1}$ to $5f^2(J=4): 15\,148\ cm^{-1}$. Each subfigure shows the experimental data (connected dots) together with the positions of the individual resonances as predicted by MCDF calculations and the resulting theoretical spectrum (dashed line).

For detection, the fluorescence line from the decay of the $5f^2(J=0): 29\,300\ cm^{-1}$ state to $5f6d(J=1): 7921\ cm^{-1}$ was chosen.

Results and discussion. The hyperfine coefficients for $^{229}Th^{3+}$ were measured with high precision [29] and theoretical calculations of these coefficients have been presented in Ref. [13], including the extraction of the values $\mu_{gr} = 0.36\mu_N$ and $Q_{gr} = 3.11$ eb for the moments of the ground-state ^{229}Th nucleus. We used these moments to obtain the hyperfine constants for the ground and the first few excited states of $^{229}Th^{3+}$ using the MCDF method. We found these results to be in good agreement with previous calculations and thus the experimental values. Although triply charged thorium is a considerably simpler system, it resembles a very good test case for our calculations for Th^{2+}, because in both ions f and d orbitals are populated for the two lowest states, favoring strong core-valence correlation effects. The good agreement with the experiment thus gives us confidence that we are able to numerically control these correlations, also in the case of Th^{2+}.

While our calculations for triply charged thorium were an important benchmark, the complexity of the problem for doubly charged thorium is still considerably higher. The Th^{2+} ion has 45 levels in the desired energy range between 0 and 25 000 cm^{-1}, ranging from three ($J^\Pi = 1^-$) to six ($J^\Pi = 2^+$ and $J^\Pi = 3^-$) for each pair of J and Π [cf. Eq. (3)]. Although only a few levels were addressed in the experiment, all of these levels need to be described to the same accuracy to obtain reliable theoretical results. Therefore the achievable accuracy of our calculations is worse than in other effective two-electron systems.

To obtain results for the level structure of the $^{229}Th^{2+}$ ion with the MCDF method, we first performed calculations, where the set of CSFs was constructed from a closed radon core allowing for double excitations of the two valence electrons. We added correlation layers until the energies of the calculated levels completely converged. These results were then used to perform calculations, where we subsequently added single excitations from the core up to the argon shell. After also allowing for core-valence excitations from the $6p$ and $5d$ orbitals we eventually achieved a very good convergence of the results. As it can be seen from Table I, our agreement with experimental excitation energies [30] is always better than 10%, except for the lowest $6d^2(J=2): 63\ cm^{-1}$ state. The energy of this state is particularly difficult to obtain, because it is almost degenerate with the $5f6d(J=4): 0\ cm^{-1}$ ground state. The accuracy of the CI+MBPT calculation is somewhat lower. The reason is strong correlations between two valence electrons and the outermost core shells. In order to increase the accuracy, one needs to go beyond the second-order MBPT and use CI+AO (CI+all-order) [31–33]. Our main goal here is to check that two very different methods give consistent results. For this purpose our CI+MBPT calculation is sufficient.

After we obtained the many-electron wave functions, we calculated the hyperfine coefficients for all states that were investigated experimentally. First, we used these results to analyze the spectra that have been obtained using the single-step excitation scheme (cf. Fig. 1). As seen in Fig. 2, the limited resolution of these spectra does not allow us to extract experimental values of the hyperfine constants for the electronic ground and the two $5f^2(J=4)$ states. Instead, we utilized the MCDF results for the A and B constants of these states (cf. Table I) to make a prediction for the positions of the individual resonances and the overall shape of the hyperfine spectrum. In Fig. 2 this prediction is shown alongside the

TABLE I. Magnetic dipole and electric quadrupole hyperfine constants A and B for the ground and four excited states of $^{229}Th^{2+}$. The theoretical results are obtained using CI+MBPT and the MCDF method. In lines two and four a comparison is drawn to experimental values presented in Ref. [7]. For the calculation, $\mu_{gr} = 0.36\mu_N$ and $Q_{gr} = 3.11|e|b$ have been used [13]. The experimental energies have been taken from Ref. [30].

Level		Energy (cm^{-1})			A (MHz)			B (MHz)		
Configuration	J^Π	CI+MBPT	MCDF	Expt. [30]	CI+MBPT	MCDF	Expt. [7]	CI+MBPT	MCDF	Expt. [7]
$[Rn] + 5f6d$	4^-	0	0	0	64(17)	81(4)		3287(630)	3008(260)	
$[Rn] + 6d^2$	2^+	2933	447	63	143(47)	162(8)	151(8)	68(23)	71(7)	73(27)
$[Rn] + 5f^2$	4^+	23223	14891	15148	38(3)	72(3)		1221(390)	1910(200)	
$[Rn] + 5f6d$	1^-	21193	22121	20711	109(36)	90(4)	88(5)	839(220)	689(110)	901(18)
$[Rn] + 5f^2$	4^+	19946	21959	21784	8(36)	26(2)		65(21)	39(45)	

experimentally recorded spectra. While the positions of the main resonances match rather well, some discrepancies in the line intensities occur, especially for the $5f6d(J = 4) : 0\ cm^{-1}$ to $5f^2(J = 4) : 21\,784\ cm^{-1}$ transition. Moreover, the overall width of the calculated spectrum is slightly smaller than it was measured.

In contrast to the spectra recorded from the single-step excitation which were limited in resolution by Doppler broadening, the Doppler-free spectra, presented in Ref. [7], of the $6d^2(J = 2) : 63\ cm^{-1}$ and $5f6d(J = 1) : 20\,711\ cm^{-1}$ states allowed for a precise extraction of the hyperfine constants A and B. In Table I we show our numerical results alongside these experimentally extracted values. The theoretical uncertainty of the MCDF results is obtained from a convergence analysis with respect to the addition of correlation layers as well as the number of opened core shells. The uncertainty of the CI+MBPT results is determined by the neglected high-order MBPT terms. We estimated them from the size of the second-order MBPT and random phase approximation (RPA) corrections. We can see in Table I that the agreement between theory and experiment is very good for the magnetic hyperfine constant A. In the case of the electric quadrupole constant B, the agreement is slightly worse but still satisfying.

To obtain the values for the hyperfine constants A and B [cf. Eqs. (2)] shown in Table I, we used the nuclear moments of ^{229}Th from Ref. [13]. While these values for the ground-state nucleus are commonly accepted, the measured value of the nuclear dipole moment of the nuclear isomer ^{229m}Th [7] disagrees strongly with previous theoretical works [10,14]. As an example for a possible application of our calculations and to help to resolve this controversy, we calculated the atomic parts A/μ_{iso} and B/Q_{iso} of the hyperfine constants in the doubly charged nuclear isomer $^{229m}Th^{2+}$, which has a nuclear spin of $I_{iso} = \frac{3}{2}$ in contrast to the nuclear ground state with $I_{gr} = \frac{5}{2}$. By combining these calculations with measurements for A and B, we can extract the nuclear moments of the nuclear isomer to a high precision. The results of these calculations are shown in Table II. In Ref. [7], μ_{iso} has been determined by measuring the ratio μ_{iso}/μ_{gr} and using μ_{gr} from Ref. [13]. The obtained value of $\mu_{iso} = -0.37(6)\mu_N$ coincides with our consideration, which gives an average value of $\mu_{iso}-0.35\mu_N$. Therefore, our calculations affirm the measurements and thus provide a stronger foundation for the obtained value of the magnetic dipole moment of the nuclear isomer ^{229m}Th. An analog consideration for Q_{iso} shows a very good agreement between the value obtained using the CI+MBPT method and the experimental value of $Q_{iso} = 1.74(8)$ eb, while the result from the MCDF method is slightly above the measured result.

Concluding remarks. In summary, we aimed for a theoretical prediction of the hyperfine structure of doubly charged thorium with the nucleus being in the ground, and the first isomeric state. Therefore we employed two different approaches: (i) a combination of many-body perturbation theory and configuration interaction and (ii) the multiconfigurational Dirac-Fock method. We performed large-scale calculations for the hyperfine constants A and B in $^{229}Th^{2+}$. The results of these calculations were based on the nuclear moments [13] and reproduced the experimental data very well. That is, we provide an independent confirmation of the calculations presented by Safranova *et al.* in a system with a more complicated electronic structure and a different experimental setup. Finally, we also obtained the magnetic dipole moment of the nuclear isomer

TABLE II. Atomic part of the magnetic dipole hyperfine constant A/μ_{iso} for two excited states of $^{229m}Th^{2+}$. The results have been obtained using (a) the CI+MBPT and (b) the MCDF method. The experimental values presented in Ref. [7] are utilized to extract the magnetic dipole μ_{iso} and electric quadrupole Q_{iso} moment of the ^{229m}Th nuclear isomer.

Energy level			A/μ_{iso} (MHz/μ_N)		A (MHz)	μ_{iso} (μ_N)		B/Q_{iso} (MHz/eb)		B (MHz)	Q_{iso} (eb)	
Configuration	J^Π	Energy (cm^{-1})	(a)	(b)	Expt. [7]	(a)	(b)	(a)	(b)	Expt. [7]	(a)	(b)
$[Rn] + 6d^2$	2^+	63	660	749	−263(29)	−0.40	−0.35	22	23	53(65)		
$[Rn] + 5f6d$	1^-	20711	506	419	−151(22)	−0.30	−0.36	270	222	498(15)	1.84	2.24

using measurements of the hyperfine constant A and calculations for the ratio $A/\mu_{\rm iso}$. Our result of $\mu_{\rm iso} = -0.35\mu_{\rm N}$ rules out a previous theoretical work that estimated the magnetic dipole moment to be $\mu_{\rm iso} = -0.076\mu_{\rm N}$. This discrepancy arose first in Ref. [7], where Ref. [13] has been used to obtain $\mu_{\rm iso}$. Our work complements these studies by providing an independent value for the nuclear magnetic dipole moment of ^{229m}Th. Therefore our theory allows for a better understanding of the low-lying nuclear isomer. Combined with further theoretical and experimental investigations, our results will moreover help to use thorium as a testground for fundamental physics [8–10].

Acknowledgments. R.A.M. and A.V.M. would like to thank Mikhail Kozlov for his support and many helpful discussions. R.A.M. acknowledges support by the RS-APS. A.V.M. acknowledges support by the Ministry of Education and Science of the Russian Federation (Grant No. 3.1463.2017/4.6) and by RFBR (Grant No. 17-02-00216). We thank Lars von der Wense, Benedikt Seiferle, and Peter Thirolf from LMU Munich for their contributions to joint experiments. We acknowledge financial support from the European Union's Horizon 2020 Research and Innovation Programme under Grant Agreement No. 664732 (nuClock) and from DFG through CRC 1227 (DQ-mat, project B04).

[1] L. Kroger and C. Reich, Nucl. Phys. A **259**, 29 (1976).
[2] C. W. Reich and R. G. Helmer, Phys. Rev. Lett. **64**, 271 (1990).
[3] Z. O. Guimarães-Filho and O. Helene, Phys. Rev. C **71**, 044303 (2005).
[4] E. Peik and M. Okhapkin, C. R. Phys. **16**, 516 (2015).
[5] C. J. Campbell, A. G. Radnaev, A. Kuzmich, V. A. Dzuba, V. V. Flambaum, and A. Derevianko, Phys. Rev. Lett. **108**, 120802 (2012).
[6] G. A. Kazakov, A. N. Litvinov, V. I. Romanenko, L. P. Yatsenko, A. V. Romanenko, M. Schreitl, G. Winkler, and T. Schumm, New J. Phys. **14**, 083019 (2012).
[7] J. Thielking, M. V. Okhapkin, P. Głowacki, D. M. Meier, L. von der Wense, B. Seiferle, C. E. Düllmann, P. G. Thirolf, and E. Peik, Nature (London) **556**, 321 (2018).
[8] V. V. Flambaum, Phys. Rev. Lett. **97**, 092502 (2006).
[9] J. C. Berengut, V. A. Dzuba, V. V. Flambaum, and S. G. Porsev, Phys. Rev. Lett. **102**, 210801 (2009).
[10] E. Litvinova, H. Feldmeier, J. Dobaczewski, and V. Flambaum, Phys. Rev. C **79**, 064303 (2009).
[11] B. R. Beck, J. A. Becker, P. Beiersdorfer, G. V. Brown, K. J. Moody, J. B. Wilhelmy, F. S. Porter, C. A. Kilbourne, and R. L. Kelley, Phys. Rev. Lett. **98**, 142501 (2007).
[12] E. V. Tkalya, C. Schneider, J. Jeet, and E. R. Hudson, Phys. Rev. C **92**, 054324 (2015).
[13] M. S. Safronova, U. I. Safronova, A. G. Radnaev, C. J. Campbell, and A. Kuzmich, Phys. Rev. A **88**, 060501 (2013).
[14] A. M. Dykhne and E. V. Tkalya, JETP Lett. **67**, 251 (1998).
[15] L. von der Wense, B. Seiferle, M. Laatiaoui, J. B. Neumayr, H.-J. Maier, H.-F. Wirth, C. Mokry, J. Runke, K. Eberhardt, C. E. Düllmann, N. G. Trautmann, and P. G. Thirolf, Nature (London) **533**, 47 (2016).
[16] I. P. Grant, *Relativistic Quantum Theory of Atoms and Molecules: Theory and Computation* (Springer, Berlin, 2007).
[17] V. A. Yerokhin, A. N. Artemyev, V. M. Shabaev, M. M. Sysak, O. M. Zherebtsov, and G. Soff, Phys. Rev. Lett. **85**, 4699 (2000).
[18] A. N. Artemyev, V. M. Shabaev, I. I. Tupitsyn, G. Plunien, and V. A. Yerokhin, Phys. Rev. Lett. **98**, 173004 (2007).
[19] N. S. Oreshkina, D. A. Glazov, A. V. Volotka, V. M. Shabaev, I. I. Tupitsyn, and G. Plunien, Phys. Lett. A **372**, 675 (2008).
[20] V. A. Yerokhin and A. Surzhykov, Phys. Rev. A **86**, 042507 (2012).
[21] M. Kozlov, S. Porsev, M. Safronova, and I. Tupitsyn, Comput. Phys. Commun. **195**, 199 (2015).
[22] V. A. Dzuba, V. V. Flambaum, and M. G. Kozlov, Phys. Rev. A **54**, 3948 (1996).
[23] V. A. Dzuba, Phys. Rev. A **71**, 032512 (2005).
[24] V. A. Dzuba and V. V. Flambaum, Phys. Rev. A **75**, 052504 (2007).
[25] P. Jönsson, G. Gaigalas, J. Bieroń, C. F. Fischer, and I. Grant, Comput. Phys. Commun. **184**, 2197 (2013).
[26] O. A. Herrera-Sancho, M. V. Okhapkin, K. Zimmermann, C. Tamm, E. Peik, A. V. Taichenachev, V. I. Yudin, and P. Głowacki, Phys. Rev. A **85**, 033402 (2012).
[27] J. E. Bjorkholm and P. F. Liao, Phys. Rev. A **14**, 751 (1976).
[28] W. Kälber, J. Rink, K. Bekk, W. Faubel, S. Göring, G. Meisel, H. Rebel, and R. C. Thompson, Z. Phys. A: At. Nucl. **334**, 103 (1989).
[29] C. J. Campbell, A. G. Radnaev, and A. Kuzmich, Phys. Rev. Lett. **106**, 223001 (2011).
[30] A. Kramida, Yu. Ralchenko, J. Reader, and NIST ASD Team, (2015) published: NIST Atomic Spectra Database (ver. 5.3) (online), available at http://physics.nist.gov/asd (25 September 2017), National Institute of Standards and Technology, Gaithersburg, MD.
[31] M. G. Kozlov, Int. J. Quantum Chem. **100**, 336 (2004).
[32] M. S. Safronova, M. G. Kozlov, W. R. Johnson, and D. Jiang, Phys. Rev. A **80**, 012516 (2009).
[33] M. V. Okhapkin, D. M. Meier, E. Peik, M. S. Safronova, M. G. Kozlov, and S. G. Porsev, Phys. Rev. A **92**, 020503 (2015).

Electronic level structure of Th^+ in the range of the ^{229m}Th isomer energy

D.-M. Meier,[1] J. Thielking,[1] P. Głowacki,[1,*] M. V. Okhapkin,[1] R. A. Müller,[1] A. Surzhykov,[1,2] and E. Peik[1,†]
[1]*Physikalisch-Technische Bundesanstalt, 38116 Braunschweig, Germany*
[2]*Technische Universität Braunschweig, 38106 Braunschweig, Germany*

(Received 22 February 2019; published 29 May 2019)

Using resonant two-step laser excitation of trapped $^{232}Th^+$ ions, we observe 166 previously unknown energy levels of even parity within the energy range from 7.8 to 9.8 eV and angular momenta from $J = 1/2$ to $7/2$. We also classify the high-lying levels observed in our earlier experiments by the total angular momentum and perform multiconfiguration Dirac-Fock calculations to compare their results with the observed level density. The observed levels can be relevant for the excitation or decay of the ^{229m}Th isomeric nuclear state which lies in this energy range. The high density of electronic levels promises a strongly enhanced electronic bridge excitation of the isomer in $^{229}Th^+$.

DOI: 10.1103/PhysRevA.99.052514

I. INTRODUCTION

The atomic structure of thorium, the third-heaviest naturally occurring element, has been a subject of study because of applications in various fields. With four valence electrons in neutral Th and strongly mixed $5f$, $6d$, $7s$, and $7p$ configurations the atomic spectrum is dense and complex [1]. The high density of lines makes thorium discharge lamps suitable for the calibration of spectrographs over wide spectral ranges, for example, in astronomical observatories [2,3]. In a recent analysis of the spectra of Th, Th^+, and Th^{2+}, Ritz wavelengths of about 20000 lines are given together with 787 energy levels of Th and 516 of Th^+ [3].

In our earlier work [4] on Th^+ we have seen the onset of repulsion in the energy spacing between levels of identical parity and angular momentum, as it is expected for strong configuration mixing, leading to the appearance of chaotic quantum dynamics [5].

Work on excited states in Th^+ is motivated by the search for laser excitation of the ^{229m}Th nuclear isomer at 7.8eV excitation energy. This energy has been inferred from γ spectrocopy [6,7] with an uncertainty $\sigma = 0.5$ eV, that is large on the scale of optical spectroscopy. No direct optical spectroscopy of the nuclear transition has been possible so far. Since the electronic level density in this energy range is high, it can be expected that laser excitation of the isomer and radiative decay are dominated by so-called electronic bridge processes, where the electron shell enhances the coupling of the nucleus to the radiation field [8–11], determined by the detuning between nuclear and electronic resonance. Therefore, it is likely to find strong enhancement in a system with high electronic level density. A tentative experimental indication of this mechanism could be conjectured from the observation of a strongly reduced lifetime of the isomer in Th^+ in comparison to Th^{2+} and Th^{3+} [12,13].

In a previous publication [4] 44 unknown energy levels of Th^+ were reported within the energy range from 7.3 to 8.3 eV, obtained from two-step laser excitation of trapped Th^+ ions. Extending this study, we present here 166 additional levels of even parity up to 9.8 eV energy and classify these and the levels reported earlier according to their total angular momentum. In order to excite different configurations and different values of the angular momentum, 15 different intermediate levels are used as first excitation steps from the ground state. Figure 1 gives a schematic overview of the excitation schemes and Table I lists the leading electronic configurations of the intermediate levels used in our experiments.

The range of excitation energy that is investigated here covers more than 2σ above the ^{229m}Th isomer energy of 7.8 ± 0.5 eV, but is still well below the ionization potential of Th^+ of 12.1(2) eV [4]. A further increase in level density by up to a factor 10 has been predicted in approaching the ionization energy [17]. Multiconfigurational Dirac-Fock (MCDF) calculations are used to estimate the level density in the range of the excitation energy of the nuclear isomer.

II. EXPERIMENT

For the experiments we use a linear Paul trap with the capacity to store up to 10^6 $^{232}Th^+$ ions, described in Refs. [18,19]. The trap is loaded by ablating a metallic ^{232}Th target using a Nd:YAG laser emitting 5ns pulses with an energy of $\leqslant$1 mJ at 1064 nm. Argon buffer gas at 0.1 Pa pressure is used to cool the trapped ions to room temperature and to depopulate metastable states by collisional quenching [18,19]. We dissociate Th^+ molecular compounds which are formed in the trap with impurities of the buffer gas (see [4]) with the fourth harmonic radiation of a Q-switched solid state laser at 266 nm and a pulse energy of $\approx$10 μJ.

The search of new levels is carried out by a two-step excitation: an odd-parity intermediate level (see Table I) is excited from the ground state and the radiation frequency of

*Present address: Poznań University of Technology, Poznań, Poland.
†Corresponding author: ekkehard.peik@ptb.de

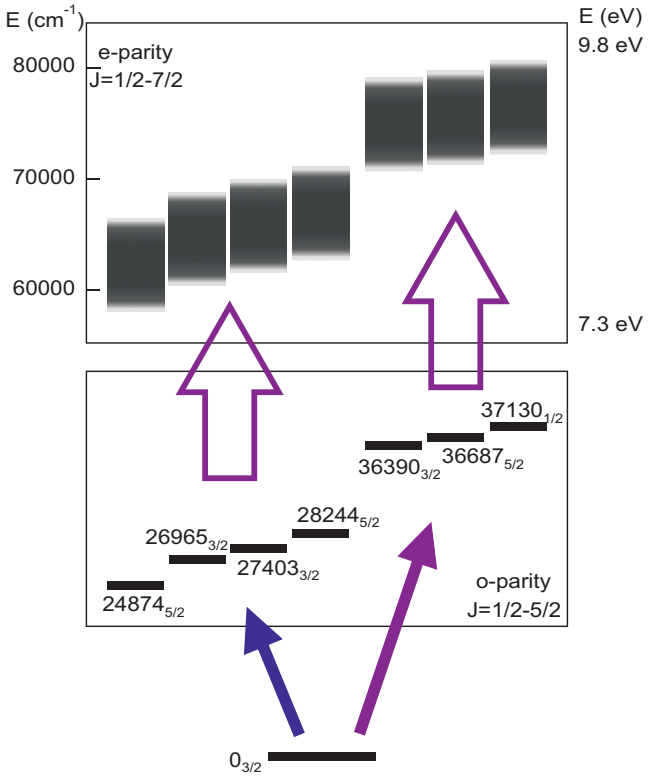

FIG. 1. Two-step laser excitation scheme in Th^+, starting from the ground state through different odd-parity intermediate levels (middle panel) to high-lying levels within the indicated energy ranges (upper panel). Levels are labeled by their energy in cm^{-1} and their total angular momentum J.

a second laser is tuned over a wide frequency range to excite unknown even-parity high-lying levels from the intermediate level. A scheme of the experimental setup is shown in Fig. 2. The first excitation step is provided by the radiation of a second harmonic (SHG) or third harmonic generation (THG) of a pulsed Ti:Sa laser (TU model, Photonics Industries). For the second excitation step we use the radiation of a THG of a second pulsed Ti:Sa laser (Credo, Sirah Lasertechnik).

Both lasers emit synchronized pulses with a duration of ≈20 ns and a repetition rate of 1kHz. The beam diameters of both lasers, which are matched at the position of the ions in the linear Paul trap, are ≈1 mm and the peak powers used in the experiment are up to 0.1 kW, which corresponds to intensities of 10 kW/cm^2. The wavelengths of both lasers are measured by a Fizeau wavemeter (HighFinesse/Angstrom WS-7). The first laser wavelength is stabilized to the center of the Doppler-broadened line of one of a set of selected intermediate levels by a computer-based locking scheme using the wavemeter readout. The second laser is tunable by controlling an intracavity diffraction grating and simultaneously adjusting the orientation of the frequency conversion crystals. The third harmonic radiation is tuned in the range from 240 to 293 nm at a tuning rate of 0.001 nm/s in frequency steps of ≈500 MHz (0.1 pm) or ≈100 MHz for fine scans. In the search for new levels we determine the line center of each transition by repeated fine scanning over the line.

TABLE I. Intermediate levels of the two-step excitation, sorted by angular momentum J. Energies and leading configurations are taken from Ref. [14], with the exception of the corrected classification of the 25027 cm^{-1} state described in Ref. [15]. Labels in the first column are introduced for reference in the Supplemental Material [16].

Ref.	Level (cm^{-1})	J	Configuration
a	25027.040	1/2	$7s7p + 6d7s7p$
b	26626.478	1/2	$6d7s(^3D)7p\ ^4D^o + (^3D)\ ^2P^o$
c	35198.990	1/2	$6d^2(^3P)7p\ ^4D^o + 6d7s(^3D)7p\ ^4P^o$
d	37130.340	1/2	$5f(^1G^o)6d^2\ 2P^o + 6d^2(^3P)7p\ ^4D^o$
e	37716.322	1/2	$6d^2(^1D)7p\ ^2P^o + (^3F)\ ^4D^o$
f	26965.202	3/2	$5f(^3F^o)6d^2\ 4S^o + (^3F^o)\ ^2P^o$
g	27403.180	3/2	$5f(^1D^o)6d^2\ 2D^o + (^3P^o)\ ^4D^o$
h	36390.527	3/2	$6d^2(^3F)7p\ ^4F^o + 5f(^1G^o)6d^2\ 2P^o$
i	36581.568	3/2	$6d^2(^3F)7p\ ^4F^o + 5f(^1G^o)6d^2\ 2D^o$
j	24873.981	5/2	$6d7s(^3D)7p\ ^4F^o + 5f(^3P^o)6d^2\ 4F^o$
k	26424.480	5/2	$5f(^3P^o)6d^2\ 4F^o + (^3P^o)\ ^4D^o$
l	28243.812	5/2	$6d7s(^3D)7p\,4F^o + 6d^2(^3F)7p\ ^4G^o$
m	35156.916	5/2	$5f(^1G^o)6d^2\ 2D^o + (^1G^o)\ ^2F^o$
n	36687.992	5/2	$6d^2(^3F)7p\,4F^o + 6d7s(^3D)7p\ ^4P^o$
o	37846.174	5/2	$6d^2(^3P)7p\,2D^o + (^3P)\ ^4D^o$

For the detection of the fluorescence decay of the high-lying electronic levels we use two photomultiplier tubes (PMT) for different spectral ranges. Photons are detected in the range from 300 to 650 nm with a PMT which is equipped with a long-pass edge interference filter to block laser stray light from the Ti:Sa laser pulses. A second PMT is used for the detection of VUV photons in the wavelength range from 115 to 230 nm. Fast gated integrators are used to evaluate the PMT signals during a detection window of 100 ns, starting after the excitation pulses. Counters are used to detect photons in the interval from 1 to 10 μs after the excitation pulses.

We try to excite each observed level via several intermediate levels with different values of the angular momentum (see

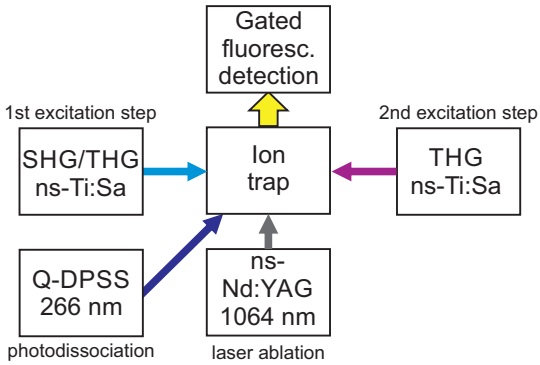

FIG. 2. Experimental setup for laser excitation of trapped Th^+ ions. The first step excitation is provided by the second harmonic (SHG) or third harmonic (THG) radiation of a nanosecond Ti:Sa laser, locked to a Fizeau wavemeter. The second excitation step is provided by the THG of a second ns-Ti:Sa laser. Th^+ ions are loaded via laser ablation (ns-Nd:YAG laser at 1064 nm). Molecular compounds of Th^+ are photodissociated by pulses from a Q-switched diode-pumped solid-state laser (Q-DPSS) at 266 nm.

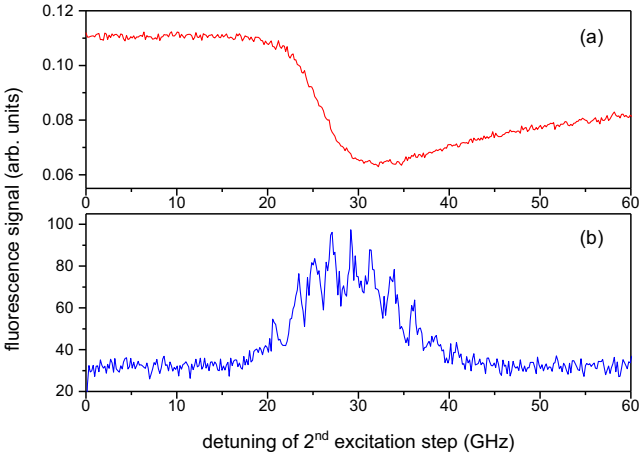

FIG. 3. Two-step excitation of the level 74195.13 cm^{-1} via the intermediate level $35156.9_{5/2}$ cm^{-1}. Graph (a) shows the decrease of the fluorescence signal of the intermediate level (wavelength range from 325 to 650 nm) due to three-photon ionization during the scan from negative to positive detunings. The slight increase of the signal after the excitation occurs due to redistribution of Th^+ ions in the trap. Graph (b) shows the simultaneously recorded VUV fluorescence signal of the decay of the high-lying level. The line shape is determined by the multimode spectrum of the Ti:Sa laser radiation. The start of the scan at 0GHz laser detuning corresponds to the wave number 39039.15 cm^{-1} of the second excitation step laser radiation.

Table I) to confirm them as high-lying levels and determine their total angular momenta.

III. NEWLY OBSERVED LEVELS

Within the search scans we not only observe direct two-step excitation to high-lying levels, but also single-photon transitions originating from the ground state, thermally populated metastable levels (up to 4490 cm^{-1}), and levels populated by a decay of the intermediate level (N-scheme transition). Most of these transitions can be identified based on the existing energy level database [14]. In order to unambiguously identify new levels at an excitation energy corresponding to the sum of the two laser photon energies, we are required to observe the excitation via at least two intermediate levels.

Excitation of a high-lying level is inferred by observing either fluorescence at a wavelength different from the excitation wavelength, depletion of fluorescence from the decay of the intermediate level, or a loss of ions because of resonance-enhanced three-photon ionization; see Fig. 3. Due to the high pulse power of the Ti:Sa laser radiation there is a significant probability of absorption of a third photon when a high-lying level is excited. The absorption of this photon leads to ionization of the Th^+ ions to Th^{2+} ions [4]. We select the operating parameters of our ion trap so that Th^{2+} is not stably trapped. Nevertheless, ionization alone cannot be a confirmation of the high-lying level excitation, because it can also occur as a resonant four-photon process in an N-scheme excitation through levels with an energy of about 20000 cm^{-1}, listed in Ref. [14].

By applying the aforementioned criteria, two-photon excitations to 166 previously unknown high-lying energy levels in the investigated energy range from 7.3 to 9.8 eV are identified and listed in Table II. In a table given in the Supplemental Material [16] a complete list with the successful excitation pathways via the different intermediate levels is provided. We achieve a total uncertainty for the energy determination of $\sigma_{tot} \sim 0.2$ cm^{-1}, limited by the uncertainty of identifying the center of the Ti:Sa laser spectrum from the wavemeter readout. The energy of a high-lying level is derived as the mean value from the different excitation pathways, weighted with the statistical uncertainty of the individual measurements. The measured center wavelengths of the transitions from the ground state to the intermediate levels mentioned in Table I are in coincidence with the values given in Ref. [14].

In comparison to the previous experiment [4] we see an agreement of the measured energies of these levels, except for one level. The energy of the level marked with a double asterisk in Table II is measured to be 65738.54 cm^{-1}, shifted by $\approx 2\sigma$ from the previous value. We verified the existence of the level and update its energy to the new value, which is based on the excitations from three intermediate levels. A level mentioned at 66427.14 cm^{-1} in Ref. [3] is not observed in our experiment.

IV. DETERMINATION OF THE TOTAL ANGULAR MOMENTA

The observed signal strengths at the applied second step laser intensities in the range of 10 kW/cm^2 are in the range expected for electric dipole transitions [4]. Therefore, we assume that the observed transitions are electric dipole allowed. Selection rules then require these high-lying levels to have even parity and angular momenta from $J = 1/2$ to $7/2$, since we are using intermediate levels with $J = 1/2$ to $5/2$.

Analyzing the excitation through different intermediate levels allows for the determination of the total angular momentum of the newly found levels. In our experiment high-lying levels with $J = 3/2$ can be accessed via all intermediate levels. These states can therefore be unambiguously classified. Angular momenta $J = 1/2$, $5/2$, and $7/2$ can only be identified by the absence of excitation through intermediate levels that would not fulfill the $\Delta J = 0, \pm 1$ selection rule.

In these cases, the absence of a single excitation path does not allow a sure assignment of the J value, as we observe that some high-lying levels can be excited through only one out of two intermediate levels with the same J (see, e.g., level 67577.7 cm^{-1} in the Supplemental Material [16]). This is because intermediate levels with the same total angular momenta can have different electronic configurations (see Table I) and therefore the excitation probabilities of the high-lying levels can be substantially different. Hence we require the absence of excitation through at least two intermediate levels with the same J to consider the level not being excitable via this particular J. In all other cases we give the range of possible angular momenta.

Using the same excitation scheme we also determine the angular momenta of levels which could not be classified in Ref. [4].

TABLE II. Newly found electronic levels in $^{232}Th^{+}$ in the energy range from 7.8 to 9.8 eV, total uncertainties σ_{tot} of the energy determination, and possible angular momenta. The angular momentum value $J = 3/2$ is assigned with certainty; otherwise, the most likely values of J are given (see text). Levels marked with an asterisk were found in the previous investigation [4] with an uncertainty of 0.2 cm^{-1} and are classified in this investigation. We update the energy value of a previously found level, marked with a double asterisk.

Energy (cm^{-1})	σ_{tot} (cm^{-1})	J	Energy (cm^{-1})	σ_{tot} (cm^{-1})	J	Energy (cm^{-1})	σ_{tot} (cm^{-1})	J
58875.5	*	3/2–7/2	68564.19	0.18	3/2 or 5/2	74195.13	0.17	3/2–7/2
59387.1	*	3/2–7/2	68598.83	0.18	3/2 or 5/2	74201.68	0.16	1/2 or 3/2
59477.4	*	3/2	68752.06	0.17	3/2	74255.11	0.17	3/2 or 5/2
59803.0	*	3/2–7/2	68812.64	0.18	3/2 or 5/2	74328.90	0.17	3/2 or 5/2
60380.1	*	3/2	68898.67	0.17	3/2 or 5/2	74396.40	0.16	3/2 or 5/2
60618.6	*	3/2	68921.30	0.17	3/2 or 5/2	74461.06	0.17	3/2–7/2
60721.3	*	3/2–7/2	69582.93	0.17	3/2	74503.38	0.18	3/2 or 5/2
61032.4	*	3/2	70036.57	0.17	3/2	74554.39	0.16	3/2
61388.0	*	3/2–7/2	70602.32	0.16	3/2 or 5/2	74642.51	0.17	3/2 or 5/2
61428.6	*	3/2 or 5/2	70618.40	0.16	3/2 or 5/2	74646.94	0.16	1/2 or 3/2
61726.3	*	3/2	70747.82	0.16	3/2–7/2	74781.76	0.17	3/2 or 5/2
61963.6	*	3/2	70924.75	0.16	3/2 or 5/2	74823.59	0.16	3/2 or 5/2
62307.2	*	3/2 or 5/2	71038.37	0.16	3/2	74881.76	0.17	3/2
62373.8	*	3/2	71043.67	0.15	3/2–7/2	75009.01	0.18	3/2 or 5/2
62477.0	*	3/2 or 5/2	71148.96	0.16	3/2 or 5/2	75058.06	0.17	3/2–7/2
62560.1	*	3/2 or 5/2	71153.87	0.16	3/2	75108.36	0.17	3/2 or 5/2
62562.2	*	3/2	71278.32	0.16	1/2 or 3/2	75129.42	0.17	1/2–5/2
62753.1	*	3/2 or 5/2	71309.24	0.16	3/2 or 5/2	75172.74	0.19	3/2 or 5/2
62873.11	0.17	1/2 or 3/2	71345.59	0.16	1/2 or 3/2	75324.44	0.17	3/2–7/2
63257.5	*	3/2–7/2	71457.82	0.16	3/2–7/2	75380.56	0.17	3/2 or 5/2
63268.90	0.17	1/2 or 3/2	71543.05	0.16	3/2	75434.83	0.17	3/2–7/2
63298.4	*	3/2–7/2	71544.12	0.16	1/2 or 3/2	75553.70	0.17	1/2 or 3/2
63557.7	*	3/2–7/2	71595.39	0.17	1/2–5/2	75568.80	0.17	3/2 or 5/2
63680.29	0.16	3/2	71648.63	0.16	1/2–5/2	75613.54	0.17	3/2
64107.51	0.17	3/2 or 5/2	71682.08	0.16	1/2 or 3/2	75690.72	0.17	1/2 or 3/2
64122.0	*	3/2–7/2	71704.43	0.16	3/2 or 5/2	75783.69	0.17	3/2 or 5/2
64150.3	*	3/2	71893.76	0.16	3/2	75840.96	0.16	3/2 or 5/2
64368.24	0.17	3/2 or 5/2	71980.22	0.17	3/2 or 5/2	75889.36	0.17	1/2 or 3/2
64442.11	0.16	1/2 or 3/2	71995.47	0.16	3/2–7/2	75950.56	0.17	3/2–7/2
64560.4	*	3/2	72027.87	0.16	3/2	75966.37	0.16	3/2
64813.7	*	3/2–7/2	72070.57	0.16	1/2 or 3/2	76122.62	0.16	1/2 or 3/2
64860.4	*	3/2 or 5/2	72183.47	0.17	3/2 or 5/2	76157.73	0.16	1/2 or 3/2
64887.80	0.16	1/2 or 3/2	72195.77	0.17	3/2 or 5/2	76158.83	0.17	3/2–7/2
64920.1	*	3/2 or 5/2	72353.67	0.17	3/2–7/2	76169.30	0.17	1/2–5/2
65037.7	*	3/2	72395.99	0.18	3/2 or 5/2	76227.32	0.17	1/2–5/2
65144.4	*	3/2 or 5/2	72403.45	0.16	3/2	76371.41	0.16	1/2 or 3/2
65191.1	*	3/2–7/2	72437.78	0.16	1/2 or 3/2	76445.96	0.16	1/2 or 3/2
65730.4	*	3/2	72443.68	0.16	3/2 or 5/2	76508.84	0.17	3/2–7/2
65738.54	0.18**	3/2–7/2	72612.99	0.18	3/2 or 5/2	76521.57	0.17	3/2 or 5/2
65753.45	0.17	1/2 or 3/2	72624.83	0.16	3/2	76552.60	0.16	3/2
65799.6	*	3/2	72644.97	0.16	3/2–7/2	76616.44	0.17	3/2–7/2
65910.0	*	3/2–7/2	72711.86	0.16	3/2–7/2	76788.94	0.16	1/2 or 3/2
65946.9	*	3/2–7/2	72748.31	0.16	3/2	76895.40	0.16	3/2
66052.0	*	3/2 or 5/2	72756.38	0.17	3/2–7/2	76954.26	0.16	3/2
66141.2	*	3/2 or 5/2	72849.84	0.16	3/2	76999.66	0.16	3/2–7/2
66324.52	0.17	1/2 or 3/2	72904.32	0.16	3/2–7/2	77069.42	0.17	3/2 or 5/2
66333.7	*	3/2	72937.01	0.17	3/2 or 5/2	77154.88	0.17	1/2–5/2
66388.81	0.17	1/2 or 3/2	72967.30	0.16	3/2	77185.31	0.16	3/2–7/2
66429.64	0.17	3/2 or 5/2	73007.80	0.16	1/2 or 3/2	77208.86	0.17	3/2 or 5/2
66558.0	*	3/2–7/2	73141.86	0.16	3/2	77278.24	0.16	1/2 or 3/2
66609.0	*	3/2 or 5/2	73171.82	0.17	3/2–7/2	77295.28	0.17	3/2 or 5/2
66666.96	0.17	1/2 or 3/2	73225.52	0.17	3/2	77311.25	0.16	3/2
66702.9	*	3/2	73245.52	0.17	3/2 or 5/2	77429.20	0.16	1/2 or 3/2
66831.1	*	3/2	73314.63	0.16	3/2–7/2	77506.72	0.16	1/2–5/2
66855.6	*	3/2 or 5/2	73349.33	0.18	1/2 or 3/2	77668.89	0.17	3/2 or 5/2
67066.2	*	3/2–7/2	73427.59	0.16	3/2	77715.95	0.17	1/2 or 3/2

TABLE II. (*Continued.*)

Energy (cm^{-1})	σ_{tot} (cm^{-1})	J	Energy (cm^{-1})	σ_{tot} (cm^{-1})	J	Energy (cm^{-1})	σ_{tot} (cm^{-1})	J
67154.05	0.16	3/2	73486.18	0.18	3/2 or 5/2	77914.52	0.16	1/2 or 3/2
67177.76	0.18	3/2–7/2	73506.20	0.16	1/2 or 3/2	77992.06	0.16	3/2–7/2
67378.61	0.19	3/2–7/2	73514.42	0.17	3/2–7/2	78004.65	0.16	3/2
67509.63	0.17	3/2	73571.40	0.17	3/2 or 5/2	78079.15	0.16	3/2 or 5/2
67577.71	0.20	3/2 or 5/2	73637.54	0.16	3/2 or 5/2	78106.22	0.16	1/2 or 3/2
67657.30	0.18	1/2 or 3/2	73717.33	0.16	3/2	78147.89	0.17	3/2–7/2
67737.62	0.18	3/2 or 5/2	73720.66	0.19	3/2–7/2	78311.97	0.17	1/2 or 3/2
67803.24	0.17	3/2 or 5/2	73856.76	0.16	3/2 or 5/2	78365.42	0.17	3/2
67843.31	0.17	3/2 or 5/2	73927.39	0.17	3/2 or 5/2	78486.07	0.17	1/2 or 3/2
67866.10	0.18	3/2 or 5/2	74015.17	0.17	3/2–7/2	78643.42	0.17	1/2 or 3/2
68033.33	0.21	3/2–7/2	74035.55	0.16	3/2	78671.36	0.16	1/2 or 3/2
68088.03	0.17	3/2	74041.31	0.16	3/2–7/2	78746.08	0.16	1/2 or 3/2
68278.65	0.20	3/2–7/2	74077.59	0.17	1/2–5/2	78780.27	0.17	1/2 or 3/2
68497.88	0.18	3/2 or 5/2	74159.76	0.17	3/2 or 5/2	79056.55	0.17	1/2 or 3/2

V. LEVEL DENSITY CALCULATIONS

To reassure that we did not miss a relevant number of levels in the experiment we calculated the densities of even levels in Th^+ up to 85000 cm^{-1} using the multiconfigurational Dirac-Fock (MCDF) method implemented in a modified version of the GRASP2K package [20]. A detailed description of the methods involved can be found, e.g., in Refs. [21,22]. Thorium in its singly ionized state has three valence electrons above a closed radon core. The basis for our calculations has been set up with single and double excitations of the valence electrons from six reference configurations: $6d^27s$, $5f^27s$, $5f^26d$, $5f7s7p$, $5f6d7p$, and $6d^3$. Moreover, we add to the basis the configurations produced by single excitations from the core opened up to xenon.

Singly charged thorium is a very complicated system with strong electron-electron correlations. Therefore, we cannot expect to reproduce the energies of particular levels accurately, especially for high-lying levels. Instead we compare the number of levels per 5000 cm^{-1} interval. Generally, the size of the basis used in an MCDF calculation determines the number of energy levels that can be constructed, each approximation being a solution of the many-electron Dirac equation. However, due to numerical uncertainties, not all of these energy levels have a physical meaning. Especially those that consist only of basis elements constructed from weakly bound single-electron orbitals are numerically unstable. Fortunately such energy levels are collected at energies close to the ionization threshold. This can be checked by observing the convergence of the level density at different energy ranges. While the level density converges and is stable for the energy range under consideration in the present work, an increasing number of nonphysical energy levels can be observed at higher energies.

With this setup we achieve a good convergence of the calculated level density; however, it has to be noted that the accuracy of our level energies does not go beyond the chosen 5000 cm^{-1} energy interval. In Fig. 4 we show a comparison of the number of known electronic levels from the database of Ref. [3], our investigations (including Ref. [4]), and the MCDF calculations for even-parity levels with $J = 1/2$ to $7/2$. The calculated level density shows a qualitative agreement with the measurements apart from a prevailing shift to higher energies. The most apparent feature of the level density plot is the minimum around 60000 cm^{-1}. The existence of this minimum comes with an experimental uncertainty, because it lies on the border of the covered energy range of both measurements. Our calculations, however, reproduce this qualitative behavior, confirming the experimental findings.

Based on our calculations and the experimental findings we can estimate the enhancement factor β for the excitation of the ^{229}Th nuclear transition via an electronic bridge process [10]. Following Ref. [17] we find the average energy interval between two levels in the desired energy range between 60000 cm^{-1} and 65000 cm^{-1} to be 160 $cm^{-1} < D_p <$ 280 cm^{-1}. Assuming that the electronic bridge starts from the $J_i = 3/2$ ground state of Th^+ via an even-parity intermediate level with angular momentum in the range $1/2 < J_n < 7/2$, and with the present value and uncertainty for the nuclear

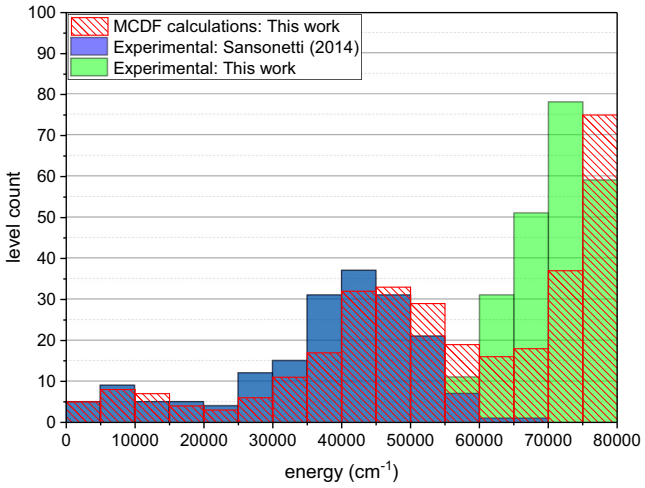

FIG. 4. Histogram of the number of electronic levels in Th^+ with $J = 1/2$ to $7/2$ and even parity in the energy range up to 80 000 cm^{-1}. The calculated level numbers are shown in red and the measured level numbers in blue (Ref. [3]) and green (this work).

transition frequency ω_N, we get $0.5 \times 10^3 < \beta < 6 \times 10^3$. However, this value strongly depends on ω_N and increases rapidly for $\omega_N > 70000\,\mathrm{cm}^{-1}$. A similar result has recently been obtained for the electronic bridge decay rate in Th^+ [13].

VI. CONCLUSION

We have measured the energies of 166 previously unknown high-lying levels in the energy range from 7.8 to 9.8 eV in $^{232}Th^+$ and have determined the angular momenta of many of the newly found levels, as well as for previously unclassified levels reported in Ref. [4]. We furthermore have performed MCDF calculations which allow us to predict the electronic level density with acceptable accuracy in the investigated energy range.

The good agreement between measured and calculated level density gives rise to the assumption that most of the even-parity levels with $J = 1/2$ to $7/2$ in the energy range from 7.8 to 9.8 eV were found.

The resonant excitation of the nuclear isomer through high-lying levels in $^{229}Th^+$ is expected to be enhanced compared to the direct optical excitation [8–10,23]. In comparison to the investigated energy range in the previous experiment [4] and *ab initio* calculations [17,24], the level density measured in this work is significantly higher. Therefore, we can expect an increased excitation probability for the nuclear isomer via these newly found high-lying levels.

ACKNOWLEDGMENTS

We thank O. A. Herrera-Sancho and K. Zimmermann for contributions to the experimental setup and S. Klein for assistance in the experiment. We furthermore thank T. Leder, M. Menzel, B. Lipphardt, and A. Hoppmann for providing expert technical support. We acknowledge financial support from the European Union's Horizon 2020 Research and Innovation Programme under Grant Agreement No. 664732 (nuClock) and from Deutsche Forschungsgemeinschaft (DFG) through CRC 1227 (DQ-mat, Project No. B04).

[1] E. F. Worden, J. Blaise, M. Fred, N. Trautmann, and J.-F. Wyart, in *The Chemistry of the Actinide and Transactinide Elements, Chap. 16*, 3rd ed., edited by L. R. Morss, N. Edelstein, J. Fuger, and J. J. Katz (Springer, Netherlands, 2006), Vol. 3.

[2] C. Lovis and F. Pepe, Astron. Astrophys. **468**, 1115 (2007).

[3] S. L. Redman, G. Nave, and C. J. Sansonetti, Astrophys. J. Suppl. Ser. **211**, 4 (2014).

[4] O. A. Herrera-Sancho, N. Nemitz, M. V. Okhapkin, and E. Peik, Phys. Rev. A **88**, 012512 (2013).

[5] N. Rosenzweig and C. E. Porter, Phys. Rev. **120**, 1698 (1960).

[6] B. R. Beck, J. A. Becker, P. Beiersdorfer, G. V. Brown, K. J. Moody, J. B. Wilhelmy, F. S. Porter, C. A. Kilbourne, and R. L. Kelley, Phys. Rev. Lett. **98**, 142501 (2007).

[7] B. R. Beck, G. V. Brown, R. L. Kelley, J. A. Becker, C. Y. Wu, F. S. Porter, J. B. Wilhelmy, C. A. Kilbourne, J. K. Moody, *et al.*, Report No. LLNL-PROC-415170, 2009, https://e-reports-ext.llnl.gov/pdf/375773.pdf.

[8] E. V. Tkalya, V. O. Varlamov, V. V. Lomonosov, and S. A. Nikulin, Phys. Scr. **53**, 296 (1996).

[9] F. Karpeshin, I. Band, and M. Trzhaskovskaya, Nucl. Phys. A **654**, 579 (1999).

[10] S. G. Porsev, V. V. Flambaum, E. Peik, and C. Tamm, Phys. Rev. Lett. **105**, 182501 (2010).

[11] E. Peik and M. Okhapkin, C. R. Phys. **16**, 516 (2015).

[12] B. Seiferle, L. von der Wense, and P. G. Thirolf, Phys. Rev. Lett. **118**, 042501 (2017).

[13] F. F. Karpeshin and M. B. Trzhaskovskaya, Nucl. Phys. A **969**, 173 (2018).

[14] R. Zalubas and C. H. Corliss, J. Res. Natl. Bur. Stand., Sect. A **78A**, 163 (1974).

[15] M. V. Okhapkin, D. M. Meier, E. Peik, M. S. Safronova, M. G. Kozlov, and S. G. Porsev, Phys. Rev. A **92**, 020503(R) (2015).

[16] See Supplemental Material at http://link.aps.org/supplemental/10.1103/PhysRevA.99.052514 for a list of all observed two-photon excitation channels and machine-readable lists of the newly observed levels and transition wavelengths.

[17] V. A. Dzuba and V. V. Flambaum, Phys. Rev. Lett. **104**, 213002 (2010).

[18] O.-A. Herrera-Sancho, Ph.D. thesis, Leibniz Universität Hannover, 2012.

[19] O. A. Herrera-Sancho, M. V. Okhapkin, K. Zimmermann, C. Tamm, E. Peik, A. V. Taichenachev, V. I. Yudin, and P. Głowacki, Phys. Rev. A **85**, 033402 (2012).

[20] P. Jönsson, G. Gaigalas, J. Bieron, C. F. Fischer, and I. Grant, Comput. Phys. Commun. **184**, 2197 (2013).

[21] C. Froese-Fischer and T. Brage, *Computational Atomic Structure: An MCHF Approach* (CRC Press, Boca Raton, FL, 1997).

[22] I. P. Grant, *Relativistic Quantum Theory of Atoms and Molecules: Theory and Computation*, 1st ed., Springer Series on Atomic, Optical, and Plasma Physics Vol. 40 (Springer-Verlag, New York, 2007).

[23] F. Karpeshin, I. Band, M. Trzhaskovskaya, and M. Listengarten, Phys. Lett. B **372**, 1 (1996).

[24] S. G. Porsev and V. V. Flambaum, Phys. Rev. A **81**, 032504 (2010).

Nuclear Instruments and Methods in Physics Research B 408 (2017) 84–88

Contents lists available at ScienceDirect

Nuclear Instruments and Methods in Physics Research B

journal homepage: www.elsevier.com/locate/nimb

Theoretical analysis of the electron bridge process in $^{229}Th^{3+}$

R.A. Müller [a,b,*], A.V. Volotka [c], S. Fritzsche [c,d], A. Surzhykov [a,b]

[a] Physikalisch-Technische Bundesanstalt, D-38116 Braunschweig, Germany
[b] Technische Universität Braunschweig, D-38106 Braunschweig, Germany
[c] Helmholtz-Institute Jena, D-07743 Jena, Germany
[d] Theoretisch-Physikalisches Institut, Friedrich-Schiller-Universität Jena, D-07743 Jena, Germany

ARTICLE INFO

Article history:
Received 9 December 2016
Received in revised form 2 May 2017
Accepted 3 May 2017
Available online 12 May 2017

Keywords:
Electron bridge
Thorium 229
Nuclear excitation

ABSTRACT

We investigate the deexcitation of the ^{229}Th nucleus via the excitation of an electron. Detailed calculations are performed for the enhancement of the nuclear decay width due to the so called *electron bridge* (EB) compared to the direct photoemission from the nucleus. The results are obtained for triply ionized thorium by using a B-spline pseudo basis approach to solve the Dirac equation for a local x_α potential. This approach allows for an approximation of the full electron propagator including the positive and negative continuum. We show that the contribution of continua slightly increases the enhancement compared to a propagator calculated by a direct summation over bound states. Moreover we put special emphasis on the interference between the direct and exchange Feynman diagrams that can have a strong influence on the enhancement.

1. Introduction

Because of its extremely low lying first excited metastable state the ^{229}Th nucleus has been object of intense investigation during the last decades [1–10]. Due to its extremely narrow linewidth the transition between this isomeric and the nuclear ground state is planned to be the working transition of the future nuclear clock [11–13]. This clock will be very important for benchmarking existing atomic clocks and might help to provide a new optical frequency standard [14]. Moreover this clock will be accurate enough to test predictions for the fifth force and the time variation of fundamental constants [15,16]. Triply charged thorium is a good candidate to study in particular because it has been successfully laser cooled and was already studied in ion trap experiments [17].

So far the exact energy of the low lying nuclear resonance in ^{229}Th remains unknown. Its currently accepted value is 7.8 ± 0.5 eV [18]. The large uncertainty of this value, however, does not allow for a direct laser spectroscopy of this level. Therefore many alternative scenarios have been put forward how to address the low lying nuclear isomeric state [19,10,20]. Meanwhile the majority of these scenarios have been realized in experiments aiming for a precise determination of the resonance energy [1–3,13,21,22,11]. A key property here is the lifetime of the isomeric state that is strongly influenced by the electronic environment, inter alia because of the electron bridge (EB) process [8]. In this process the ^{229}Th nucleus does not decay via emission of a photon but by exciting the electron shell. We present here an approach to analyze the influence of the EB onto the decay width of the first excited state of the ^{229}Th nucleus. Our approach extends the analysis shown in Ref. [8] by two means. First our method allows to include the experimental energies of the important transitions in Th^{3+} and does not necessarily rely on many-electron calculations that are not always in good agreement with the measured spectra. Second we approximate the full electron propagator, including the coupling to the positive and negative continuum, in contrast to Ref. [8], where a direct summation over bound states is performed.

After we have sketched our theory in Section 2 we will present results in Section 4, where we will discuss the role of the positive an negative continuum in the electron propagator as well as interference effects between the participating quantum processes. Natural units ($\hbar = c = 1$) are used throughout this work.

2. Theory

The EB is described by two Feynman diagrams shown in Fig. 1. The *direct diagram* describes the process where the nuclear isomeric state $|e\rangle$ decays to the ground state $|g\rangle$ via exchanging a virtual photon with the electron shell from which, in turn, a real photon is emitted. In the *exchange diagram* the real photon is emitted before the deexcitation of the nucleus takes place. It is known

* Corresponding author at: Physikalisch-Technische Bundesanstalt, D-38116 Braunschweig, Germany.
E-mail address: robert.mueller@ptb.de (R.A. Müller).

http://dx.doi.org/10.1016/j.nimb.2017.05.004
0168-583X/

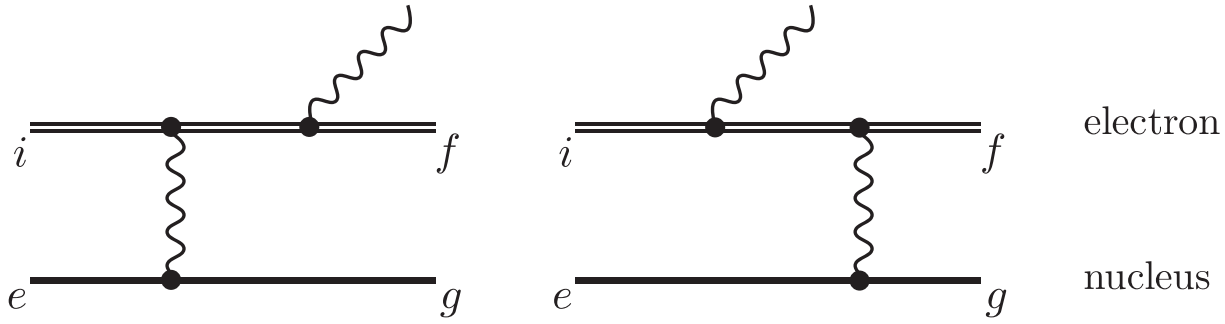

Fig. 1. Feynman diagrams for the electronic bridge process. e and g are the first excited and the ground state of the nucleus, i and f the initial and final electronic states.

experimentally that the $|e\rangle \rightarrow |g\rangle$ transition in ^{229}Th is of magnetic dipole type ($M1$). As shown in Fig. 2 this transition leads to an $M1$ excitation of the electron to a, possibly virtual, intermediate state. We will employ the dipole approximation for the emitted real photon so that the transition from the intermediate to the final electronic state is of electric dipole type ($E1$).

In order to quantify the influence of the EB on the total decay width of the ^{229}Th nucleus we will derive an expression for the ratio β between the width Γ_{EB} of the EB process and the width of the direct $M1$ photo decay of the nucleus:

$$\beta = \frac{\Gamma_{EB}}{\Gamma_N(M1, e \rightarrow g)} \tag{1}$$

The spontaneous decay width $\Gamma_N(M1, e \rightarrow g)$ has not been measured yet. Only a theoretical estimate has been given [23]. We will see later, that β is especially useful because it is largely independent on $\Gamma_N(M1, e \rightarrow g)$. This makes the coefficient β a convenient quantity for the comparison of different theories and scenarios.

The calculation of the EB-width Γ_{EB} can be traced back to an evaluation of the transition amplitudes. We apply the Feynman rules to the diagrams shown in Fig. 1 to obtain expressions for these. Assuming that the angular momentum projections of the initial and final nuclear and electronic states are not observed, we obtain for Γ_{EB}:

$$\begin{aligned}\Gamma_{EB} = &\left(\frac{\omega}{\omega_N}\right)^3 \frac{\alpha \Gamma_N(M1, e \rightarrow g)}{4\pi(2j_i+1)} \\ &\times \left[\sum_n \frac{1}{2j_n+1} \left(\left| \frac{\langle f||\hat{D}||n\rangle \langle n||\hat{T}_1||i\rangle}{\omega_{in}+\omega_N} \right|^2 + \left| \frac{\langle f||\hat{T}_1||n\rangle \langle n||\hat{D}||i\rangle}{\omega_{fn}-\omega_N} \right|^2 \right) \right. \\ &\left. + \sum_{nn'} (-1)^{j_n+j_{n'}} \begin{Bmatrix} j_i & L & j_n \\ j_f & 1 & j_{n'} \end{Bmatrix} \frac{\langle f||\hat{D}||n\rangle \langle n||\hat{T}_1||i\rangle \langle f||\hat{T}_1||n'\rangle^* \langle n'||\hat{D}||i\rangle^*}{(\omega_{in}+\omega_N)(\omega_{fn'}-\omega_N)} \right]\end{aligned} \tag{2}$$

where the electronic states $|i\rangle$ have angular momentum j_i and energy ϵ_i. The energy of the emitted photon is $\omega = \epsilon_i - \epsilon_f + \omega_N$, α is the fine structure constant and ω_N the energy splitting between the nuclear ground and first excited state. The electron propagator is represented by summing and integrating over all possible intermediate states n. The energy splitting between these intermediate and the initial or final electronic states is labeled by $\omega_{i/fn}$. We can see that Γ_{EB} increases drastically if the resonance condition $\omega_{in} + \omega_N = 0$ is fulfilled. In this resonant case it is important to include the width of the atomic states to resolve the divergence of the denomiators in Eq. (2). Moreover Γ_{EB} scales linearly with $\Gamma_N(M1, e \rightarrow f)$, which cancels with the denomiator of Eq. (1) and makes β independent of the width of isomeric nuclear state.

The transition operators in Eq. (2) are the dipole operator $\hat{D}$ describing the photon emission from the electron shell and the operator $\hat{T}_{1M}$ which is part of the virtual photon exchange in the electron nucleus interaction (cf. Fig. 1). Following similar steps to Refs. [24–26] find for $\hat{T}_{1M}$:

$$\hat{T}_{1M} = -e\sqrt{\frac{4\pi}{3}} \frac{[\hat{\vec{r}} \times \vec{\alpha}]_M}{r^3}, \tag{3}$$

where $\vec{\alpha}$ is the vector of Dirac matrices and e is the electron charge.

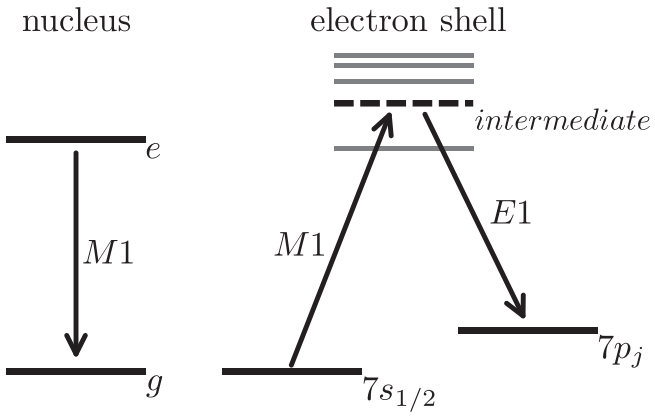

Fig. 2. Sketch of the electronic bridge process for the deexcitation of the nucleus via the $M1$-excitation of a $7s_{1/2}$ electron to a (virtual) intermediate state. In a second step the intermediate state decays via an $E1$ electric dipole transition to a $7p_j$ state.

3. Computational details

After we have derived an expression for the EB-width Γ_{EB} (2) we need to obtain a basis set for all (bound and continuum) electronic states to evaluate the matrix elements and the sum and integral in Eq. (2). In order to do this, we restrict ourselves here to the single active electron (SAE) approximation, which is well justified since Th^{3+} has only one valence electron. In order to generate the wave function for this valence electron, we solve the Dirac-Equation for a x_α potential, that is assembled from the Coulomb potential $V_{nuc}(r)$ of the extended nucleus and the static potential generated by the other electrons:

$$V_{x_\alpha}(r) = V_{nuc}(r) + \alpha \int_0^\infty dr\prime \frac{\varrho(r\prime)}{\max(r, r\prime)} - x_\alpha \frac{\alpha}{r} \left(\frac{81}{32\pi^2} r\varrho(r) \right)^{\frac{1}{3}}, \tag{4}$$

where $\varrho(r)$ is the electron density obtained by means of the Dirac-Hartree–Fock method. For the usual Kohn–Sham potential the pref-

actor of the last term is $x_\alpha = \frac{2}{3}$. In our case we take x_α as a free parameter and vary it so that the corresponding binding energies accurately match the transition energy between the initial and final electronic state. Following Refs. [27,28] we construct for this potential a finite pseudo basis set consisting of B-spline wave functions that are solutions of the Dirac equation. This reduces the infinite sum and integral in Eq. (2) to a finite sum and allows for a very good approximation of the electron propagator [29,30]. Now by plugging Eq. (2) into Eq. (1), we can calculate the enhancement β.

4. Results and discussion

Before we present calculations for the enhancement β [Eq. (1)], we want to convince ourselves that the approximations we made to obtain the electron wavefunctions are valid. Therefore we will use our potential to calculate the spectrum of Th^{3+} and compare these calculations with experimental data. Th^{3+} has one electron above a closed radon core, the ground state configuration is $[Rn]5f^1$. Thus, for brevity, we can name the ionic configurations by the state of the valence electron. Many experiments are performed not using the ground but excited states of Th^{3+}. The $7s_{1/2}$ state is of particular interest here because the $7s_{1/2} \rightarrow 8s_{1/2}$ resonance is close to the expected nuclear excitation energy. Due to the dipole transition matrix elements in Eq. (2), the final state has to be of opposite parity and we will restrict ourselves here to a final $7p_j$ state. Therefore we vary the parameter x_α in Eq. (4) to match the calculations with the experimental values [31] for the transitions $7s_{1/2} \rightarrow 7p_{1/2}$ and $7s_{1/2} \rightarrow 7p_{3/2}$. After variation we obtain $x_\alpha = 1.06$ for the $7p_{1/2}$ and $x_\alpha = 1.01$ for the $7p_{3/2}$ case. With these potentials we can now compare the calculated spectra with the measured level energies as shown in Table 1. It can be seen from the table that our agreement with the experimental energies is always better than 2% for states above the 6*d*-shell. Calculations for the Th^{3+} spectrum that we performed using the GRASP2k package [32] help us to explain the strong disagreement for the lower lying levels. These calculations show us that for these levels correlation effects play an important role which are not covered by the approximation (4).

Above we have shown that our approximation provides good results for the desired transition from the initial $7s_{1/2}$ to the final $7p_j$ state. This allows us to perform calculations for the coefficient β. Because the nuclear excitation energy ω_N is unknown we take it as a free parameter and evaluate β as a function of ω_N as shown in Fig. 3. In this case the general behaviour of β is determined by the denomiator $\omega_{in} + \omega_N$ in Eq. (2) that becomes zero if the energy splitting between the initial and intermediate state ω_{in} matches the nuclear excitation energy ω_N. Therefore we will see β increase if ω_{in} and ω_N approach each other and decrease if the denomiator increases again. In Fig. 3 we see β becoming larger towards higher energies. This is due to the closeby $7s_{1/2} \rightarrow 8s_{1/2}$ resonance. Therefore the β is larger than one over a wide energy range, which means that the deexcitation via the EB process is more probable than the emission of a photon from the nucleus.

Table 1
Comparison between the experimental spectrum [31] and the spectra obtained using our screening potentials (4) varied to match the transition energy between $7s_{1/2} \rightarrow 7p_{1/2}$ and $7s_{1/2} \rightarrow 7p_{3/2}$, respectively. All energies are given in eV with respect to the ionization threshold.

State	Experiment [31]	x_α fit to $7s_{1/2} \rightarrow 7p_{1/2}$	x_α fit to $7s_{1/2} \rightarrow 7p_{3/2}$
$[Rn]5f_{5/2}$	−28.811	−36.403	−35.142
$[Rn]5f_{7/2}$	−28.275	−35.508	−34.271
$[Rn]6d_{3/2}$	−27.672	−28.843	−28.238
$[Rn]6d_{5/2}$	−27.015	−27.859	−27.287
$[Rn]7s_{1/2}$	−25.944	−26.094	−25.808
$[Rn]7p_{1/2}$	−21.343	−21.493	−21.301
$[Rn]7p_{3/2}$	−19.754	−19.766	−19.621
$[Rn]8s_{1/2}$	−13.980	−14.133	−14.038
$[Rn]7d_{3/2}$	−13.972	−14.170	−14.074
$[Rn]7d_{5/2}$	−13.756	−13.943	−13.846
$[Rn]6f_{5/2}$	−13.033	−13.163	−13.067
$[Rn]6f_{7/2}$	−12.964	−13.099	−13.005
$[Rn]8p_{1/2}$	−12.133	−12.225	−12.147
$[Rn]8p_{3/2}$	−11.469	−11.480	−11.415
$[Rn]9s_{1/2}$	−8.8837	−8.9192	−8.8756

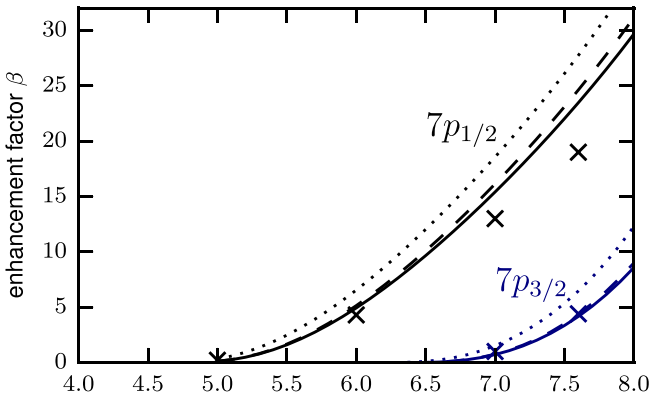

Fig. 3. Calculations for the enhancement β as a function of ω_N for two different transition paths (i) $7s_{1/2} \rightarrow 7p_{1/2}$ (black lines and symbols, upper set) and (ii) $7s_{1/2} \rightarrow 7p_{3/2}$ (blue lines and symbols, lower set). The crosses are values published in Ref. [8] and the solid lines correspond to results obtained with our screening potential fitted to the energies and the basis set shown in Ref. [8]. The dashed lines correspond to results obtained with the same potential but the full basis set, while the dotted lines are results where we varied the potential to match the experimental transition energies. (For interpretation of the references to colour in this figure legend, the reader is referred to the web version of this article.)

In order to draw a comparison to previous results, we modified our approach to mimic the theory put forward by Porsev and Flambaum [8]. Therefore we (i) varied our potential to match the energies published in Ref. [8] ($x_\alpha = 1.12$ for $7s_{1/2} \rightarrow 7p_{1/2}, x_\alpha = 1.07$ for $7s_{1/2} \rightarrow 7p_{3/2}$) and (ii) truncated our basis to the same set of states used by Porsev and Flambaum. The results of these calculations are shown as solid lines in Fig. 3 together with the set of values presented by Porsev and Flambaum [8] (crosses) for both final states $7p_{1/2}$ (upper black set) and $7p_{3/2}$ (lower blue set). It is seen that we achieve a very good agreement with these previous calculations, especially for the $7p_{3/2}$ final state. But it is important to note, that due to the incomplete set of intermediate states the theory is not gauge invariant. The dashed lines in contrast show the results for the same potential but the full B-spline pseudo basis. In order to check the gauge invariance of this approximation we performed calculations in length and velocity gauge. These results turn out to agree up to the order 10^{-5}. Compared to the calculations with the truncated basis set β is slightly increased if the full set of B-splines is used. The dotted lines show results again for the complete pseudo basis and a potential where the binding energies are matched to the experimental values. The fact that β is again larger in this case is mainly due to the fact that the experimental energy of the nearest resonance, where $\omega_N = \epsilon_{8s_{1/2}} - \epsilon_{7s_{1/2}}$, is about 0.3 eV lower than calculated in Ref. [8]. This shows us that even in the regime where ω_N is far from an electronic resonance it is important to have an accurate representation of the electronic spectrum.

All results shown above in Fig. 3 were obtained including the contributions of both the direct and the exchange diagram (cf. Fig. 1). In Fig. 4 we show a more detailed investigation of the different contributions to β from both diagrams involved. The calcu-

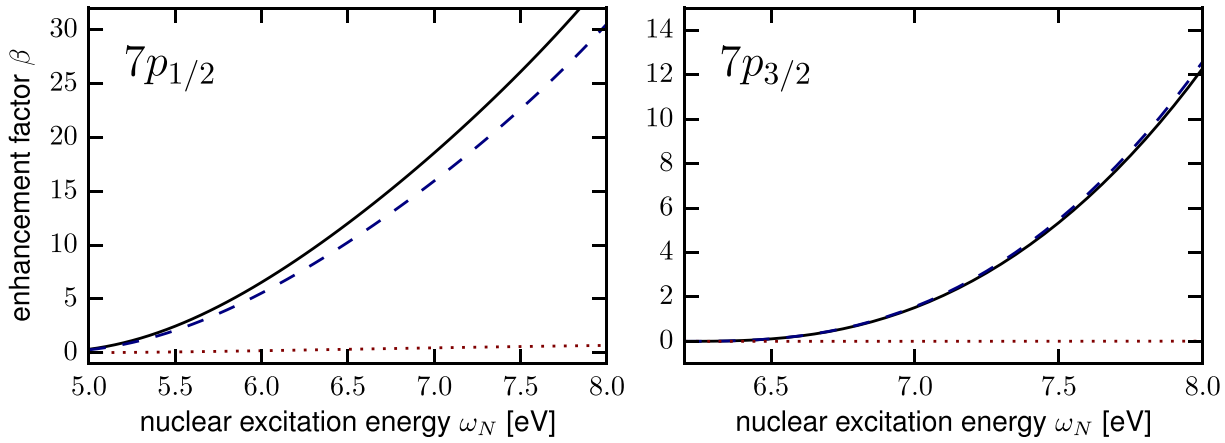

Fig. 4. Calculations for the enhancement β for the initial state $7s_{1/2}$ and the final state $7p_{1/2}$ (left panel) and $7p_{3/2}$ (right panel). The solid lines are the full result with the potential fitted to the experimental spectrum just as shown already in Fig. 3. The blue dashed lines show β calculated only for the direct and the red dotted lines only for the exchange diagram. (For interpretation of the references to colour in this figure legend, the reader is referred to the web version of this article.)

lations are performed again for two final states and with the use of the potential fitted to the experimental transition energies as presented in Table 1. In each panel of Fig. 4 the solid black lines correspond to the full results (2) as already shown in Fig. 3. The dashed blue and dotted red lines show β calculated only for the direct or the exchange diagram, respectively. It can be seen that in the case of the final state being $7p_{1/2}$ the full result does not correspond to the sum of direct and exchange amplitudes. While the contribution from the exchange diagram is almost zero, the full result is about 10% larger than the calculation from the direct diagram. This increase is due to the interference between the two processes. For the final state $7p_{3/2}$ this interference effect is negative but negligible. Conclusively Fig. 4 shows us that, however the contribution from the exchange diagram is small, it cannot always be neglected because of strong interference effects.

5. Summary

We have investigated the enhancement of the decay width of the low lying nuclear isomeric state due to the EB process in $^{229}Th^{3+}$. Our method allows us to obtain results for this enhancement as a function of the nuclear excitation energy ω_N, where we are able to accurately match the important transition energies to the experimental values. We have shown that a good representation of the spectrum is important even in the off-resonance regime. Moreover we found out that the enhancement due to the EB is slightly underestimated if the electron propagator is approximated by a direct sum over bound electron states. However the contribution from the exchange diagram has been rightly neglected in some works [9,10] we have shown that in some cases interference effects between the direct and the exchange diagram can have a large influence on the width of the EB.

Acknowledgements

The authors are grateful for many useful discussions with Maksim Okhapkin. RAM acknowledges support of the RS-APS and the HGS-HIRe.

References

[1] L. Kroger, C. Reich, Features of the low-energy level scheme of 229th as observed in the a-decay of 233u, Nucl. Phys. A 259 (1) (1976) 29–60, http://dx.doi.org/10.1016/0375-9474(76)90494-2, URL http://linkinghub.elsevier.com/retrieve/pii/0375947476904942.

[2] C.W. Reich, R.G. Helmer, Energy separation of the doublet of intrinsic states at the ground state of Th 229, Phys. Rev. Lett. 64 (3) (1990) 271–273, http://dx.doi.org/10.1103/PhysRevLett. 64.271.

[3] Z.O. Guimarães Filho, O. Helene, Energy of the 3/ 2 + state of Th 229 reexamined, Phys. Rev. C 71 (4) (2005) 044303, http://dx.doi.org/10.1103/PhysRevC.71.044303.

[4] B.R. Beck, J.A. Becker, P. Beiersdorfer, G.V. Brown, K.J. Moody, J.B. Wilhelmy, F.S. Porter, C.A. Kilbourne, R.L. Kelley, Energy splitting of the ground-state doublet in the nucleus Th 229, Phys. Rev. Lett. 98 (14) (2007) 142501, http://dx.doi.org/10.1103/PhysRevLett. 98.142501.

[5] F.F. Karpeshin, M.R. Harston, F. Attallah, J.F. Chemin, J.N. Scheurer, I.M. Band, M. B. Trzhaskovskaya, Subthreshold internal conversion to bound states in highly ionized Te 125 ions, Phys. Rev. C 53 (4) (1996) 1640, URL http://journals.aps.org/prc/abstract/10.1103/PhysRevC.53.1640.

[6] F. Karpeshin, I. Band, M. Trzhaskovskaya, 3.5-eV isomer of 229mth: how it can be produced, Nucl. Phys. A 654 (3–4) (1999) 579–596, http://dx.doi.org/10.1016/S0375-9474(99)00303-6, URL http://linkinghub.elsevier.com/retrieve/pii/S0375947499003036.

[7] F.F. Karpeshin, M.B. Trzhaskovskaya, Excitation of the 229m Th nuclear isomer via resonance conversion in ionized atoms, Phys. At. Nucl. 78 (6) (2015) 715–719, http://dx.doi.org/10.1134/S1063778815060125.

[8] S.G. Porsev, V.V. Flambaum, Effect of atomic electrons on the 7.6-eV nuclear transition in Th 229 3+, Phys. Rev. A 81(3) doi:http://dx.doi.org/10.1103/PhysRevA.81.042516.

[9] S.G. Porsev, V.V. Flambaum, Electronic bridge process in Th 229 +, Phys. Rev. A 81 (4) (2010) 042516, http://dx.doi.org/10.1103/PhysRevA.81.042516.

[10] S.G. Porsev, V.V. Flambaum, E. Peik, C. Tamm, Excitation of the isomeric Th 229 m nuclear state via an electronic bridge process in Th + 229, Phys. Rev. Lett. 105 (18) (2010) 182501, http://dx.doi.org/10.1103/PhysRevLett. 105.182501.

[11] E. Peik, C. Tamm, Nuclear laser spectroscopy of the 3.5 eV transition in Th-229, EPL (Europhys. Lett.) 61 (2) (2003) 181, URL http://iopscience.iop.org/article/10.1209/epl/i2003-00210-x/fulltext/7463.html.

[12] E. Peik, M. Okhapkin, Nuclear clocks based on resonant excitation of *gamma*-transitions, C.R. Phys. 16 (5) (2015) 516–523, http://dx.doi.org/10.1016/j.crhy.2015.02.007, URL http://linkinghub.elsevier.com/retrieve/pii/S1631070515000213.

[13] L. von der Wense, B. Seiferle, M. Laatiaoui, J.B. Neumayr, H.-J. Maier, H.-F. Wirth, C. Mokry, J. Runke, K. Eberhardt, C.E. Düllmann, N.G. Trautmann, P.G. Thirolf, Direct detection of the 229th nuclear clock transition, Nature 533 (7601) (2016) 47–51, http://dx.doi.org/10.1038/nature17669.

[14] E. Peik, K. Zimmermann, M. Okhapkin, C. Tamm, Prospects for a nuclear optical frequency standard based on Thorium-229, arXiv preprint arXiv:0812.3548. URL http://arxiv.org/abs/0812.3548.

[15] J.C. Berengut, V.A. Dzuba, V.V. Flambaum, S.G. Porsev, Proposed experimental method to determine a sensitivity of splitting between ground and 7.6 eV isomeric states in Th 229, Phys. Rev. Lett. 102 (21). doi:http://dx.doi.org/10.1103/PhysRevLett.102.210801.

[16] W.G. Rellergert, D. DeMille, R.R. Greco, M.P. Hehlen, J.R. Torgerson, E.R. Hudson, Constraining the evolution of the fundamental constants with a solid-state optical frequency reference based on the Th 229 nucleus, Phys. Rev. Lett. 104 (20) (2010) 200802, http://dx.doi.org/10.1103/PhysRevLett. 104.200802.

[17] C.J. Campbell, A.V. Steele, L.R. Churchill, M.V. DePalatis, D.E. Naylor, D.N. Matsukevich, A. Kuzmich, M.S. Chapman, Multiply charged thorium crystals for nuclear laser spectroscopy, Phys. Rev. Lett. 102 (23) (2009) 233004, http://dx.doi.org/10.1103/PhysRevLett. 102.233004.

[18] E.V. Tkalya, C. Schneider, J. Jeet, E.R. Hudson, Radiative lifetime and energy of the low-energy isomeric level in Th 229, Phys. Rev. C 92 (5). doi:http://dx.doi.org/10.1103/PhysRevC.92.054324.

[19] A. Pálffy, W. Scheid, Z. Harman, Theory of nuclear excitation by electron capture for heavy ions, Phys. Rev. A 73 (1). doi:http://dx.doi.org/10.1103/PhysRevA.73.012715.
[20] F.F. Karpeshin, Electron shell as a resonator, Hyperfine Interact. 143 (1–4) (2002) 79–96, URL http://link.springer.com/article/10.1023/A:1024056828718.
[21] M.V. Okhapkin, D.M. Meier, E. Peik, M.S. Safronova, M.G. Kozlov, S.G. Porsev, Observation of an unexpected negative isotope shift in Th + 229 and its theoretical explanation, Phys. Rev. A 92 (2) (2015) 020503, http://dx.doi.org/10.1103/PhysRevA.92.020503.
[22] A. Yamaguchi, M. Kolbe, H. Kaser, T. Reichel, A. Gottwald, E. Peik, Experimental search for the low-energy nuclear transition in 229Th with undulator radiation, New J. Phys. 17 (5) (2015) 053053, http://dx.doi.org/10.1088/1367-2630/17/5/053053, URL http://stacks.iop.org/1367-2630/17/i=5/a=053053?key=crossref.203df8f549067fa2d47b30d3c36d4532.
[23] A.M. Dykhne, E.V. Tkalya, Matrix element of the anomalously low-energy (3.5±0.5 eV) transition in 229th and the isomer lifetime, J. Exp. Theor. Phys. Lett. 67 (4) (1998) 251–256, URL http://link.springer.com/article/10.1134/1.567659.
[24] G. Plunien, B. Müller, W. Greiner, G. Soff, Nuclear polarization in heavy atoms and superheavy quasiatoms, Phys. Rev. A 43 (11) (1991) 5853, URL http://journals.aps.org/pra/abstract/10.1103/PhysRevA.43.5853.
[25] E.V. Tkalya, E.V. Akhrameev, R.V. Arutyunyan, L.A. Bol'shov, P.S. Kondratenko, Excitation of atomic nuclei in hot plasma through resonance inverse electron bridge, Phys. Rev. C 90 (3) (2014) 034614, http://dx.doi.org/10.1103/PhysRevC.90.034614.
[26] A. Volotka, A. Surzhykov, S. Trotsenko, G. Plunien, T. Stühlker, S. Fritzsche, Nuclear Excitation by Two-Photon Electron Transition, Phys. Rev. Lett. 117 (24). doi:http://dx.doi.org/10.1103/PhysRevLett.117.243001.
[27] J. Sapirstein, W.R. Johnson, The use of basis splines in theoretical atomic physics, J. Phys. B: At. Mol. Opt. Phys. 29 (22) (1996) 5213, URL http://iopscience.iop.org/article/10.1088/0953-4075/29/22/005/meta.
[28] V.M. Shabaev, I.I. Tupitsyn, V.A. Yerokhin, G. Plunien, G. Soff, Dual kinetic balance approach to basis-set expansions for the dirac equation, Phys. Rev. Lett. 93 (13) (2004) 130405, http://dx.doi.org/10.1103/PhysRevLett.93.130405.
[29] A.V. Volotka, A. Surzhykov, V.M. Shabaev, G. Plunien, Interelectronic-interaction effects on the two-photon decay rates of heavy He-like ions, Phys. Rev. A 83 (6) (2011) 062508, http://dx.doi.org/10.1103/PhysRevA.83.062508.
[30] A.V. Volotka, V.A. Yerokhin, A. Surzhykov, T. Stöhlker, S. Fritzsche, Many-electron effects on x-ray Rayleigh scattering by highly charged He-like ions, Phys. Rev. A 93 (2) (2016) 023418, http://dx.doi.org/10.1103/PhysRevA.93.023418.
[31] P. Klinkenberg, Spectral structure of trebly ionized thorium, Th IV, Phys. B+C 151 (3) (1988) 552–567, http://dx.doi.org/10.1016/0378-4363(88)90312-9, URL http://linkinghub.elsevier.com/retrieve/pii/0378436388903129.
[32] P. Jönsson, G. Gaigalas, J. Bieron, C.F. Fischer, I. Grant, New version: Grasp2k relativistic atomic structure package, Comput. Phys. Commun. 184 (9) (2013) 2197–2203, http://dx.doi.org/10.1016/j.cpc.2013.02.016, URL http://linkinghub.elsevier.com/retrieve/pii/S0010465513000738.

Excitation of the ^{229}Th nucleus via a two-photon electronic transition

Robert A. Müller,[1,2,*] Andrey V. Volotka,[3,4] and Andrey Surzhykov[1,2]
[1]*Physikalisch-Technische Bundesanstalt, D-38116 Braunschweig, Germany*
[2]*Technische Universität Braunschweig, D-38106 Braunschweig, Germany*
[3]*Helmholtz Insitute Jena, D-07743 Jena, Germany*
[4]*GSI Helmholtzzentrum für Schwerionenforschung, D-64291 Darmstadt, Germany*

(Received 13 February 2019; published 26 April 2019)

We investigate the process of nuclear excitation via a two-photon electron transition (NETP) for the case of the doubly charged thorium. The theory of the NETP process was originally devised for heavy-helium-like ions. In this work, we study this process in the nuclear clock isotope ^{229}Th in the 2+ charge state. For this purpose we employ a combination of configuration interaction and many-body perturbation theory to calculate the probability of NETP in resonance approximation. The experimental scenario we propose for the excitation of the low-lying isomeric state in ^{229}Th is a circular process starting with a two-step pumping stage followed by NETP. The ideal intermediate steps in this process depends on the supposed energy $\hbar\omega_N$ of the nuclear isomeric state. For each of these energies, the best initial state for NETP is calculated. Special focus is put on the most recent experimental results for $\hbar\omega_N$.

DOI: 10.1103/PhysRevA.99.042517

I. INTRODUCTION

Atomic clocks are among the most precise measurement instruments available to date [1,2]. Accurate time measurements and clock comparisons offer the opportunity to investigate fundamental physics and possible physics beyond the standard model [3–5]. Fifteen years ago, Peik and co-workers proposed to build a clock based on a nuclear transition [6]. The most suitable of such transitions is found in the thorium isotope with mass number $A = 229$ between the nuclear ground and the first-excited isomeric state, nowadays sometimes referred to as *nuclear clock isomer*. Therefore, intense research, theoretically and experimentally, has been performed on ^{229}Th and especially the nucleus in its first-excited state, the isomer ^{229m}Th [7–10]. Recently, for example, the nuclear moments of ^{229m}Th have been determined [11,12], which may give insight into the energy of the nuclear isomeric state [13]. Moreover, the emission of internal conversion electrons from the ^{229m}Th $\rightarrow$ ^{229}Th transition has been observed [14]. However, a controlled excitation of the nuclear isomer has not been achieved yet [15].

A large number of different processes have been proposed to produce the ^{229m}Th nuclear isomer, ranging from direct laser excitation to the interaction with hot plasmas [6,16–20]. Out of these, the excitation of nuclei by the energy excess from electronic processes appears to be very efficient and is much stronger than, e.g., direct laser excitation [12,18,21]. However, all such electronic bridge processes come with a major challenge: For the process to be sufficiently strong, the electronic transition needs to be in proximity to the transition between the nuclear ground and the low-lying isomeric state of ^{229}Th. In the classic electron bridge process, the energy difference between the electronic and nuclear transition is accounted for by the absorption of a photon. Instead of absorbing a photon with an energy that needs to be precisely tuned, we consider a two-photon decay in the electron shell [22]. In such a transition, one virtual photon excites the nucleus, while the other is emitted as a real photon. The energy share between both photons is continuous and, thus, there is no scanning necessary to excite the nucleus. This so-called nuclear excitation by a two-photon electron transition (NETP) has been introduced for heavy highly charged ions to access nuclear excited states in the keV regime [22].

In this work, we want to investigate NETP in ^{229m}Th. In contrast to other nuclear levels, the ^{229m}Th isomeric state is found only about 8 eV above the ^{229}Th ground state. Therefore, the electronic transition needs to be in the same energy range. Consequently, lower charge states, especially ^{229}Th^{2+}, are promising candidates to observe NETP in thorium.

In contrast to the scenario discussed in Ref. [22] for heliumlike ions, Th^{2+} has many real intermediate resonances between the upper and the final state of the NETP process, provided by the rich level structure of the thorium ion. Ideally, such a resonance is close to the nuclear excitation energy, thus enhancing the probability of the NETP process. The location and number of the resonances, however, strongly depend on the initially pumped upper state. Therefore, the upper state which offers the highest probability for NETP depends on the energy of the nuclear isomeric state. In this paper, we therefore provide detailed calculations for NETP in ^{229}Th^{2+} and give clear recommendations for the levels to excite, depending on the energy range in which the isomer is searched.

Hartree atomic units ($\hbar = m_e = e = 1$) are used throughout this paper, unless stated otherwise.

*robert.mueller@ptb.de

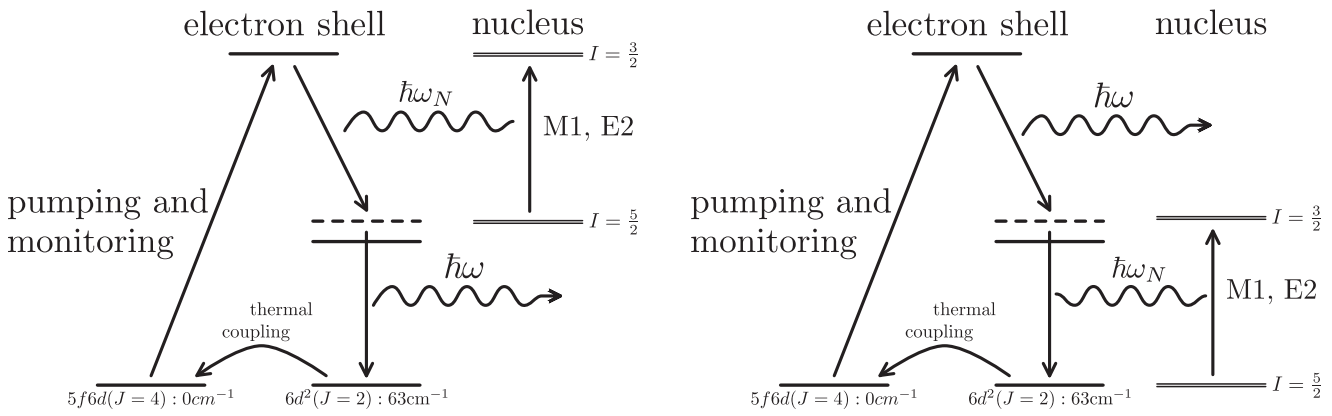

FIG. 1. Sketch of the NETP process together with the initial pumping of the excited state via two-step laser excitation. There are two equivalent scenarios to be considered: either the first (left picture) or the second photon (right picture) excites the nucleus. The excitation is assumed to start from the $6d^2(J = 2) : 63\ \text{cm}^{-1}$ state, which is assumed to always be thermally populated in the sample.

II. SCENARIO

A sketch of the scheme we propose for the excitation of the low-lying isomeric state in ^{229}Th can be seen in Fig. 1. First, starting from the $5f6d(J = 4) : 0\,\text{cm}^{-1}$ ground state, the electron shell of the thorium ion is excited to an upper state with odd parity. From this upper state, the NETP process occurs, where the nuclear excitation energy either corresponds to the energy splitting between the upper and the intermediate (left panel) or the intermediate and the lower state. The NETP decay is either of $E1{+}M1$ or $E1{+}E2$ type; therefore, the final state of the process is of even parity. In this work, we consider the $6d^2(J = 2) : 63\,\text{cm}^{-1}$ state as the final state, which is almost degenerate with the $5f6d(J = 4) : 0\,\text{cm}^{-1}$ ground state. In previous experiments on Th^+ and Th^{2+} with a buffer gas quenched sample, no significant population of dark states was observed. Thus, we can safely assume that the $6d^2(J = 2) : 63\,\text{cm}^{-1}$ state decays quickly to the ground state due to collisional coupling [11,12,23–25].

III. THEORY

A. NETP transition amplitudes and rates

In the previous section, we have described the process we propose for the excitation of ^{229}Th. Now we will derive the probability of NETP in doubly charged thorium below. To simplify our considerations, we will assume that the pumping of the upper state (cf. Fig. 1) is very efficient so that it is always populated. Therefore, the probability of the process is given by the last two deexcitation steps, which resemble the NETP process as discussed in Ref. [22].

In this work, we will identify each many-electron state by its total angular momentum J, the projection μ of J onto the quantization (z) axis, and a set of additional quantum numbers summarized by γ. The nuclear states are labeled by the nuclear spin I and its projection M. The theoretical description of NETP consists of two interfering channels. As also seen in Fig. 1, either the first or the second photon can excite the nucleus. Consequently, the NETP matrix element M_{fi} consists of two terms:

$$M_{\text{fi}} = \sum_{\gamma_n J_n \mu_n} \left(\frac{\langle \gamma_f J_f \mu_f, I_e M_e | \boldsymbol{\alpha} \cdot \boldsymbol{u}_\lambda e^{i\boldsymbol{k}\cdot\boldsymbol{r}} | \gamma_n J_n \mu_n, I_e M_e \rangle \langle \gamma_n J_n \mu_n, I_e M_e | H_{\text{int}} | \gamma_i J_i \mu_i, I_g M_g \rangle}{\epsilon_i - \omega_N - \epsilon_n - i\frac{\Gamma_n}{2}} \right.$$
$$\left. + \frac{\langle \gamma_f J_f \mu_f, I_e M_e | H_{\text{int}} | \gamma_n J_n \mu_n, I_g M_g \rangle \langle \gamma_n J_n \mu_n, I_g M_g | \boldsymbol{\alpha} \cdot \boldsymbol{u}_\lambda e^{i\boldsymbol{k}\cdot\boldsymbol{r}} | \gamma_i J_i \mu_i, I_g M_g \rangle}{\epsilon_f + \omega_N - \epsilon_n - i\frac{\Gamma_n}{2}} \right), \tag{1}$$

where ω_N is the frequency of the nuclear transition and $\boldsymbol{\alpha}$ denotes the vector of Dirac matrices. State energies and widths are denoted by ϵ and Γ, respectively, while the subscripts i, n, and f specify the initial, intermediate, and final states. Generally, the intermediate state can be virtual and, thus, we have to sum over the entire spectrum $|\gamma_n J_n \mu_n\rangle$, where we assume that the continuous spectrum can be neglected. Note that in Eq. (1) we have omitted the width of the nuclear excited state since it is much narrower than the electronic states.

Both terms in Eq. (1) each split into two matrix elements of the operators H_{int} and $\boldsymbol{\alpha} \cdot \boldsymbol{u}_\lambda e^{i\boldsymbol{k}\cdot\boldsymbol{r}}$. The latter is the usual interaction of the electron shell with a plane-wave photon with momentum $\boldsymbol{k}$ polarized along $\boldsymbol{u}_\lambda$, where λ is the helicity. The interaction Hamiltonian H_{int} mediates the interaction between the electron shell and the nucleus, thus acting on both electronic and nuclear degrees of freedom.

To obtain the probability of the NETP process, we can use Fermi's golden rule:

$$\mathcal{W}_{\text{fi}} = \frac{\alpha^3 \omega}{2\pi} \sum_{\mu_i \mu_f M_g M_e \lambda} [J_i, I_g]^{-1} \int |M_{\text{fi}}|^2 d\Omega_k, \tag{2}$$

where $[k] = 2k + 1$, α is the fine-structure constant, $d\Omega_k$ is the differential emission angle of the real photon, and ω is

the frequency of the real, emitted photon. In Eq. (2), we average over M_g and μ_i, assuming that the initial electronic and nuclear states are unpolarized. Moreover, neither μ_f and M_e nor the emission direction of the real photon are observed, and thus we sum over the magnetic quantum numbers of the final states and integrate over Ω_k.

To express Eq. (2) in a more convenient way, the photon emission operator $\boldsymbol{\alpha}\cdot\boldsymbol{u}_\lambda e^{i\boldsymbol{k}\cdot\boldsymbol{r}}$ is readily expanded into electric ($p=1$) and magnetic ($p=0$) multipoles L with magnetic quantum number M [26,27]:

$$\boldsymbol{u}_\lambda e^{i\boldsymbol{k}\cdot\boldsymbol{r}} = \sqrt{2\pi}\sum_{LMp} i^L [L]^{\frac{1}{2}} (i\lambda)^p D^L_{M\lambda}(\phi_k,\theta_k,0)\boldsymbol{a}^{(p)}_{LM}, \tag{3}$$

where $D^L_{M\lambda}(\phi_k,\theta_k,0)$ is the Wigner-D matrix and $\boldsymbol{a}^{(p)}_{LM}$ are irreducible tensors of rank L resembling the multipole fields.

Similar to the photon interaction operator, the electron-nucleus interaction $\hat{H}_{\rm int}$ can be expanded into multipoles [28,29],

$$\hat{H}_{\rm int} = \sum_{qr} \hat{T}_{qr}\hat{M}^*_{qr}, \tag{4}$$

where it is important to note that for each multipole, the operator $\hat{H}_{\rm int}$ splits into the hyperfine interaction operators $\hat{T}_{qr}$ acting only on electronic degrees of freedom and $\hat{M}_{qr}$ interacting with the nuclear part of the wave function. That way, we can find the NETP probability for each multipolarity q of the nuclear transition and electronic transitions L and p,

$$\mathcal{W}^{(Lpq)}_{\rm fi} = \frac{8\pi\alpha^3\omega}{[J_i,I_g]}\sum_{Lpq}\frac{|\langle I_e||\hat{M}_q||I_g\rangle|^2}{[q]} \times\left(G^{(Lpq)}_1 + G^{(Lpq)}_2 + G^{(Lpq)}_{12}\right), \tag{5}$$

where the total probability of the process would be the sum over all possible L, p, and q, and

$$G^{(Lpq)}_1 = \sum_{J_n}\frac{1}{[J_n]}\left|\sum_{\gamma_n}\frac{\langle\gamma_f J_f||\boldsymbol{\alpha}\cdot\boldsymbol{a}^{(p)}_L||\gamma_n J_n\rangle\,\langle\gamma_n J_n||\hat{T}_q||\gamma_i J_i\rangle}{\epsilon_i-\omega_N-\epsilon_n-i\frac{\Gamma_n}{2}}\right|^2, \tag{6a}$$

$$G^{(Lpq)}_2 = \sum_{J_n}\frac{1}{[J_n]}\left|\sum_{\gamma_n}\frac{\langle\gamma_f J_f||\hat{T}_q||\gamma_n J_n\rangle\,\langle\gamma_n J_n||\boldsymbol{\alpha}\cdot\boldsymbol{a}^{(p)}_L||\gamma_i J_i\rangle}{\epsilon_f+\omega_N-\epsilon_n-i\frac{\Gamma_n}{2}}\right|^2, \tag{6b}$$

$$G^{(Lpq)}_{12} = 2(-1)^{q+L}\sum_{\substack{\gamma_n\gamma'_n\\ J_nJ'_n}}(-1)^{J_n+J'_n}\begin{Bmatrix} J_i & q & J_n\\ J_f & L & J'_n\end{Bmatrix}\mathrm{Re}\left(\frac{\langle\gamma_f J_f||\boldsymbol{\alpha}\cdot\boldsymbol{a}^{(p)}_L||\gamma_n J_n\rangle\,\langle\gamma_n J_n||\hat{T}_q||\gamma_i J_i\rangle}{\epsilon_i-\omega_N-\epsilon_n-i\frac{\Gamma_n}{2}} \times\frac{\langle\gamma_f J_f||\hat{T}_q||\gamma'_n J'_n\rangle^*\,\langle\gamma'_n J'_n||\boldsymbol{\alpha}\cdot\boldsymbol{a}^{(p)}_L||\gamma_i J_i\rangle^*}{\epsilon_f+\omega_N-\epsilon'_n+i\frac{\Gamma'_n}{2}}\right). \tag{6c}$$

The equations above show that the NETP probability for each multipole (5) splits into three parts proportional to the amplitudes $G^{(Lpq)}_i$. The first two amplitudes $G^{(Lpq)}_1$ and $G^{(Lpq)}_2$ correspond here to the cases illustrated in Fig. 1, where the real photon is emitted either due to the transition between the initial and the intermediate states or the intermediate and the final states. The last amplitude $G^{(Lpq)}_{12}$ covers the interference between these two coherent processes.

B. Resonance approximation

For our specific case, the probability (5) can be further simplified. In contrast to the very simple electronic structure of heliumlike systems, for which NETP has been first discussed [22], Th^{2+} has a rich and dense level structure. Therefore, it is safe to assume that only the closest resonance will contribute to the NETP probability. This allows for the application of the so-called resonance approximation. In this approximation, all interference terms vanish, and, thus, $G^{(Lpq)}_{12}$ can be neglected and the terms $G^{(Lpq)}_1$ and $G^{(Lpq)}_2$ become

$$G^{(Lpq)}_1 \approx \sum_{\gamma_n J_n}\frac{1}{[J_n]} \times\left|\frac{\langle\gamma_f J_f||\boldsymbol{\alpha}\cdot\boldsymbol{a}^{(p)}_L||\gamma_n J_n\rangle\,\langle\gamma_n J_n||\hat{T}_q||\gamma_i J_i\rangle}{\epsilon_i-\omega_N-\epsilon_n-i\frac{\Gamma_n}{2}}\right|^2, \tag{7a}$$

$$G^{(Lpq)}_2 \approx \sum_{\gamma_n J_n}\frac{1}{[J_n]}\frac{\Gamma_i+\Gamma_n}{\Gamma_n} \times\left|\frac{\langle\gamma_f J_f||\hat{T}_q||\gamma_n J_n\rangle\,\langle\gamma_n J_n||\boldsymbol{\alpha}\cdot\boldsymbol{a}^{(p)}_L||\gamma_i J_i\rangle}{\epsilon_f+\omega_N-\epsilon_n-i\frac{\Gamma_i+\Gamma_n}{2}}\right|^2, \tag{7b}$$

where we incorporated the width of the initial state in resonance approximation following Ref. [30].

Now, the remaining task to calculate the NETP probability (5) in resonance approximation is the evaluation of the reduced nuclear and electronic matrix elements. The nuclear transition amplitudes $\langle I_e||\hat{M}_q||I_g\rangle$ are known from elaborate nuclear calculations, e.g., by Minkov and Pálffy [31], where previous estimates by Tkalya *et al.* [32] have been refined.

C. Enhancement factor β

Due to the complexity of nuclear calculations, the nuclear amplitudes provided, e.g., in Ref. [31] are a major source of uncertainty in our calculations of the NETP probability (5). To circumvent these uncertainties, one can define the *enhancement factor* β (cf. Refs. [28,29]), which is independent of the nuclear transition probability,

$$\beta^{(Lpq)} = \frac{\mathcal{W}^{(Lpq)}_{\rm fi}}{\Gamma_q}, \tag{8}$$

where the nuclear decay width Γ_q is defined by

$$\Gamma_q = \frac{8\pi(q+1)}{q((2q+1)!!)^2}\frac{(\alpha\omega_N)^{2q+1}}{[I_g]}|\langle I_e||\hat{M}_q||I_g\rangle|^2. \tag{9}$$

The enhancement factor (8) is defined in analogy to Refs. [28,29] and given here mainly to make a connection to these works and to test our theory with respect to effects coming from the electronic structure of Th^{2+}.

Specifically, for the case of ^{229}Th, the leading multipoles of the nuclear transition are $M1$ and $E2$, so q is either 1 or 2. From now on, we will assume that all radiative electronic transitions are of the $E1$ type, so that $L = 1$ and $p = 1$. Therefore, in resonance approximation, the enhancement factors of interest are

$$\beta^{(111)} = \frac{3\omega}{2\omega_N^3}\frac{1}{[J_i]}\left(G_1^{(111)} + G_2^{(111)}\right), \tag{10a}$$

$$\beta^{(112)} = \frac{30\omega}{\alpha^2\omega_N^5}\frac{1}{[J_i]}\left(G_1^{(112)} + G_2^{(112)}\right). \tag{10b}$$

IV. NUMERICAL DETAILS

Up to now, we have shown how the NETP process may be discussed by taking the nuclear transition amplitude from the literature or by investigating the enhancement factor instead. Now we will briefly sketch the evaluation of the electronic matrix elements. To calculate these, we apply a combination of configuration interaction (CI) and many-body perturbation theory (MBPT), which has been described in detail in Refs. [33–35]. In particular, we used the package assembled by Kozlov *et al.* [36]. The CI configuration state functions have been set up using Dirac-Hartree-Fock wave functions for the core orbitals and the $5f$, $6d$, $7s$, and $7p$ valence orbitals. For the higher-lying orbitals, we use b-splines and orbitals constructed using the method described, e.g., in Ref. [37]. The CI basis is constructed by virtual excitations from the $[Rn] + 6d^2$ and $[Rn] + 5f6d$ configuration.

The CI+MBPT method is a powerful method to calculate reliable transition matrix elements. Level energies, however, especially for complicated systems such as Th^{2+}, are determined more accurately in experiments. Because the exact position of the resonances is important to determine the NETP probability accurately, we take the experimental values [38] for all level energies instead of the theoretical ones. We will discuss the importance of this step in the section below.

V. RESULTS AND DISCUSSION

Before we discuss the probability of the NETP process in Th^{2+}, we will have a brief look at the enhancement factor $\beta^{(111)}$ [cf. Eq. (8)]. In particular, we want to investigate how the replacement of the calculated level energies by the experimental ones influences the results. Therefore, we performed calculations for $\beta^{(111)}$ as a function of the nuclear excitation energy ω_N using both. The results of these calculations are shown in Fig. 2: the theoretical (black solid line) and the experimental (red dashed line) level energies. The first feature we notice in Fig. 2 is the different number of resonance peaks for different J_i of the upper (initial) state. This can be explained by the sheer number of available decay paths to the $6d^2(J=2): 63\,\mathrm{cm}^{-1}$ state from each of these upper states. While for $J_i = 4$ and a $E1$ radiative transition, the intermediate state must have $J_n = 3$, for $J_i = 2$, there are three possible J_n and, therefore, more intermediate resonances available. But there are two more important things to notice. Foremost, we see that the high-energy cutoff of β is reduced for the case of the experimental level energies. Therefore, we note that it is very important to take the energy splitting between the initial and final electronic state accurately into account. Moreover, we see that the replacement of the energies of the intermediate states to their experimental values does not change the qualitative behavior of $\beta^{(111)}$ and, thus, can be safely done to achieve accurate results.

The primary aim of this paper is to provide information about the most promising excitation paths to observe the NETP process in $^{229}Th^{2+}$. Therefore, we assume according to available experimental setups that the exciting lasers are tunable between 3.45 eV and 5.25 eV [41] (cf. Fig. 1). With such lasers, 19 possible upper states $|\gamma_i J_i\rangle$ can be pumped. This number reduces to 16 if we fix the final state to be the level $6d^2(J=2): 63\,\mathrm{cm}^{-1}$, in order to be able to cycle through the process multiple times. For each of these 16 possible upper states, we calculated the NETP probability (5) summing over $1 \leqslant q \leqslant 2$ in order to account for both the $M1$ and $E2$ nuclear transition channels. This step is necessary

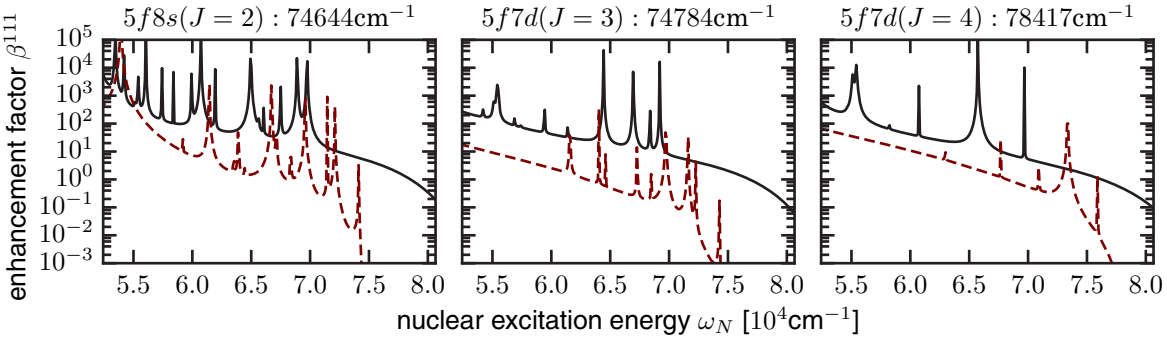

FIG. 2. Comparison of the enhancement factor β before (black solid line) and after (red dashed line) the resonance energies have been shifted to the experimental values [38]. Exemplarily shown here are the transitions from the $5f8s(J=2): 74\,644\,\mathrm{cm}^{-1}$ (left panel), $5f8s(J=3): 74\,784\,\mathrm{cm}^{-1}$ (center panel), and $5f7d(J=4): 78\,417\,\mathrm{cm}^{-1}$ (right panel) states to the $6d^2(J=2): 63\,\mathrm{cm}^{-1}$ state.

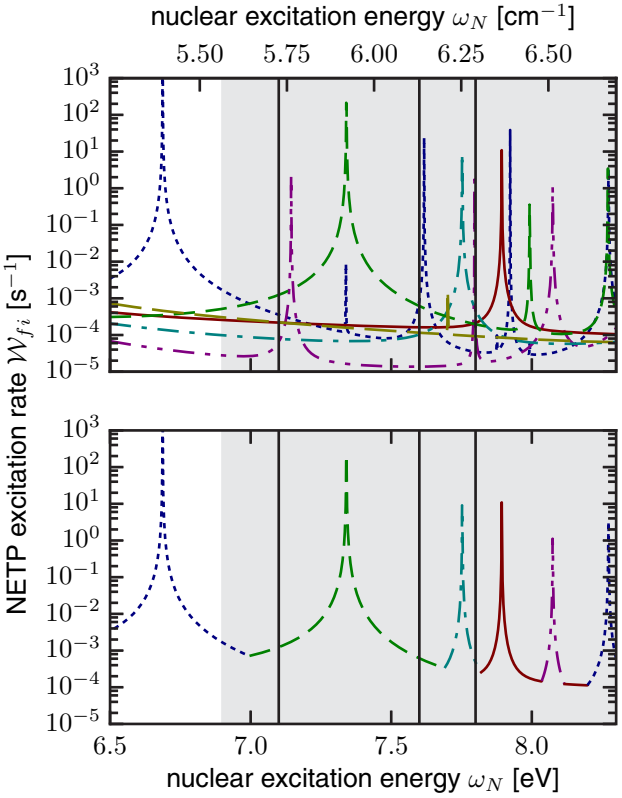

FIG. 3. Probability of NETP for different upper states (top panel) and the envelope of these probabilities (bottom panel), where contributions narrower than 0.1 eV are neglected. The colors are distributed as follows: blue dotted line: $5f8s(J=2): 74\,644\,\mathrm{cm}^{-1}$; green dashed line: $5f7d(J=2): 79\,916\,\mathrm{cm}^{-1}$; turquoise dash-dotted line: $5f7d(J=2): 83\,237\,\mathrm{cm}^{-1}$; red solid line: $5f7d(J=3): 84\,374\,\mathrm{cm}^{-1}$; and purple dash-double-dotted line: $5f7d(J=2): 78\,333\,\mathrm{cm}^{-1}$. The black vertical lines show the supposed energies of the low-lying isomeric state according to Refs. [32,39,40] with the corresponding uncertainty interval shown by the gray-shaded area.

because it has been shown recently that both the $M1$ and the $E2$ channels may contribute equally to the NETP probability [42]. Similar to Fig. 2, we display the NETP probability $\mathcal{W}_{\mathrm{fi}} = \sum_{q=1}^{2} \mathcal{W}_{\mathrm{fi}}^{(E1,q)}$ as a function of the nuclear excitation energy ω_N. This data, however, is not very conclusive. Thus, it needed to be processed, which is illustrated in Fig. 3. In the upper panel of this figure, we display the NETP probability for four upper states as a function of the nuclear excitation energy ω_N. To get our final result, we take the envelope of this family of curves, as shown in the bottom panel of Fig. 3. Moreover, we omit resonance peaks narrower than 0.1 eV for it would make the figure impractical to use, especially at higher ω_N, where the resonances get more dense. Note also that we do not show the NETP probability for those of the 16 possible upper states that do not contribute to the envelope. The vertical lines in Fig. 3 denote the most recent values for the energy of the nuclear isomeric state, ranging from 7.1 to 7.6 and 7.8 eV [32,39,40]. The gray shaded area denotes the combined uncertainties of all three measurements and, thus, a recommended initial search area for the nuclear isomer.

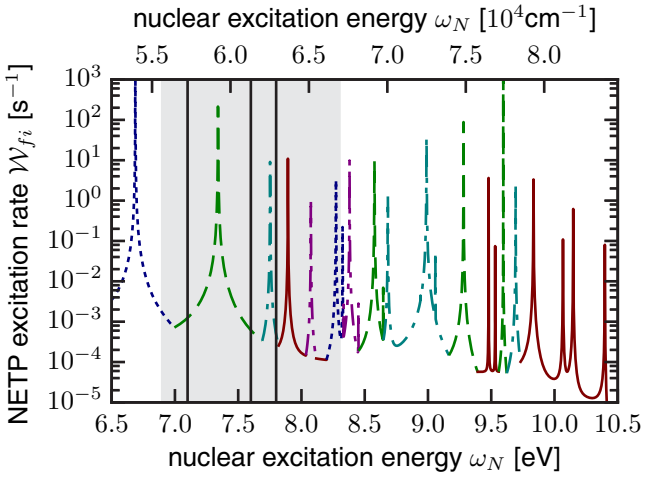

FIG. 4. Same as Fig. 3 (bottom panel) but for the energy range between 6.5 and 10.5 eV.

With the preparation of the data explained above, we are now able to generate the main result of this work. In Fig. 4, we show which is the ideal upper state to observe the NETP process in ^{229}Th^{2+} as a function of ω_N. It can also be seen that for the entire energy range between 6.5 and 10.5 eV, only 5 of the possible 16 upper states need to be considered for a possible experiment. Again, the vertical lines and the gray area in Fig. 4 mark the recommended initial search area for the nuclear isomeric state.

Let us finally discuss how the excitation of the nucleus could be monitored in the experiment we propose. Recently, the hyperfine structure of the electronic levels in Th^{2+} has proven to be a good indicator of whether the nucleus is in its ground or first-excited state [11]. This would also be possible in the scenario proposed in the present work by either applying an additional laser or observing the fluorescence from one of the pumping stages. Another common option would be to observe the time-delayed photoemission from the nuclear decay. This, however, would not be recommended for the scenario proposed here because we could cycle through the process, no matter if the upper state decayed via NETP or the more likely two-photon cascade. This allows for a good statistics and does not require a shot-by-shot analysis of the data with accurate timing.

VI. CONCLUDING REMARKS

The NETP process has been shown to be a promising candidate to investigate the nuclear structure of highly charged ions [22]. In the present work, this process is discussed for many electron systems within the resonance approximation. To excite the ^{229}Th nucleus, we propose a combination of a two-step pumping of an upper state from which the NETP process occurs. To overcome the difficulty of a small branching ratio between NETP and a generic radiative two-step decay of the upper state, the proposed process can be cycled independent of the way the ion decays.

With several promising experiments on the horizon that aim for a precise determination of $\hbar\omega_N$ [20,43], the scenario described in this work aims for a controlled excitation of the

^{229}Th. Therefore, a challenge that comes with many proposed electronic bridge processes for the excitation of the ^{229}Th nucleus, i.e., the requirement of a continuous scanning with a tunable laser, does not apply in the scenario described in this paper. In the proposed experiment, the lasers are adjusted only once to ensure the most efficient pumping of the upper state. For a first test of our theory, we recommend to pump the $5f7d(J=2): 83\,237\,\mathrm{cm}^{-1}$ and the $5f7d(J=3): 84\,374\,\mathrm{cm}^{-1}$ states, both of which have resonances close to the currently assumed value of 7.8 eV of the nuclear excitation energy.

ACKNOWLEDGMENTS

R.A.M. acknowledges support form the RS-APS and many useful discussions with David-Marcel Meier and Johannes Thielking.

[1] B. J. Bloom, T. L. Nicholson, J. R. Williams, S. L. Campbell, M. Bishof, X. Zhang, W. Zhang, S. L. Bromley, and J. Ye, Nature (London) **506**, 71 (2014).

[2] N. Huntemann, C. Sanner, B. Lipphardt, C. Tamm, and E. Peik, Phys. Rev. Lett. **116**, 063001 (2016).

[3] V. A. Kostelecký and C. D. Lane, Phys. Rev. D **60**, 116010 (1999).

[4] T. Rosenband, D. B. Hume, P. O. Schmidt, C. W. Chou, A. Brusch, L. Lorini, W. H. Oskay, R. E. Drullinger, T. M. Fortier, J. E. Stalnaker, S. A. Diddams, W. C. Swann, N. R. Newbury, W. M. Itano, D. J. Wineland, and J. C. Bergquist, Science **319**, 1808 (2008).

[5] M. S. Safronova, V. A. Dzuba, V. V. Flambaum, U. I. Safronova, S. G. Porsev, and M. G. Kozlov, Phys. Rev. Lett. **113**, 030801 (2014).

[6] E. Peik and C. Tamm, Europhys. Lett. **61**, 181 (2003).

[7] L. von der Wense, *On the Direct Detection of ^{229m}Th* (Springer, Berlin, 2017).

[8] E. V. Tkalya, Phys. Rev. Lett. **120**, 122501 (2018).

[9] B. Seiferle, L. von der Wense, and P. G. Thirolf, Phys. Rev. Lett. **118**, 042501 (2017).

[10] M. S. Safronova, S. G. Porsev, M. G. Kozlov, J. Thielking, M. V. Okhapkin, P. Głowacki, D.-M. Meier, and E. Peik, Phys. Rev. Lett. **121**, 213001 (2018).

[11] J. Thielking, M. V. Okhapkin, P. Głowacki, D.-M. Meier, L. von der Wense, B. Seiferle, C. E. Düllmann, P. G. Thirolf, and E. Peik, Nature (London) **556**, 321 (2018).

[12] R. A. Müller, A. V. Maiorova, S. Fritzsche, A. V. Volotka, R. Beerwerth, P. Głowacki, J. Thielking, D.-M. Meier, M. Okhapkin, E. Peik, and A. Surzhykov, Phys. Rev. A **98**, 020503(R) (2018).

[13] K. Beloy, Phys. Rev. Lett. **112**, 062503 (2014).

[14] L. von der Wense, B. Seiferle, M. Laatiaoui, J. B. Neumayr, H.-J. Maier, H.-F. Wirth, C. Mokry, J. Runke, K. Eberhardt, C. E. Düllmann, N. G. Trautmann, and P. G. Thirolf, Nature (London) **533**, 47 (2016).

[15] S. Stellmer, G. Kazakov, M. Schreitl, H. Kaser, M. Kolbe, and T. Schumm, Phys. Rev. A **97**, 062506 (2018).

[16] F. F. Karpeshin, Hyperfine Interact. **143**, 79 (2002).

[17] A. Pálffy, W. Scheid, and Z. Harman, Phys. Rev. A **73**, 012715 (2006).

[18] J. Gunst, Y. A. Litvinov, C. H. Keitel, and A. Pálffy, Phys. Rev. Lett. **112**, 082501 (2014).

[19] A. V. Andreev, A. B. Savel'ev, S. Y. Stremoukhov, and O. A. Shoutova, Phys. Rev. A **99**, 013422 (2019).

[20] L. von der Wense, B. Seiferle, S. Stellmer, J. Weitenberg, G. Kazakov, A. Pálffy, and P. G. Thirolf, Phys. Rev. Lett. **119**, 132503 (2017).

[21] J. Gunst, Y. Wu, N. Kumar, C. H. Keitel, and A. Pálffy, Phys. Plasmas **22**, 112706 (2015).

[22] A. V. Volotka, A. Surzhykov, S. Trotsenko, G. Plunien, T. Stöhlker, and S. Fritzsche, Phys. Rev. Lett. **117**, 243001 (2016).

[23] M. Knoop, M. Vedel, and F. Vedel, Phys. Rev. A **58**, 264 (1998).

[24] O. A. Herrera-Sancho, M. V. Okhapkin, K. Zimmermann, Chr. Tamm, E. Peik, A. V. Taichenachev, V. I. Yudin, and P. Głowacki, Phys. Rev. A **85**, 033402 (2012).

[25] J. Thielking (private communication).

[26] J. Eisenberg and W. Greiner, *Nuclear Theory: Excitation Mechanisms of the Nucleus*, Nuclear Theory (North-Holland, Amsterdam, 1976).

[27] M. E. Rose, *Elementary Theory of Angular Momentum* (Dover, New York, 1995).

[28] S. G. Porsev, V. V. Flambaum, E. Peik, and C. Tamm, Phys. Rev. Lett. **105**, 182501 (2010).

[29] S. G. Porsev and V. V. Flambaum, Phys. Rev. A **81**, 042516 (2010).

[30] V. M. Shabaev, A. V. Volotka, C. Kozhuharov, G. Plunien, and T. Stöhlker, Phys. Rev. A **81**, 052102 (2010).

[31] N. Minkov and A. Pálffy, Phys. Rev. Lett. **118**, 212501 (2017).

[32] E. V. Tkalya, C. Schneider, J. Jeet, and E. R. Hudson, Phys. Rev. C **92**, 054324 (2015).

[33] V. A. Dzuba, V. V. Flambaum, and M. G. Kozlov, Phys. Rev. A **54**, 3948 (1996).

[34] V. A. Dzuba, Phys. Rev. A **71**, 032512 (2005).

[35] V. A. Dzuba and V. V. Flambaum, Phys. Rev. A **75**, 052504 (2007).

[36] M. Kozlov, S. Porsev, M. Safronova, and I. Tupitsyn, Comput. Phys. Commun. **195**, 199 (2015).

[37] M. G. Kozlov, S. G. Porsev, and V. V. Flambaum, J. Phys. B **29**, 689 (1996).

[38] A. Kramida, Yu. Ralchenko, J. Reader, and NIST ASD Team, NIST Atomic Spectra Database (ver. 5.6.1) National Institute of Standards and Technology, Gaithersburg, MD, 2018 https://physics.nist.gov/asd.

[39] B. R. Beck, J. A. Becker, P. Beiersdorfer, G. V. Brown, K. J. Moody, J. B. Wilhelmy, F. S. Porter, C. A. Kilbourne, and R. L. Kelley, Phys. Rev. Lett. **98**, 142501 (2007).

[40] P. V. Borisyuk, E. V. Chubunova, N. N. Kolachevsky, Yu. Y. Lebedinskii, O. S. Vasiliev, and E. V. Tkalya, arXiv:1804.00299.

[41] D.-M. Meier (private communication).

[42] P. V. Bilous, N. Minkov, and A. Pálffy, Phys. Rev. C **97**, 044320 (2018).

[43] B. Seiferle, L. von der Wense, I. Amersdorffer, N. Arlt, B. Kotulski, and P. G. Thirolf, arXiv:1812.04621.

6

SUMMARY AND OUTLOOK

This thesis is devoted to the interactions between atomic nuclei and their electron shells beyond electrostatic attraction. Therefore we laid down the theory of the kinetic and nuclear volume isotope shifts and hyperfine interaction. We have shown how these effects can be used to derive nuclear properties from spectroscopic measurements. Finally, we have discussed how transitions in the electron shell can influence the state of the nucleus, ending with a proposal for the excitation of ^{229}Th via a two-photon transition in doubly charged thorium.

Isotope Shift Calculations and King Plots

In theory, we distinguish two kinds of isotope shifts. The mass shift is caused by the motion of the nucleus about the center of mass of the atom and the field shift arises due to the change of the nuclear charge radius for different isotopes. As we have shown this difference can be obtained with a combination of many-body calculations and experimental results. In particular we derived the mean square radius difference for ^{232}Th and ^{229}Th using the MCDF approach (cf. Sec. 2.4). More importantly, we were also able to reproduce the results by Safranova *et al.* [14] for the charge radius difference between ^{229}Th and the first excited isomeric state of this thorium nucleus ^{229m}Th using a conceptually different theoretical way for the calculation of many-electron dynamics than the authors.

The measurement of isotope shifts can not only be used to extract the charge radii of atomic nuclei. With a so-called King plot it is possible to measure and calculate a very robust quantity being the ratio $f = F_{f_2 i_2} / F_{f_1 i_1}$ of the field shift constants of two transitions $|i_{1/2}\rangle \rightarrow |f_{1/2}\rangle$. This ratio is given by the slope of the King plot that is strictly linear if we can assume that only the first order of both the relativistic mass and field shift contribute significantly to the total isotope shift. This and the fact that f can be obtained very precisely by electronic structure calculations supposedly makes it a very sensitive tool for the search for physics beyond the standard model [16, 17]. In particular, the authors of the references above suggest looking for nonlinearities in the King plot that can be attributed to unknown interactions. But before any interpretation of such nonlinearities is even possible, we first need to benchmark both theory and experiment at the desired precision. This is necessary to understand the involved theories and complex numerics and get possible experimental systemat-

ics under control. Recently an experiment has shown that this is not entirely achieved yet. In a measurement of the isotope shifts of two transitions in Ca^+, a yet unresolved discrepancy between the theoretical and experimental value for the field shift ratio has been found [78]. To gain a better understanding of this discrepancy we performed an analogue study on the about three times as heavy Ba^+ ion [RAM1]. We used the measured isotope shifts that were about one order of magnitude more precise than previous values to derive the experimental ratio of field shift constants $f_{exp} = 1.0186(9)$. This number was then compared to theoretical values for f that have been obtained in three different ways. The hydrogenic model yielded a value for $f_{hyd} = 1.04231$ that was significantly larger than the experimental result. With the more advanced DHF model we obtained $f_{DHF} = 1.0201$ and eventually used the MCDF approach to calculate our final result of $f_{MCDF} = 1.0206(3)_{num}(4)_{sys}$. To estimate the systematic and numerical uncertainties of this result we performed an elaborate convergence analysis according to section 2.3 and estimated the Breit, self-energy and vacuum polarization contributions to the field shift from analytical single-electron models. The excellent agreement between our calculations and the experimental results helped to narrow down the possible reasons for the discrepancy in the Ca^+ case. Either there were theoretical errors in the treatment of correlations in the electron shell or experimental systematics that have not been taken into account.

For the continuation of our investigations it is important to be aware that besides those caused by physics beyond the standard model, there are King plot nonlinearities that can appear in precise spectroscopic measurements that are theoretically already well understood. These contributions have not been observed in any experiment yet, however only if they are under control and if we can find systems and scenarios where they are suppressed, we can use King plot nonlinearities as an indicator for physics beyond the standard model. The precision that can be achieved by experiments that are currently being prepared seem to make the observation of higher-order contributions to the isotope shift feasible, including even more complex contributions like the polarization of the nucleus due to its level structure. Therefore a comparative study of such nonlinearities introduced by quantum electrodynamical effects has to be conducted and the magnitude of their contributions needs to be estimated.

Due to the variety of systems that are available for high-precision experiments, future research needs to employ a variety of theoretical approaches to investigate small contributions to the isotope shift. For few-electron systems, a rigorous treatment of quantum electrodynamical effects within CI calculations is possible (cf. Sec. 2.3), as shown in Refs. [93, 94]. In more complex systems the possible precision of calculations is limited by the available computational power and is usually smaller and different theoretical approaches like MCDF and CI-MBPT may be required (cf. Secs. 2.4 and 2.5).

Hyperfine Structure of Th^{2+}

Supposedly the nuclear transition between ^{229}Th and the isomeric ^{229m}Th is orders of magnitude more sensitive to possible variations of fundamental constants than any electronic transition known to date. To verify this claim Berengut *et al.* [13] derived a model that allows expressing this sensitivity in terms of quantities that can be derived from electronic observables. The first observable needed is the difference between the mean square radii of both the ground state nucleus and the isomer. This has been obtained by us in Sec. 4.1. The second quantity that is needed is the ratio between the nuclear electric quadrupole moments of ^{229}Th and ^{229m}Th. Therefore we performed a set of MCDF and CI-MBPT calculations (cf. Ch. 2). These calculations are the first theoretical investigation of the hyperfine structure of doubly charged thorium and agree very well with the experimental findings and, therefore, mark one of the milestones reached in this thesis. We used our theoretical results to extract the ratio Q/Q_m for the first time independent on previous calculations (for details see [RAM2]). Similar to Ref. [73], our results indicate that the nuclear transition in thorium is by about three orders of magnitude more sensitive to α-variations than most electronic transitions. However, the experimental and theoretical uncertainty of these results does not allow to settle this question satisfactorily.

The fact that the sensitivity of the nuclear transition in ^{229}Th to variations of α is one of the main justifications for the extensive research on this unique nucleus makes further studies more than interesting. One factor limiting the accuracy of our results is the description of the complex electronic structure of Th^{2+}, requiring up to half a million CSFs. Therefore analogue measurements as in Ref. [73] in Th^{3+} will be necessary. This ion has a comparably simple electronic structure with one electron above a closed radon core and can be treated theoretically with good precision. Moreover, it has been shown that it can be laser cooled and trapped for spectroscopic experiments [79].

Electronic Bridge Processes

Related to our studies of nuclear properties using atomic structure calculations we also wanted to apply these theories to influence the state of the nucleus itself. This is achieved by a coupling of the electron shell to the nuclear current that is very similar to the hyperfine interaction (see Sec. 4.2). Such a coupling allows for the excitation of the nucleus via the exchange of a virtual photon. If the corresponding transition in the electron shell is between two bound states both, the energy of the nuclear and the electronic transitions, need to be close to each other. One possibility to weaken

this resonance condition is to choose a system with a dense level structure like Th^+. For this ion, we performed a study of the level density and compared our results to spectroscopic measurements of the level structure of Th^+ up to 9.8 eV [RAM3]. Furthermore, we obtained the so-called enhancement factor β in Th^+ that is the ratio between the width of the electron bridge process and the spontaneous decay width of the nucleus. Our value of $\beta \sim 10^3$ is consistent with previous works [36] but now based on the experimental electronic structure of Th^+. A more detailed investigation of the properties of β has been performed by us in Ref. [RAM4], where we studied different approximation schemes that are commonly applied in calculations of the enhancement with special emphasis on the construction of the electron propagator. There we come to the conclusion that the direct summation approach is a good approximation for this propagator if the possible interference between the contributing Feynman diagrams is taken into account.

Both, our work on the theoretical details of electron bridge processes in Th^{3+} [RAM4] and the estimation of the enhancement of the same process in Th^+ rely on a weakening of the resonance condition (4.32) due to the energetic proximity of an electronic transition to the nuclear resonance or a dense level structure. We have shown that this can be overcome by considering a two-photon decay of the electron shell. One of these photons participates in the electron bridge process, while the other one is emitted. The ratio of both photon energies is continuous and, thus, the resonance condition can always be fulfilled. There are, however, several ways how this nuclear excitation by a two-photon electronic transition (NETP) can be implemented experimentally. Using the example of doubly charged thorium we studied the best way of monitoring and preparing the excited state of the electron shell from which the NETP process occurs to achieve the optimal probability for the nuclear excitation [RAM5]. This study resulted in a guideline that shows the recommended excitation paths for Th^{2+}, depending on the frequency ω_N of the nuclear resonance that is only known up to a precision of 0.17 eV. Thus it enables us to choose the best experimental scenario depending on the energy at which the nuclear isomer ^{229m}Th is searched.

Besides the trapping of weakly charged thorium and its excitation by a two-photon transition, there are other promising mechanisms that are close to an experimental realization. These processes are theoretically only sparsely investigated, opening opportunities for future research. Many of these mechanisms aim for taking advantage of the newly developed electron beam ion traps (EBITs) for the preparation of highly charged ions and subsequent cooling and trapping of these ions in a cryogenic Paul trap [95, 96]. In such highly charged ions, the overlap between wave function of the remaining electrons and the nucleus is much larger than in neutral systems. Therefore the electron-nuclear interaction is expected to be enhanced, increasing the probability of electron bridge processes. The transition energies between atomic levels in

highly charged ions are, however, much higher than the energy of the ^{229m}Th nuclear isomer. Thus, we will investigate the possibility of using transitions between hyperfine states in an electron bridge process such as NETP to excite the thorium nucleus. This idea may be later transferred to the case of ^{235}U to gain a better understanding of the emergence of low lying nuclear excited states in general.

The presence of an electron beam in an EBIT might enable another process that also does not suffer from the resonance condition. As it has been shown for muonic atoms, nuclei can be excited by a non-resonant process by an external electromagnetic field [97]. A similar process might be observed in an EBIT. The high-energy ($\sim$ keV) electrons of the trap passing by the highly charged ions will polarize their electron shell. The relaxation of this polarization usually happens via the emission of a photon and is known as polarization bremsstrahlung [98, 99]. The spectrum of this radiation is continuous and located at much lower energies than the kinetic energy of the passing electron and can be in the order of $\sim 10\,\mathrm{eV}$. Thus this radiation might be used in a non-resonant electron bridge process for the excitation of the thorium nucleus.

In recent years more and more effort is spent to finally get a hold of the transition in the thorium nucleus. If these efforts lead to success eventually it is worth thinking of the next steps towards a technical implementation of the ^{229}Th$\rightarrow^{229m}$Th transition. Therefore, we plan to investigate how this transition can be interrogated as a frequency standard in a nuclear clock. Although the nuclear isomer can be accessed with optical lasers, a frequency comb in this energy range is feasible but challenging to realize [32]. Therefore we plan to propose the option of a hybrid interrogation of the nuclear transition involving an electron bridge process. Our proposal is based on the idea of quantum logic spectroscopy that is nowadays commonly applied in optical atomic clocks (see e.g. Ref. [27] and references therein). But instead or additionally to logic ions in the trap, the electron shell serves as the telltale for the nuclear excitation.

Closing Remarks

In summary atomic physics has reached a point, where experiments have become so precise that they can be used to investigate processes and effects that were only known theoretically and have been neglected for decades. In fact, these experiments exceed the precision of theoretical calculations in many cases. But as we have shown in this thesis theoretical calculations serve as a guideline for these investigations and are necessary for the distinction of all involved interactions and effects. Moreover, as we could only indicate above, there is much theoretical work to be done in the field of electron-nucleus interactions to make the most of the exciting possibilities that opened up in recent years.

7

APPENDIX A: SUPPLEMENT MATERIAL OF REF. [RAM3]

For completeness, we provide here the supplement material for our work on the level structure of singly charged thorium. This material provides a complete list of the excitation paths that were chosen narrow down the total angular momentum of the newly identified levels in Th^+. We only considered levels that were observed via at least two different intermediate levels (cf. Tab. 1 below).

Supplemental Material for: Electronic level structure of Th^+ in the range of the ^{229m}Th isomer energy

D.-M. Meier,[1] J. Thielking,[1] P. Głowacki,[1,*] M. V. Okhapkin,[1] R. A. Müller,[1] A. Surzhykov,[1,2] and E. Peik[1,†]

[1] *Physikalisch-Technische Bundesanstalt, 38116 Braunschweig, Germany*
[2] *Technische Universität Braunschweig, 38106 Braunschweig, Germany*

(Dated: February 22, 2019)

TABLE I. Intermediate states of the two-step excitation, sorted by angular momentum J. Energies and leading configurations are taken from Ref. [1], with the exception of the corrected classification of the 25027cm^{-1} state described in Ref. [2]. Labels in the first column are introduced for reference in Tab. II.

Ref.	Level [cm^{-1}]	J	Configuration
a	25027.040	1/2	$7s7p + 6d7s7p$
b	26626.478	1/2	$6d7s(^3\mathrm{D})7p\ ^4\mathrm{D^o} + (^3\mathrm{D})\ ^2\mathrm{P^o}$
c	35198.990	1/2	$6d^2(^3P)7p\ ^4\mathrm{D^o} + 6d7s(^3\mathrm{D})7p\ ^4\mathrm{P^o}$
d	37130.340	1/2	$5f(^1\mathrm{G^o})6d^2\ ^2\mathrm{P^o} + 6d^2(^3\mathrm{P})7p\ ^4\mathrm{D^o}$
e	37716.322	1/2	$6d^2(^1\mathrm{D})7p\ ^2\mathrm{P^o} + (^3\mathrm{F})\ ^4\mathrm{D^o}$
f	26965.202	3/2	$5f(^3\mathrm{F^o})6d^2\ ^4\mathrm{S^o} + (^3\mathrm{F^o})\ ^2\mathrm{P^o}$
g	27403.180	3/2	$5f(^1\mathrm{D^o})6d^2\ ^2\mathrm{D^o} + (^3\mathrm{P^o})\ ^4\mathrm{D^o}$
h	36390.527	3/2	$6d^2(^3\mathrm{F})7p\ ^4\mathrm{F^o} + 5f(^1\mathrm{G^o})6d^2\ ^2\mathrm{P^o}$
i	36581.568	3/2	$6d^2(^3\mathrm{F})7p\ ^4\mathrm{F^o} + 5f(^1\mathrm{G^o})6d^2\ ^2\mathrm{D^o}$
j	24873.981	5/2	$6d7s(^3\mathrm{D})7p\ ^4\mathrm{F^o} + 5f(^3\mathrm{P^o})6d^2\ ^4\mathrm{F^o}$
k	26424.480	5/2	$5f(^3\mathrm{P^o})6d^2\ ^4\mathrm{F^o} + (^3\mathrm{P^o})\ ^4\mathrm{D^o}$
l	28243.812	5/2	$6d7s(^3\mathrm{D})7p\ ^4\mathrm{F^o} + 6d^2(^3\mathrm{F})7p\ ^4\mathrm{G^o}$
m	35156.916	5/2	$5f(^1\mathrm{G^o})6d^2\ ^2\mathrm{D^o} + (^1\mathrm{G^o})\ ^2\mathrm{F^o}$
n	36687.992	5/2	$6d^2(^3\mathrm{F})7p\ ^4\mathrm{F^o} + 6d7s(^3\mathrm{D})7p\ ^4\mathrm{P^o}$
o	37846.174	5/2	$6d^2(^3\mathrm{P})7p\ ^2\mathrm{D^o} + (^3\mathrm{P})\ ^4\mathrm{D^o}$

TABLE II: Newly observed high-lying states excited through the intermediate levels listed in Tab. I together with levels observed in our previous experiment [3] (marked with "**"). The symbol "**x**" marks levels which are successfully excited via the specified intermediate level and the symbol "–" denotes that no excitation is observed. If no symbol is given, the excitation has not been checked. Where possible, the levels are given with their total angular momenta derived from the experiment. The energy of the level marked with ** from Ref. [3] is updated. Levels with angular momentum $J = 3/2$ are classified unambiguously.

	Intermediate levels			
Level	J = 1/2	J = 3/2	J = 5/2	
[cm^{-1}]	a b c d e	f g h i	j k l m n o	J_{exp}
58875.5 *	-		x	3/2 - 7/2
59387.1 *	-		x	3/2 - 7/2
59477.4 *	x		x	3/2
59803.0 *	-		x	3/2 - 7/2
60380.1 *	x		x	3/2
60618.6 *	x		x	3/2
60721.3 *	-		x	3/2 - 7/2
61032.4 *	x	x	x	3/2
61388.0 *	-	-	x	3/2 - 7/2
61428.6 *	-	x	x	3/2 or 5/2
61726.3 *	x x	x x	x	3/2
61963.6 *	x x	x x	x	3/2
62307.2 *	-	x x	x	3/2 or 5/2
62373.8 *	x x	x x	x x	3/2
62477.0 *	-	x x	x x	3/2 or 5/2
62560.1 *	-	- -	x x	3/2 or 5/2
62562.2 *	x x	x x	x x	3/2
62753.1 *	-	x x	x x	3/2 or 5/2
62873.11	x	x x	- -	1/2 or 3/2
63257.5 *	-	- -	x x	3/2 - 7/2
63268.90	x x	x x	- -	1/2 or 3/2
63298.4 *	-	- -	x x	3/2 - 7/2
63557.7 *	-	- -	x x	3/2 - 7/2
63680.29	x x	x x	x x	3/2
64107.51	- -	x x	x x	3/2 or 5/2
64122.0 *	-	- -	x x	3/2 - 7/2
64150.3 *	x x	x -	x x	3/2
64368.24	- -	x x	x x	3/2 or 5/2
64442.11	x x	x x	- -	1/2 or 3/2
64560.4 *	x x	x x	x x	3/2
64813.7 *	-	- -	x x	3/2 - 7/2
64860.4 *	-	x x	x x	3/2 or 5/2
64887.80	x x	x x	- -	1/2 or 3/2
64920.1 *	-	x x	x x	3/2 or 5/2
65037.7 *	x x	x x	x x	3/2
65144.4 *	-	x x	x x	3/2 or 5/2
65191.1 *	-	- -	x x	3/2 - 7/2
65730.4 *	x x	- x	x x	3/2
65738.54 **	-	- -	x x	3/2 - 7/2
65753.45	x x	x x	- -	1/2 or 3/2
65799.6 *	x x	x x	x x	3/2
65910.0 *	-	- -	x x	3/2 - 7/2
65946.9 *	-	- -	x x	3/2 - 7/2
66052.0 *	-	- x	x x	3/2 or 5/2
66141.2 *	-	x x	x x	3/2 or 5/2
66324.52	x x	x x	- -	1/2 or 3/2
66333.7 *	x x	- x	x x	3/2
66388.81	x x	x x	- -	1/2 or 3/2
66429.64	- -	x x	- x	3/2 or 5/2
66558.0 *	-	- -	x x	3/2 - 7/2
66609.0 *	-	x x	x x	3/2 or 5/2
66666.96	x x	- x	- -	1/2 or 3/2
66702.9 *	x x	x x	x x	3/2
66831.1 *	x x	x x	x x	3/2
66855.6 *	-	x x	x x	3/2 or 5/2
67066.2 *	-	- -	x x	3/2 - 7/2
67154.05	x -	x x	x x	3/2
67177.76	- -	- -	x x	3/2 - 7/2
67378.61	-	- -	x x	3/2 - 7/2
67509.63	x	x x	x x	3/2
67577.71	-	x -	- x	3/2 or 5/2
67657.30	x	x x	- -	1/2 or 3/2
67737.62	-	x x	x x	3/2 or 5/2
67803.24	-	x -	- x	3/2 or 5/2
67843.31	-	x x	- x	3/2 or 5/2
67866.10	-	- x	x x	3/2 or 5/2
68033.33	-	- -	x x	3/2 - 7/2
68088.03	x	x x	- x	3/2
68278.65	-	- -	x x	3/2 - 7/2
68497.88	-	- x	- x	3/2 or 5/2
68564.19	-	x x	- x	3/2 or 5/2

* Present address: Poznań University of Technology, Poznań, Poland
† Corresponding author e-mail address: ekkehard.peik@ptb.de

	Intermediate levels															
Level	J = 1/2					J = 3/2				J = 5/2						
[cm^{-1}]	a	b	c	d	e	f	g	h	i	j	k	l	m	n	o	J_{exp}
68598.83	-					x	x			-	x					3/2 or 5/2
68752.06	x					x	x				x					3/2
68812.64	-					x	x				x					3/2 or 5/2
68898.67						x	x				x					3/2 or 5/2
68921.30						-	x				x					3/2 or 5/2
69582.93		x									x					3/2
70036.57		x									x					3/2
70602.32							x								x	3/2 or 5/2
70618.40							x								x	3/2 or 5/2
70747.82							-	-					x	x		3/2 - 7/2
70924.75		-					x								x	3/2 or 5/2
71038.37		x	-				x								x	3/2
71043.67		-					-	-					x	x		3/2 - 7/2
71148.96		-					x								x	3/2 or 5/2
71153.87		x					x								x	3/2
71278.32		x					x								-	1/2 or 3/2
71309.24		-					x								x	3/2 or 5/2
71345.59		x					x								-	1/2 or 3/2
71457.82		-					-	-					x	x		3/2 - 7/2
71543.05		x					x								x	3/2
71544.12		x					x								-	1/2 or 3/2
71595.39		-					x	x							-	1/2 - 5/2
71648.63		-					x	x							-	1/2 - 5/2
71682.08		x					x								-	1/2 or 3/2
71704.43		-					x								x	3/2 or 5/2
71893.76		x					x								x	3/2
71980.22		-					x								x	3/2 or 5/2
71995.47		-					-	-					x	x		3/2 - 7/2
72027.87		x					x								x	3/2
72070.57		x					x								-	1/2 or 3/2
72183.47		-					x								x	3/2 or 5/2
72195.77		-					x								x	3/2 or 5/2
72353.67		-					-	-					x	x		3/2 - 7/2
72395.99		-					x								x	3/2 or 5/2
72403.45		x					x								x	3/2
72437.78		x					x								-	1/2 or 3/2
72443.68		-					x								x	3/2 or 5/2
72612.99		-					x								x	3/2 or 5/2
72624.83		x					x								x	3/2
72644.97		-					-	-					x	x		3/2 - 7/2
72711.86		-					-	-					x	x		3/2 - 7/2
72748.31		x					x								x	3/2
72756.38		-					-	-					x	x		3/2 - 7/2
72849.84		x					x								x	3/2
72904.32		-					-	-					x	x		3/2 - 7/2
72937.01		-					x								x	3/2 or 5/2
72967.30		x					x								x	3/2
73007.80		x					x								-	1/2 or 3/2
73141.86		x					x								x	3/2
73171.82		-					-	-					x	x		3/2 - 7/2
73225.52		x					x								x	3/2
73245.52		-					x								x	3/2 or 5/2
73314.63		-					-	-					x	x		3/2 - 7/2
73349.33		x					x								-	1/2 or 3/2
73427.59		x					x								x	3/2
73486.18		-					x								x	3/2 or 5/2
73506.20		x					x								-	1/2 or 3/2
73514.42		-					-	-					x	x		3/2 - 7/2
73571.40		-					x								x	3/2 or 5/2
73637.54		-					x								x	3/2 or 5/2
73717.33		x					x								x	3/2
73720.66		-					-	-					x	x		3/2 - 7/2
73856.76		-					x								x	3/2 or 5/2
73927.39		-					x								x	3/2 or 5/2
74015.17		-					-	-					-	x	x	3/2 - 7/2
74035.55		x					x								x	3/2
74041.31		-					-	-					x	x		3/2 - 7/2

	Intermediate levels															
Level	J = 1/2					J = 3/2				J = 5/2						
[cm^{-1}]	a	b	c	d	e	f	g	h	i	j	k	l	m	n	o	J_{exp}
74077.59			-				x	x						-		1/2 - 5/2
74159.76			-				x							x		3/2 or 5/2
74195.13													x	x		3/2 - 7/2
74201.68			x				x							-		1/2 or 3/2
74255.11			-				x							x		3/2 or 5/2
74328.90			-				x							x		3/2 or 5/2
74396.40			-				x							x		3/2 or 5/2
74461.06			-				-	-					x	x		3/2 - 7/2
74503.38			-				x							x		3/2 or 5/2
74554.39			x				x							x		3/2
74642.51			-				x							x		3/2 or 5/2
74646.94			x				x							-		1/2 or 3/2
74781.76			-				x							x		3/2 or 5/2
74823.59			-				x							x		3/2 or 5/2
74881.76			x				x							x		3/2
75009.01			-				x							x		3/2 or 5/2
75058.06			-				-	-					-	x	x	3/2 - 7/2
75108.36			-				x							x		3/2 or 5/2
75129.42			-				x	x						-		1/2 - 5/2
75172.74			-				x							x		3/2 or 5/2
75324.44			-				-	-						x	x	3/2 - 7/2
75380.56			-				x							x		3/2 or 5/2
75434.83			-				-	-						x	x	3/2 - 7/2
75553.70			x				x							-		1/2 or 3/2
75568.80			-				x							x		3/2 or 5/2
75613.54			x				x							x	x	3/2
75690.72			x				x							-		1/2 or 3/2
75783.69			-				x							x		3/2 or 5/2
75840.96			-				x							x		3/2 or 5/2
75889.36			x				x							-		1/2 or 3/2
75950.56			-				-	-						x	x	3/2 - 7/2
75966.37			x				x							x		3/2
76122.62			x				x	x						-		1/2 or 3/2
76157.73			x				x							-		1/2 or 3/2
76158.83			-				-	-						x	x	3/2 - 7/2
76169.30			-				x	x						-		1/2 - 5/2
76227.32			-				x	x						-		1/2 - 5/2
76371.41			x				x	x						-		1/2 or 3/2
76445.96			x				-	x						-		1/2 or 3/2
76508.84			-				-	-						x	x	3/2 - 7/2
76521.57			-				x							x		3/2 or 5/2
76552.60			x				x							x		3/2
76616.44			-				-	-						x	x	3/2 - 7/2
76788.94			x				-	x						-		1/2 or 3/2
76895.40			x				x							x		3/2
76954.26			x				x							x		3/2
76999.66			-				-	-						x	x	3/2 - 7/2
77069.42			-				x							x		3/2 or 5/2
77154.88			-				x	x						-		1/2 - 5/2
77185.31			-				-	-						x	x	3/2 - 7/2
77208.86			-				x							x		3/2 or 5/2
77278.24			x				-	x						-		1/2 or 3/2
77295.28			-				x	-						-	x	3/2 or 5/2
77311.25			x				x							x		3/2
77429.20			x				x							-		1/2 or 3/2
77506.72			-				x	x						-		1/2 - 5/2
77668.89			-				x							x		3/2 or 5/2
77715.95			x	x			-	-						-		1/2 or 3/2
77914.52			x				x							-		1/2 or 3/2
77992.06			-				-							x	x	3/2 - 7/2
78004.65			x				x							x		3/2
78079.15			-				x							x		3/2 or 5/2
78106.22			x	x										-		1/2 or 3/2
78147.89			-											x	x	3/2 - 7/2
78311.97			x	x										-		1/2 or 3/2
78365.42			x											x		3/2
78486.07			x	x										-		1/2 or 3/2

	Intermediate levels			
Level	J = 1/2	J = 3/2	J = 5/2	
[cm^{-1}]	a b c d e	f g h i	j k l m n o	J_{exp}
78643.42	x x		-	1/2 or 3/2
78671.36	x x		-	1/2 or 3/2
78746.08	x x		-	1/2 or 3/2
78780.27	x x		-	1/2 or 3/2
79056.55	x x			1/2 or 3/2

TABLE III: Vacuum wavelengths λ and their uncertainties σ of the newly found lines in $^{232}Th^{+}$ between electronic levels in the energy range from 7.8 to 9.8 eV. The classification shows the initial and final level with energy in cm^{-1}.

λ [nm]	σ [pm]	Classification	λ [nm]	σ [pm]	Classification	λ [nm]	σ [pm]	Classification
237.3774	0.5	25027 – 67154	252.6039	0.6	36582 – 76169	269.2348	0.6	26965 – 64108
237.3854	0.6	26626 – 68752	252.6795	0.5	36391 – 75966	269.4283	0.6	36391 – 73506
238.4730	0.5	26965 – 68899	252.7839	0.6	28244 – 67803	269.5733	0.6	36391 – 73486
238.5148	0.5	37130 – 79056	252.9017	0.6	36582 – 76123	269.7499	0.5	37130 – 74202
238.9628	0.6	26965 – 68813	253.1719	0.5	36391 – 75889	269.8782	0.6	26626 – 63680
239.2760	0.6	28244 – 70037	253.2042	0.9	28244 – 67738	269.9864	0.5	27403 – 64442
239.3099	1.5	26965 – 68752	253.3508	0.6	36688 – 76159	270.0000	0.6	36391 – 73428
239.8737	0.5	36391 – 78079	253.3928	0.9	26965 – 66430	270.0321	0.8	36688 – 73721
239.9382	0.5	36688 – 78365	253.4829	0.6	36391 – 75841	270.0562	0.5	36688 – 73717
240.0962	0.5	37130 – 78780	253.4919	0.6	37846 – 77295	270.5256	0.7	27403 – 64368
240.1541	0.6	25027 – 66667	253.6557	0.7	26965 – 66389	270.5716	0.7	36391 – 73349
240.1903	0.6	26965 – 68599	253.6645	0.6	37130 – 76552	270.6395	0.5	36688 – 73638
240.2932	0.5	37130 – 78746	253.7101	0.5	25027 – 64442	270.9641	0.5	37130 – 74036
240.3025	0.6	36391 – 78005	253.8512	0.6	36391 – 75784	271.1246	0.6	36688 – 73571
240.3337	1.2	26424 – 68033	254.0696	0.7	26965 – 66324	271.3337	0.5	36391 – 73246
240.3905	0.7	26965 – 68564	254.1993	0.5	37846 – 77185	271.4550	0.6	35157 – 71995
240.7252	0.5	37130 – 78671	254.2338	0.9	28244 – 67578	271.4809	0.5	36391 – 73226
240.8251	0.5	36391 – 77914	254.3518	0.5	37130 – 76446	271.5441	0.5	36688 – 73514
240.8585	0.6	27403 – 68921	254.3619	0.7	26424 – 65739	271.7525	0.9	36688 – 73486
240.8879	0.5	37130 – 78643	254.4261	0.6	35157 – 74461	272.0991	0.5	36391 – 73142
240.9901	0.6	27403 – 68899	254.4506	1.0	36391 – 75691	272.1860	0.8	36688 – 73428
241.1881	0.6	26626 – 68088	254.5932	0.5	36688 – 75966	272.3679	0.5	26965 – 63680
241.1969	0.5	36688 – 78148	254.6741	0.5	28244 – 67510	272.4475	0.6	27403 – 64108
241.3031	0.7	26424 – 67866	254.6875	0.6	27403 – 66667	272.9075	0.7	26626 – 63269
241.4906	0.6	27403 – 68813	254.6952	0.6	36688 – 75951	273.0251	0.7	36688 – 73315
241.5974	0.4	36688 – 78079	254.8353	0.5	37130 – 76371	273.0951	0.5	36391 – 73008
241.7691	0.5	25027 – 66389	254.9522	0.8	36391 – 75614	273.3214	0.6	37130 – 73717
241.8040	0.5	37130 – 78486	255.2435	0.5	36391 – 75569	273.3974	0.5	36391 – 72967
241.8445	0.5	27403 – 68752	255.3419	0.5	36391 – 75554	273.5413	0.6	36688 – 73246
241.8936	0.8	37716 – 79057	255.4066	0.6	37846 – 76999	273.6242	0.7	36391 – 72937
241.9013	0.6	28244 – 69583	255.4080	0.5	36688 – 75841	273.6915	0.8	36688 – 73225
242.0322	0.7	36688 – 78005	255.5270	0.6	28244 – 67379	274.0937	0.5	36688 – 73172
242.0537	1.3	26424 – 67738	255.5784	0.6	26626 – 65753	274.2783	0.5	36391 – 72850
242.1069	0.5	36688 – 77992	255.7825	0.7	36688 – 75784	274.3188	0.9	36688 – 73142
242.1455	0.6	25027 – 66325	256.1596	2.1	35157 – 74195	274.9072	0.5	37130 – 73506
242.2577	0.5	36391 – 77669	256.2301	0.5	37130 – 76158	275.0443	0.5	36391 – 72748
242.3828	0.7	26586 – 67843	256.2361	0.6	27403 – 66430	275.4539	0.8	26965 – 63269
242.5118	0.6	37130 – 78365	256.4610	0.5	37130 – 76123	275.4751	0.7	35157 – 71458
242.7445	0.9	27403 – 68599	256.4758	0.5	36391 – 75381	275.5027	0.5	37130 – 73428
242.8248	0.6	37130 – 78312	256.5036	0.7	27403 – 66389	275.6395	0.6	36688 – 72967
242.9481	0.6	27403 – 68564	256.8454	0.6	28244 – 67178	275.6561	0.7	27403 – 63680
243.1749	1.6	26965 – 68088	256.9013	0.6	36688 – 75613	275.8693	0.6	36688 – 72937
243.2133	0.5	36391 – 77507	256.9285	0.8	27403 – 66325	275.8881	0.6	26626 – 62873
243.3403	0.6	27403 – 68498	257.0019	0.8	28244 – 67154	275.9814	0.5	36391 – 72625
243.3971	0.6	26424 – 67510	257.1727	0.5	35157 – 74041	276.0718	0.5	36391 – 72613
243.5233	0.8	37716 – 78780	257.1963	0.6	36688 – 75569	276.0983	0.7	37130 – 73349
243.6726	0.5	36391 – 77429	257.4926	0.5	37130 – 75966	276.1184	0.5	36688 – 72904
243.7195	0.9	26626 – 67657	257.8103	0.6	26965 – 65753	276.4793	0.6	37846 – 74015
243.7263	0.4	37716 – 78746	257.8501	0.7	36391 – 75173	276.5345	0.6	36688 – 72850
244.0161	0.6	36688 – 77669	257.9293	0.6	37846 – 76616	276.8210	0.6	28244 – 64368
244.0454	0.5	37130 – 78106	258.0047	0.6	37130 – 75889	277.0452	0.8	37130 – 73226
244.1713	0.5	37716 – 78671	258.0855	0.5	36688 – 75435	277.2511	0.5	36688 – 72756
244.1757	1.8	26424 – 67379	258.1385	0.5	36391 – 75129	277.3133	0.6	36688 – 72748
244.3369	0.7	37716 – 78643	258.2791	0.7	36391 – 75108	277.3683	0.7	36391 – 72444
244.3483	0.5	36582 – 77507	258.4474	0.6	36688 – 75381	277.4136	0.5	36391 – 72438
244.3746	0.4	36391 – 77311	258.6471	0.6	37846 – 76509	277.5932	0.7	36688 – 72712
244.4703	0.5	36391 – 77295	258.7102	0.9	25027 – 63680	277.6781	0.6	36391 – 72403
244.5992	0.7	26626 – 67510	258.8228	0.5	36688 – 75324	277.6888	0.5	37130 – 73142
244.6299	0.6	26965 – 67843	258.9434	0.9	36391 – 75009	277.7356	0.6	36391 – 72396
244.6534	0.5	37130 – 78004	259.3105	0.8	35157 – 73721	278.1098	0.6	36688 – 72645
244.7108	0.7	24874 – 65739	259.3339	0.6	37130 – 75691	278.2661	0.6	36688 – 72625
244.8703	0.5	26965 – 67803	259.4178	0.7	36582 – 75129	278.3578	1.2	36688 – 72613
244.9879	0.4	36391 – 77209	259.7993	0.6	36391 – 74882	278.4901	0.5	26965 – 62873
245.1924	0.4	37130 – 77915	259.8435	1.0	36688 – 75173	278.6548	0.4	35157 – 71044
245.2641	0.6	26965 – 67738	259.8534	0.6	37130 – 75614	278.7266	0.5	37130 – 73008

TABLE III: Cont.: Newly found lines in $^{232}Th^{+}$.

λ [nm]	σ [pm]	Classification	λ [nm]	σ [pm]	Classification	λ [nm]	σ [pm]	Classification
245.2809	0.7	37716 – 78486	260.1927	0.6	36391 – 74824	278.8179	0.7	27403 – 63269
245.3122	0.5	36391 – 77155	260.2582	0.7	37130 – 75554	278.8335	0.6	28244 – 64108
245.3790	0.6	26424 – 67178	260.2784	0.5	36688 – 75108	279.0227	0.7	35199 – 71038
245.5220	0.7	26424 – 67154	260.4762	0.7	36391 – 74782	279.0418	0.7	37130 – 72967
245.5409	0.5	25027 – 65753	260.6201	0.5	36688 – 75058	279.2888	0.6	36391 – 72196
245.7206	0.4	36582 – 77278	260.7055	0.8	35157 – 73514	279.3846	0.5	36391 – 72183
245.7479	0.5	26965 – 67657	260.7547	0.6	27403 – 65753	279.6758	0.5	36688 – 72444
245.7913	0.6	27403 – 68088	260.9534	0.6	36688 – 75009	279.9593	0.5	37130 – 72850
245.8277	0.5	36391 – 77069	261.0119	0.5	37846 – 76159	279.9907	0.5	36688 – 72403
245.8363	0.5	28244 – 68921	261.3606	0.5	26626 – 64888	280.0492	0.9	36688 – 72396
245.9731	0.6	28244 – 68899	261.3941	0.6	36391 – 74647	280.2686	0.6	36391 – 72071
246.1642	0.6	36688 – 77311	261.4244	0.5	36391 – 74642	280.3815	0.5	36688 – 72354
246.2293	0.8	26965 – 67578	261.4936	1.0	25027 – 63269	280.6046	0.5	36391 – 72028
246.3333	0.5	37716 – 78312	261.8229	0.7	36688 – 74882	280.7571	0.5	37130 – 72748
246.3919	0.6	37130 – 77716	261.8774	0.6	28244 – 66430	280.9699	0.5	35157 – 70748
246.4680	0.6	36582 – 77155	262.0282	0.5	36391 – 74554	280.9798	1.5	36391 – 71980
246.4951	0.9	28244 – 68813	262.0705	0.5	35157 – 73315	281.6281	0.6	36688 – 72196
246.5258	0.5	36391 – 76954	262.2221	0.4	36688 – 74824	281.6646	0.6	36391 – 71894
246.6431	0.6	26965 – 67510	262.3787	0.6	36391 – 74503	281.7263	0.6	36688 – 72183
246.7863	0.6	36688 – 77209	262.4378	0.5	37846 – 75950	281.7341	0.5	37130 – 72625
246.8632	0.7	28244 – 68752	262.5101	0.5	36688 – 74782	281.9289	0.7	27403 – 62873
246.8845	0.7	36391 – 76895	263.0554	0.6	35157 – 73172	282.1953	0.5	28244 – 63680
246.9300	0.5	36688 – 77185	263.1173	0.6	36391 – 74396	282.9669	0.6	36688 – 72028
247.1398	0.7	27403 – 67866	263.4730	0.6	36688 – 74643	283.1745	0.6	36391 – 71704
247.2790	0.6	27403 – 67843	263.5480	0.6	26424 – 64368	283.2260	0.5	36688 – 71995
247.5877	0.5	37716 – 78106	263.5858	0.7	36391 – 74329	283.2265	0.5	37130 – 72438
247.6388	0.6	36688 – 77069	263.6953	0.6	26965 – 64888	283.3486	0.5	36688 – 71980
247.8005	0.6	28244 – 68599	264.0863	0.5	36688 – 74554	283.3539	0.5	36391 – 71682
247.9269	0.7	27403 – 67738	264.0991	0.6	36391 – 74255	283.5023	0.7	37130 – 72403
248.0138	0.9	28244 – 68564	264.4414	0.6	26626 – 64442	283.6226	0.6	36391 – 71649
248.0668	0.5	36688 – 77000	264.4425	0.9	36688 – 74503	284.0444	0.5	36688 – 71894
248.1285	0.6	37846 – 78148	264.4723	0.5	36391 – 74202	284.0516	0.6	36391 – 71595
248.1460	0.5	37130 – 77429	264.7389	0.7	36688 – 74461	284.4657	0.7	36391 – 71544
248.3469	0.6	36688 – 76954	264.7654	0.5	36391 – 74160	284.4745	0.7	36391 – 71543
248.4217	0.7	27403 – 67657	264.7791	0.6	37846 – 75614	285.1681	0.5	36582 – 71649
248.4222	0.6	28244 – 68498	264.8908	0.6	37130 – 74882	285.5804	0.5	36688 – 71704
248.7104	0.6	36688 – 76895	264.9191	0.5	35157 – 72904	285.6014	0.6	36582 – 71595
248.7107	0.4	36582 – 76789	265.1928	0.4	36688 – 74396	286.0816	0.5	36391 – 71346
248.8253	0.6	26965 – 67154	265.3429	0.5	36391 – 74078	286.2032	0.5	37130 – 72071
248.8755	0.6	37130 – 77311	265.3714	0.7	26424 – 64108	286.3793	0.5	36391 – 71309
248.9909	0.8	36391 – 76553	265.6399	0.7	36391 – 74035	286.5529	0.5	37130 – 72028
249.0787	0.6	37130 – 77278	265.6679	0.5	36688 – 74329	286.6332	0.5	36391 – 71278
249.0916	0.5	37846 – 77992	265.9613	0.8	35157 – 72756	286.9024	0.5	36688 – 71543
249.1837	0.5	36391 – 76522	266.0379	0.6	37846 – 75435	287.0462	0.6	35199 – 70037
249.3359	0.6	27403 – 67510	266.1902	0.5	36688 – 74255	287.6058	0.5	36688 – 71458
249.7475	0.7	26626 – 66667	266.2772	0.5	35157 – 72712	287.6587	0.5	37130 – 71894
250.0034	0.6	37716 – 77716	266.4047	0.6	36391 – 73927	287.6592	0.6	36391 – 71154
250.1207	0.8	36391 – 76371	266.5487	0.5	37130 – 74647	287.7000	0.5	36391 – 71149
250.4481	0.5	36688 – 76616	266.6159	0.5	36688 – 74195	288.6182	0.5	36391 – 71038
250.8486	0.5	36688 – 76553	266.6953	0.6	36582 – 74078	288.8402	0.5	36688 – 71309
250.8504	0.5	36582 – 76446	266.7042	0.9	28244 – 65739	289.4210	0.5	37130 – 71682
250.8733	0.5	25027 – 64888	266.7522	0.5	35157 – 72645	289.5678	0.5	36391 – 70925
250.9774	0.6	28244 – 68088	266.7761	0.6	27403 – 64888	290.1422	0.5	36688 – 71154
251.0241	0.5	36391 – 76227	266.8226	1.1	37846 – 75324	290.1833	0.5	36688 – 71149
251.0444	0.5	36688 – 76522	266.8315	0.6	26965 – 64442	290.5814	0.5	37130 – 71544
251.1051	0.5	37130 – 76954	266.8689	0.6	36688 – 74160	290.5905	0.5	37130 – 71543
251.1249	0.6	36688 – 76509	266.9070	0.6	36391 – 73857	290.8340	0.6	35199 – 69583
251.3195	0.4	36582 – 76372	267.2075	0.5	37130 – 74554	291.0724	0.5	36688 – 71044
251.3223	0.8	28244 – 68033	267.3579	0.9	26965 – 64368	291.1177	0.6	36688 – 71038
251.3902	0.5	36391 – 76169	267.7137	0.5	36688 – 74041	292.0836	0.5	36688 – 70925
251.4636	0.5	36391 – 76158	267.7552	0.7	36688 – 74036	292.1596	0.5	36391 – 70618
251.4767	0.5	37130 – 76895	267.9015	0.5	36688 – 74015	292.2673	0.5	37130 – 71346
251.4936	0.6	26626 – 66389	267.9039	0.5	36391 – 73717	292.2969	0.6	36391 – 70602
251.5668	0.7	27403 – 67154	268.4147	0.6	26424 – 63680	292.8431	0.5	37130 – 71278
251.6860	1.0	36391 – 76123	268.4778	0.6	36391 – 73638	293.6014	0.5	36688 – 70748
251.9026	0.8	26626 – 66324	268.5331	0.7	36688 – 73927	293.9144	0.5	37130 – 71154
252.1521	0.5	37130 – 76789	268.7301	0.7	37846 – 75058	294.7209	0.5	36688 – 70618
252.2345	0.8	36582 – 76227	268.8409	0.6	35157 – 72354	294.8605	0.5	36688 – 70602

TABLE III: Cont.: Newly found lines in $^{232}Th^{+}$.

λ [nm]	σ [pm]	Classification	λ [nm]	σ [pm]	Classification	λ [nm]	σ [pm]	Classification
252.3841	0.8	28244 – 67866	268.9555	0.6	36391 – 73571			
252.5284	0.7	28244 – 67843	269.0431	0.5	36688 – 73857			

[1] R. Zalubas and C. H. Corliss, J. Res. Natl. Bur. Stand. Sect. A **78A**, 163 (1974).
[2] M. V. Okhapkin, D. M. Meier, E. Peik, M. S. Safronova, M. G. Kozlov, and S. G. Porsev, Phys. Rev. A **92**, 020503 (2015).
[3] O. Herrera-Sancho, N. Nemitz, M. Okhapkin, and E. Peik, Phys. Rev. A **88**, 012512 (2013).

DANKSAGUNG

Auch wenn am Beginn dieser Arbeit nur mein Name steht, so wäre sie nicht möglich gewesen ohne eine Vielzahl an Personen, denen ich an dieser Stelle meinen Dank aussprechen möchte. Vor allem gilt dieser meinem Doktorvater Andrey Surzhykov, welcher mir alle Freiheiten und alle Möglichkeiten gegeben hat, die ich mir nur wünschen konnte. An zweiter Stelle sei hier Stephan Fritzsche genannt, der mich nach meinem Weggang aus Jena immer wieder, mitunter auch sehr spontan in seine Gruppe willkommen geheißen hat. Außerdem bin ich Piet Schmidt für seine Bereitschaft trotz seines voll gepackten Kalenders meine Arbeit zu begutachten sehr verbunden.

Meinen Arbeitskollegen in Braunschweig und Jena danke ich für ihre fachliche Unterstützung und offenen Ohren, wenn es darum ging Ideen zu formen. Insbesondere seien hier Randolf Beerwerth und Sebastian Ulbricht genannt. Ersterer für seine Bereitschaft sich mit mir in numerischen Details zu verlieren, um die Unberechenbarkeit von Vielelektronenmethoden in den Griff zu bekommen. Letzterer weil er mich immer wieder an die Grundlagen unserer Theorien erinnert hat und daran, wie wenig wir manche Dinge verstehen, die wir aus Gewohnheit als schlicht für gegeben ansehen.

Ich danke der Arbeitsgruppe von Vladimir Shabaev für ihre Gastfreundschaft und Offenheit im Teilen von Ideen.

Der abschließende Dank gebührt meinen Eltern, deren Unterstützung ich mir immer sicher sein konnte. Sie haben nicht nur ein beeindruckendes Verständnis für die fachlichen Details meiner Forschung entwickelt, sondern mich auch immer daran erinnert wie spannend und vielfältig wissenschaftliche Arbeit ist. Zwei Aspekte, die ich immer wieder zu vergessen drohte.

PUBLICATIONS BY THE AUTHOR

[RAM1] P. Imgram, K. König, J. Krämer, T. Ratajczyk, R. A. Müller, A. Surzhykov, W. Nörtershäuser, **Collinear laser spectroscopy at ion-trap accuracy: Transition frequencies and isotope shifts in the $6s^2S_{1/2} \rightarrow 6p^2P_{1/2,3/2}$ transitions in Ba^+**, Physical Review A **99**, 012511 (2019)

[RAM2] R. A. Müller, A. V. Maiorova, S. Fritzsche, A. V. Volotka, R. Beerwerth, P. Glowacki, J. Thielking, D.-M. Meier, M. Okhapkin, E. Peik, A. Surzhykov, **Hyperfine interaction with the ^{229}Th nucleus and its low-lying isomeric state**, Physical Review A **98**, 020503 (2018)

[RAM3] D.-M. Meier, J. Thielking, P. Głowacki, M. V. Okhapkin, R. A. Müller, A. Surzhykov, E. Peik, **Electronic level structure of Th^+ in the range of the ^{229m}Th isomer energy**, Physical Review A **99**, 052514 (2019)

[RAM4] R. Müller, A. Volotka, S. Fritzsche, A. Surzhykov, **Theoretical analysis of the electron bridge process in $^{229}Th^{3+}$**, Nuclear Instruments and Methods in Physics Research Section B: Beam Interactions with Materials and Atoms **408**, 84–88 (2017)

[RAM5] R. A. Müller, A. V. Volotka, A. Surzhykov, **Excitation of the ^{229}Th nucleus via a two-photon electronic transition**, Physical Review A **99**, 042517 (2019)

[RAM6] A. V. Maiorova, S. Fritzsche, R. A. Müller, A. Surzhykov, Elastic scattering of twisted electrons by diatomic molecules, Physical Review A **98**, 042701 (2018)

[RAM7] D. Seipt, R. A. Müller, A. Surzhykov, S. Fritzsche, Two-color above-threshold ionization of atoms and ions in XUV Bessel beams and intense laser light, Physical Review A **94**, 053420 (2016)

[RAM8] R. A. Müller, D. Seipt, R. Beerwerth, M. Ornigotti, A. Szameit, S. Fritzsche, A. Surzhykov, Photoionization of neutral atoms by X waves carrying orbital angular momentum, Physical Review A **94**, 041402 (2016)

[RAM9] R. H. Pratt, R. A. Müller, A. Surzhykov, Sum rules for the polarization correlations in photoionization and bremsstrahlung, Physical Review A **93**, 053421 (2016)

[RAM10] S. Ulbricht, R. A. Müller, A. Surzhykov, Gravitational effects on geonium and free electron g_s-factor measurements in a Penning trap, arXiv:1907.01460, submitted to Phys. Rev. D

[RAM11] Y. Duan, R. A. Müller, A. Surzhykov, Selection rules for atomic excitation by twisted light, Journal of Physics B: Atomic, Molecular and Optical Physics

[RAM12] J. Sommerfeldt, R. A. Müller, A. N. Artemyev, A. Surzhykov, Polarization effects in bound-free pair production, arXiv:1907.08025, submitted to Phys. Rev. A

All Publications that constitute parts of this thesis have titles written in **bold face**.

BIBLIOGRAPHY

[1] H. Geiger, E. Marsden, On a Diffuse Reflection of the Formula-Particles, Proceedings of the Royal Society A: Mathematical, Physical and Engineering Sciences **82**, 495–500 (1909)

[2] E. Rutherford, LXXIX. The scattering of α and β particles by matter and the structure of the atom, The London, Edinburgh, and Dublin Philosophical Magazine and Journal of Science **21**, 669–688 (1911)

[3] A. A. Michelson, Light waves and their uses, no. 3 in The Decennial Publications, The University of Chicago Press, Chicago, 1903

[4] W. Pauli, Zur Frage der theoretischen Deutung der Satelliten einiger Spektrallinien und ihrer Beeinflussung durch magnetische Felder, Die Naturwissenschaften **12**, 741–743 (1924)

[5] D. S. Hughes, C. Eckart, The Effect of the Motion of the Nucleus on the Spectra of Li I and Li II, Physical Review **36**, 694–698 (1930)

[6] W. Pauli, R. E. Peierls, Physikalische Zeitschrift **32**, 670 (1931)

[7] H. Kopfermann, Über den Kerndrehimpuls der Bleiisotope, Die Naturwissenschaften **19**, 400 (1931)

[8] J. Billowes, P. Campbell, High-resolution laser spectroscopy for the study of nuclear sizes and shapes, Journal of Physics G: Nuclear and Particle Physics **21**, 707–739 (1995)

[9] K. Blaum, J. Dilling, W. Nörtershäuser, Precision atomic physics techniques for nuclear physics with radioactive beams, Physica Scripta **T152**, 014017 (2013)

[10] B. Cheal, T. E. Cocolios, S. Fritzsche, Laser spectroscopy of radioactive isotopes: Role and limitations of accurate isotope-shift calculations, Physical Review A **86**, 042501 (2012)

[11] H. De Vries, C. De Jager, C. De Vries, Nuclear charge-density-distribution parameters from elastic electron scattering, Atomic Data and Nuclear Data Tables **36**, 495–536 (1987)

[12] V. V. Flambaum, Enhanced Effect of Temporal Variation of the Fine Structure Constant and the Strong Interaction in ^{229}Th, Physical Review Letters **97**, 092502 (2006)

[13] J. C. Berengut, V. A. Dzuba, V. V. Flambaum, S. G. Porsev, Proposed Experimental Method to Determine α Sensitivity of Splitting between Ground and 7.6 eV Isomeric States in ^{229}Th, Physical Review Letters **102**, 210801 (2009)

[14] M. S. Safronova, S. G. Porsev, M. G. Kozlov, J. Thielking, M. V. Okhapkin, P. Głowacki, D. M. Meier, E. Peik, Nuclear Charge Radii of ^{229}Th from Isotope and Isomer Shifts, Physical Review Letters **121**, 213001 (2018)

[15] W. H. King, Isotope Shifts in Atomic Spectra, Springer US, Boston, MA, 1984

[16] V. V. Flambaum, A. J. Geddes, A. V. Viatkina, Isotope shift, nonlinearity of King plots, and the search for new particles, Physical Review A **97**, 032510 (2018)

[17] J. C. Berengut, D. Budker, C. Delaunay, V. V. Flambaum, C. Frugiuele, E. Fuchs, C. Grojean, R. Harnik, R. Ozeri, G. Perez, Y. Soreq, Probing New Long-Range Interactions by Isotope Shift Spectroscopy, Physical Review Letters **120**, 091801 (2018)

[18] M. S. Safronova, U. I. Safronova, A. G. Radnaev, C. J. Campbell, A. Kuzmich, Magnetic dipole and electric quadrupole moments of the ^{229}Th nucleus, Physical Review A **88**, 060501 (2013)

[19] National Nuclear Data Center, information extracted from the NuDat 2 database (Jun. 2019)
URL `http://www.nndc.bnl.gov/nudat2/`

[20] B. Seiferle, L. von der Wense, P. V. Bilous, I. Amersdorffer, C. Lemell, F. Libisch, S. Stellmer, T. Schumm, C. E. Düllmann, A. Pálffy, P. G. Thirolf, Energy of the ^{229}Th nuclear clock transition, arXiv:1905.06308

[21] E. V. Tkalya, V. O. Varlamov, V. V. Lomonosov, S. A. Nikulin, Processes of the nuclear isomer ^{229m} Th($3/2^+$, 3.5 ± 1.0 eV) resonant excitation by optical photons, Physica Scripta **53**, 296–299 (1996)

[22] E. Peik, C. Tamm, Nuclear laser spectroscopy of the 3.5 eV transition in Th-229, EPL (Europhysics Letters) **61**, 181 (2003)

[23] E. V. Tkalya, Proposal for a Nuclear Gamma-Ray Laser of Optical Range, Physical Review Letters **106**, 162501 (2011)

[24] E. Peik, M. Okhapkin, Nuclear clocks based on resonant excitation of γ-transitions, Comptes Rendus Physique **16**, 516–523 (2015)

[25] C. J. Campbell, A. G. Radnaev, A. Kuzmich, V. A. Dzuba, V. V. Flambaum, A. Derevianko, Single-Ion Nuclear Clock for Metrology at the 19th Decimal Place, Physical Review Letters **108**, 120802 (2012)

[26] G. A. Kazakov, A. N. Litvinov, V. I. Romanenko, L. P. Yatsenko, A. V. Romanenko, M. Schreitl, G. Winkler, T. Schumm, Performance of a ^{229}Thorium solid-state nuclear clock, New Journal of Physics **14**, 083019 (2012)

[27] A. D. Ludlow, M. M. Boyd, J. Ye, E. Peik, P. Schmidt, Optical atomic clocks, Reviews of Modern Physics **87**, 637–701 (2015)

[28] M. G. Kozlov, M. S. Safronova, J. R. Crespo López-Urrutia, P. O. Schmidt, Highly charged ions: Optical clocks and applications in fundamental physics, Reviews of Modern Physics **90**, 045005 (2018)

[29] M. P. Hehlen, R. R. Greco, W. G. Rellergert, S. T. Sullivan, D. DeMille, R. A. Jackson, E. R. Hudson, J. R. Torgerson, Optical spectroscopy of an atomic nucleus: Progress toward direct observation of the ^{229}Th isomer transition, Journal of Luminescence **133**, 91–95 (2013)

[30] J. Gunst, Y. Wu, N. Kumar, C. H. Keitel, A. Pálffy, Direct and secondary nuclear excitation with x-ray free-electron lasers, Physics of Plasmas **22**, 112706 (2015)

[31] L. von der Wense, B. Seiferle, S. Stellmer, J. Weitenberg, G. Kazakov, A. Pálffy, P. G. Thirolf, A Laser Excitation Scheme for ^{229m}Th, Physical Review Letters **119**, 132503 (2017)

[32] L. C. von der Wense, B. Seiferle, C. Schneider, J. Jeet, I. Amersdorffer, N. Arlt, F. Zacherl, R. Haas, D. Renisch, P. Mosel, P. Mosel, M. Kovacev, U. Morgner, C. E. Düllmann, E. R. Hudson, P. G. Thirolf, The concept of laser-based conversion electron Mössbauer spectroscopy for a precise energy determination of ^{229m}Th, Hyperfine Interactions **240**, 240:23 (2019)

[33] V. A. Krutov, V. N. Fomenko, Influence of Electronic Shell on Gamma Radiation of Atomic Nuclei, Annalen der Physik **476**, 291–302 (1968)

[34] M. Morita, Nuclear excitation by electron transition and its application to Uranium 235 separation, Progress of Theoretical Physics **49**, 1574–1586 (1973)

[35] E. Tkalya, Nuclear excitation in atomic transitions (NEET process analysis), Nuclear Physics A **539**, 209–222 (1992)

[36] S. G. Porsev, V. V. Flambaum, E. Peik, C. Tamm, Excitation of the Isomeric ^{229m}Th Nuclear State via an Electronic Bridge Process in ^{229}Th^{+}, Physical Review Letters **105**, 182501 (2010)

[37] J. Eichler, W. E. Meyerhof, Relativistic atomic collisions, Academic Press, 1995

[38] D. R. Hartree, The Wave Mechanics of an Atom with a non-Coulomb Central Field. Part III. Term Values and Intensities in Series in Optical Spectra, Mathematical Proceedings of the Cambridge Philosophical Society **24**, 426–437 (1928)

[39] R. D. Cowan, The theory of atomic structure and spectra, no. 3 in Los Alamos series in basic and applied sciences, University of California Press, Berkeley, 1981

[40] W. Kohn, L. J. Sham, Self-Consistent Equations Including Exchange and Correlation Effects, Physical Review **140**, A1133–A1138 (1965)

[41] I. P. Grant, Relativistic Quantum Theory of Atoms and Molecules: Theory and Computation, Springer Science & Business Media, 2007

[42] W. H. Press (Ed.), Numerical recipes in C: the art of scientific computing, 2nd Edition, Cambridge University Press, Cambridge ; New York, 1992

[43] C. Froese Fischer, T. Brage, P. Jönsson, Computational atomic structure: an MCHF approach, Institute of Physics Publ, Bristol, UK ; Philadelphia, Penn, 1997

[44] V. A. Dzuba, V. V. Flambaum, M. G. Kozlov, Combination of the many-body perturbation theory with the configuration-interaction method, Physical Review A **54**, 3948–3959 (1996)

[45] I. M. Savukov, W. R. Johnson, Combined configuration-interaction and many-body-perturbation-theory calculations of energy levels and transition amplitudes in Be, Mg, Ca, and Sr, Physical Review A **65**, 042503 (2002)

[46] I. M. Savukov, W. R. Johnson, H. G. Berry, Mixed configuration-interaction and many-body perturbation-theory calculations of energies and oscillator strengths of J = 1 odd states of neon, Physical Review A **66**, 052501 (2002)

[47] V. A. Dzuba, V. V. Flambaum, Core-valence correlations for atoms with open shells, Physical Review A **75**, 052504 (2007)

[48] M. Kozlov, S. Porsev, M. Safronova, I. Tupitsyn, CI-MBPT: A package of programs for relativistic atomic calculations based on a method combining configuration interaction and many-body perturbation theory, Computer Physics Communications **195**, 199–213 (2015)

[49] W. R. Johnson, Atomic Structure Theory: lectures on atomic physics, Springer, Berlin ; London, 2007

[50] B. H. Bransden, C. J. Joachain, Physics of atoms and molecules, 2nd Edition, Prentice Hall, Harlow, England ; New York, 2003

[51] F. Salvat, R. Mayol, Accurate numerical solution of the Schrödinger and Dirac wave equations for central fields, Computer Physics Communications **62**, 65–79 (1991)

[52] F. Salvat, J. Fernández-Varea, W. Williamson, Accurate numerical solution of the radial Schrödinger and Dirac wave equations, Computer Physics Communications **90**, 151–168 (1995)

[53] W. R. Johnson, S. A. Blundell, J. Sapirstein, Finite basis sets for the Dirac equation constructed from B splines, Physical Review A **37**, 307–315 (1988)

[54] J. Sapirstein, W. R. Johnson, The use of basis splines in theoretical atomic physics, Journal of Physics B: Atomic, Molecular and Optical Physics **29**, 5213 (1996)

[55] C. De Boor, A practical guide to splines: with 32 figures, Rev. Edition, Applied mathematical sciences, Springer, New York, 2001

[56] G. W. F. Drake, S. P. Goldman, Application of discrete-basis-set methods to the Dirac equation, Physical Review A **23**, 2093–2098 (1981)

[57] V. M. Shabaev, I. I. Tupitsyn, V. A. Yerokhin, G. Plunien, G. Soff, Dual Kinetic Balance Approach to Basis-Set Expansions for the Dirac Equation, Physical Review Letters **93**, 130405 (2004)

[58] V. A. Yerokhin, A. Surzhykov, S. Fritzsche, Relativistic calculations of double K -shell-photoionization cross sections for neutral medium- Z atoms, Physical Review A **90**, 063422 (2014)

[59] V. A. Yerokhin, A. Surzhykov, A. Müller, Relativistic configuration-interaction calculations of the energy levels of the $1s^2 2l$ and $1s^2 l 2l'$ states in lithiumlike ions: Carbon through chlorine, Physical Review A **96**, 042505 (2017)

[60] K. Beloy, A. Derevianko, Application of the dual-kinetic-balance sets in the relativistic many-body problem of atomic structure, Computer Physics Communications **179**, 310–319 (2008)

[61] T. N. Rescigno, Collisional Breakup in a Quantum System of Three Charged Particles, Science **286**, 2474–2479 (1999)

[62] M. Dürr, A. Dorn, J. Ullrich, S. P. Cao, A. Czasch, A. S. Kheifets, J. R. Götz, J. S. Briggs, (e , 3 e) on Helium at Low Impact Energy: The Strongly Correlated Three-Electron Continuum, Physical Review Letters **98**, 193201 (2007)

[63] S. G. Porsev, V. V. Flambaum, Effect of atomic electrons on the 7 . 6 -eV nuclear transition in $^{229}Th^{3+}$, Physical Review A **81**, 032504 (2010)

[64] S. G. Porsev, V. V. Flambaum, Electronic bridge process in $^{229}Th^{+}$, Physical Review A **81**, 042516 (2010)

[65] P. Micke, S. Kühn, L. Buchauer, J. R. Harries, T. M. Bücking, K. Blaum, A. Cieluch, A. Egl, D. Hollain, S. Kraemer, T. Pfeifer, P. O. Schmidt, R. X. Schüssler, C. Schweiger, T. Stöhlker, S. Sturm, R. N. Wolf, S. Bernitt, J. R. Crespo López-Urrutia, The Heidelberg compact electron beam ion traps, Review of Scientific Instruments **89**, 063109 (2018)

[66] P. Micke, J. Stark, S. A. King, T. Leopold, T. Pfeifer, L. Schmöger, M. Schwarz, L. J. Spieß, P. O. Schmidt, J. R. Crespo López-Urrutia, Closed-cycle, low-vibration 4 K cryostat for ion traps and other applications, Review of Scientific Instruments **90**, 065104 (2019)

[67] T. Leopold, S. A. King, P. Micke, A. Bautista-Salvador, J. C. Heip, C. Ospelkaus, J. R. C. López-Urrutia, P. O. Schmidt, A cryogenic radio-frequency ion trap for quantum logic spectroscopy of highly charged ions, arXiv:1901.03082

[68] W. Johnson, G. Soff, The lamb shift in hydrogen-like atoms, $1 \leq Z \leq 110$, Atomic Data and Nuclear Data Tables **33**, 405–446 (1985)

[69] S. A. Blundell, P. E. G. Baird, C. W. P. Palmer, D. N. Stacey, G. K. Woodgate, A reformulation of the theory of field isotope shift in atoms, Journal of Physics B: Atomic and Molecular Physics **20**, 3663–3681 (1987)

[70] V. M. Shabaev, Mass corrections in a strong nuclear field, Theoretical and Mathematical Physics **63**, 588–596 (1985)

[71] C. W. P. Palmer, Reformulation of the theory of the mass shift, Journal of Physics B: Atomic and Molecular Physics **20**, 5987–5996 (1987)

[72] I. I. Tupitsyn, V. M. Shabaev, J. R. Crespo López-Urrutia, I. Draganić, R. Soria Orts, J. Ullrich, Relativistic calculations of isotope shifts in highly charged ions, Physical Review A **68**, 022511 (2003)

[73] J. Thielking, M. V. Okhapkin, P. Głowacki, D. M. Meier, L. von der Wense, B. Seiferle, C. E. Düllmann, P. G. Thirolf, E. Peik, Laser spectroscopic characterization of the nuclear-clock isomer ^{229m}Th, Nature **556**, 321–325 (2018)

[74] W. Kälber, J. Rink, K. Bekk, W. Faubel, S. Göring, G. Meisel, H. Rebel, R. C. Thompson, Nuclear radii of thorium isotopes from laser spectroscopy of stored ions, Zeitschrift für Physik A Atomic Nuclei **334**, 103–108 (1989)

[75] V. A. Dzuba, W. R. Johnson, M. S. Safronova, Calculation of isotope shifts for cesium and francium, Physical Review A **72**, 022503 (2005)

[76] M. V. Okhapkin, D. M. Meier, E. Peik, M. S. Safronova, M. G. Kozlov, S. G. Porsev, Observation of an unexpected negative isotope shift in ^{229}Th^{+} and its theoretical explanation, Physical Review A **92**, 020503 (2015)

[77] A. C. Hayes, J. L. Friar, P. Möller, Splitting sensitivity of the ground and 7.6 eV isomeric states of ^{229}Th, Physical Review C **78**, 024311 (2008)

[78] C. Shi, F. Gebert, C. Gorges, S. Kaufmann, W. Nörtershäuser, B. K. Sahoo, A. Surzhykov, V. A. Yerokhin, J. C. Berengut, F. Wolf, J. C. Heip, P. O. Schmidt, Unexpectedly large difference of the electron density at the nucleus in the $4p\,^2P_{1/2,3/2}$ fine-structure doublet of Ca^{+}, Applied Physics B **123**, 123:2 (2017)

[79] C. J. Campbell, A. G. Radnaev, A. Kuzmich, Wigner Crystals of ^{229}Th for Optical Excitation of the Nuclear Isomer, Physical Review Letters **106**, 223001 (2011)

[80] A. M. Dykhne, E. V. Tkalya, Matrix element of the anomalously low-energy (3.5 ± 0.5)eV transition in ^{229}Th and the isomer lifetime, Journal of Experimental and Theoretical Physics Letters **67**, 251–256 (1998)

[81] E. Litvinova, H. Feldmeier, J. Dobaczewski, V. Flambaum, Nuclear structure of lowest ^{229}Th states and time-dependent fundamental constants, Physical Review C **79**, 064303 (2009)

[82] N. Minkov, A. Pálffy, Theoretical Predictions for the Magnetic Dipole Moment of ^{229m}Th, Physical Review Letters **122**, 162502 (2019)

[83] B. Seiferle, L. von der Wense, P. G. Thirolf, Lifetime Measurement of the ^{229}Th nuclear isomer, Physical Review Letters **118**, 042501 (2017)

[84] V. Barci, G. Ardisson, G. Barci-Funel, B. Weiss, O. El Samad, R. K. Sheline, Nuclear structure of ^{229}Th from γ-ray spectroscopy study of ^{233}U α-particle decay, Physical Review C **68**, 034329 (2003)

[85] L. von der Wense, B. Seiferle, M. Laatiaoui, J. B. Neumayr, H.-J. Maier, H.-F. Wirth, C. Mokry, J. Runke, K. Eberhardt, C. E. Düllmann, N. G. Trautmann, P. G. Thirolf, Direct detection of the ^{229}Th nuclear clock transition, Nature **533**, 47–51 (2016)

[86] R. Zalubas, C. H. Corliss, Energy levels and classified lines in the second spectrum of thorium (Th II), Journal of Research of the National Bureau of Standards Section A: Physics and Chemistry **78A**, 163 (1974)

[87] S. L. Redman, G. Nave, C. J. Sansonetti, The spectrum of thorium from 250nm to 5500nm: Ritz wavelengths and optimized energy levels, The Astrophysical Journal Supplement Series **211**, 4 (2014)

[88] C. W. Reich, R. G. Helmer, Energy separation of the doublet of intrinsic states at the ground state of ^{229}Th, Physical Review Letters **64**, 271–273 (1990)

[89] A. V. Volotka, A. Surzhykov, S. Trotsenko, G. Plunien, T. Stöhlker, S. Fritzsche, Nuclear Excitation by Two-Photon Electron Transition, Physical Review Letters **117**, 243001 (2016)

[90] B. R. Beck, J. A. Becker, P. Beiersdorfer, G. V. Brown, K. J. Moody, J. B. Wilhelmy, F. S. Porter, C. A. Kilbourne, R. L. Kelley, Energy Splitting of the Ground-State Doublet in the Nucleus ^{229}Th, Physical Review Letters **98**

[91] E. V. Tkalya, C. Schneider, J. Jeet, E. R. Hudson, Radiative lifetime and energy of the low-energy isomeric level in ^{229}Th, Physical Review C **92**

[92] P. V. Borisyuk, E. V. Chubunova, N. N. Kolachevsky, Y. Y. Lebedinskii, O. S. Vasiliev, E. V. Tkalya, Excitation of ^{229}Th nuclei in laser plasma: the energy and half-life of the low-lying isomeric state, arXiv:1804.00299 [nucl-ex, physics:nucl-th, physics:physics]ArXiv: 1804.00299

[93] V. A. Yerokhin, Nuclear-size correction to the Lamb shift of one-electron atoms, Physical Review A **83**, 012507 (2011)

[94] K. Pachucki, V. A. Yerokhin, Theory of the Helium Isotope Shift, Journal of Physical and Chemical Reference Data **44**, 031206 (2015)

[95] L. Schmöger, M. Schwarz, T. M. Baumann, O. O. Versolato, B. Piest, T. Pfeifer, J. Ullrich, P. O. Schmidt, J. R. Crespo López-Urrutia, Deceleration, precooling, and multi-pass stopping of highly charged ions in Be $^+$ Coulomb crystals, Review of Scientific Instruments **86**, 103111 (2015)

[96] L. Schmöger, Kalte hochgeladene Ionen für Frequenzmetrologie, Ph.D. thesis, Heidelberg University (2017)

[97] A. Shahbaz, C. Müller, T. Bürvenich, C. Keitel, Laser-induced nonresonant nuclear excitation in muonic atoms, Nuclear Physics A **821**, 106–117 (2009)

[98] V. N. Tsytovich, I. M. Oiringel (Eds.), Polarization Bremsstrahlung, Springer US, Boston, MA, 1992

[99] A. V. Korol, O. I. Obolensky, A. V. Solov'yov, I. A. Solovjev, The full relativistic description of the bremsstrahlung process in a charged particle-atom collision, Journal of Physics B: Atomic, Molecular and Optical Physics **34**, 1589–1617 (2001)